Unfolding the Potential of Transmembrane-TNFα in Cancer Therapeutics

A Thesis

Submitted in Partial Fulfillment of the Requirements

for the award of the degree of

DOCTOR OF PHILOSOPHY

by

Srirupa Bhattacharyya

(Roll No. - 156106023)

Department of Biosciences and Bioengineering

Indian Institute of Technology Guwahati

Guwahati, 781039, Assam, India

September 2020

Dedicated to My Parents

Declaration

I, hereby, declare that the research embodied in this thesis entitled "**Unfolding the Potential of Transmembrane-TNFα in Cancer Therapeutics"** is the result of investigations carried out by me under the supervision of Prof. Siddhartha Sankar Ghosh, Department of Biotechnology, Indian Institute of Technology Guwahati, India for the award of Degree of Doctor of Philosophy. This work has not been submitted elsewhere for any degree, diploma, etc. of any Institute or University to the best of my knowledge and belief.

Srirupa Bhattacharyya

Date: 15th December 2020
Place: IIT Guwahati

Srirupa Bhattacharyya
Roll No. 156106023

Indian Institute of Technology Guwahati

Department of Biosciences and Bioengineering

Certificate

This is to certify that the thesis entitled "**Unfolding the Potential of Transmembrane-TNFα in Cancer Therapeutics"** being submitted to the **Indian Institute of Technology Guwahati** by **Srirupa Bhattacharyya** (Roll No. **156106023)** for the award of the degree of **Doctor of Philosophy** in Department of Biosciences and Bioengineering, is a bonafide record of research work carried out by her. The contents of this thesis have not been submitted to any other University or Institute for the award of any degree or diploma.

Date: 15th December 2020
Place: IIT Guwahati

Prof. Siddhartha Sankar Ghosh
(Thesis Supervisor)

Acknowledgment

I want to use this opportunity to express my heartfelt gratitude to all those who have played a pivotal role in helping me reach this destination and have supported me throughout this tenure.

The love for Cell and Molecular Biology was instilled in me by my teacher Dr. Suparna Pal (Lady Brabourne College, University of Calcutta), during my college days. It was her passionate lectures, which inspired me to delve deep into this subject, which was efficiently taken over by the lessons of Dr. Sandip Das (University of Delhi) during my University days. I thank you, Sir and Ma'am, from the core of my heart.

I want to thank my Ph.D. supervisor Professor Siddhartha Sankar Ghosh, for choosing me to work in his laboratory and for believing in my capabilities. My guide has provided enough support during the days of failures when negative results paramounted. Under his able guidance, I could learn scientific perspectives of the work that has helped me to implement my thesis objectives patiently.

Next, I would like to thank my Doctoral Committee members for evaluating my progress time and again, and for giving constructive criticisms throughout this tenure. I am also highly indebted to the Department of Biosciences and Bioengineering, Centre for Nanotechnology, Central Instrumentation Facility IIT Guwahati, and DBT Program Support Facility for providing the support and assistance required to carry out my thesis work.

I am privileged to have loving and helpful senior and junior lab members. I want to thank all of them for providing a cohesive work environment. I am also fortunate to have friends who stick to me, especially when the weather is turbulent.

Last but not least, I am blessed to have parents like Ma, and Baba. Since my childhood, the main motto of their life was to make me capable enough to stand on my own feet- and particularly for that, they went to incredible extents. Despite having a hectic profession, I can not remember any single instance in which they failed to support me for my studies. I want to thank them for their guidance and support throughout my life, for everything they have done for me, and, most importantly, for giving me this Life.

Srirupa Bhattacharyya

Table of Contents

Abstract

Tumor necrosis factor-alpha (TNFα), a pleiotropic cytokine, is involved in maintaining a plethora of immune responses in the human body. Initially, TNFα is synthesized as a 26 kDa full-length transmembrane form, which is enzymatically cleaved to produce soluble 17 kDa TNFα. Although the anti-cancer potential of soluble TNFα was discovered more than a century back, its dual nature and tumor-promoting ability pose a major hindrance in its acceptance as an anti-cancer molecule. In contrast, the transmembrane TNFα (tmTNFα), the physiological precursor of soluble TNFα, holds the potential of tumor regression without initiating cell proliferation.

Section 1 is the **Introduction and Review of Literature** part, which elucidates the essential roles of cytokines in maintaining several complex physiological functions in our body. In this section, basic biology and molecular aspects of soluble TNFα and tmTNFα have been mentioned. The tmTNFα remains biologically active and is capable of initiating signaling cascades after binding with the TNFα receptors-TNF RI and TNF RII. Hence, the membrane-tethered tmTNFα form holds the potential of tumor regression. The objectives of the thesis have been framed by exploiting the ligand function of the transmembrane moiety in *in vitro* conditions. Finally, the salient features of this thesis have been delineated.

Section 2 provides a detailed description of the **materials** and **methods** used for the experiments in the current thesis. This section also encompasses the details of the protocols along with the modifications to develop recombinant tmTNFα and its microcarriers.

Section 3 describes **Results and Discussions**. This section elaborates fabrication of a novel therapeutic module by coating nontoxic, biodegradable chitosan nanoparticle core with engineered macrophage membrane-tethered TNFα. Initially, THP-1 cells were differentiated by phorbol myristate acetate (PMA) treatment. Then, the expression of membrane-bound TNFα was induced by bacterial lipopolysaccharide (LPS) in the differentiated THP-1 cells. Subsequently, the as-synthesized chitosan nanoparticle core was coated with TNFα expressed macrophage membrane through the extrusion process. Characterizations by transmission electron microscopy and Western blotting results demonstrated successful coating of chitosan nanoparticles with TNFα induced membrane. The

cell viability assays on cancer cells such as - HeLa, MDA-MB-231, and MCF-7 revealed the significant innate anti-cell proliferative potential of these membrane coated nanoparticles. Additionally, the expression of several interleukins was evaluated after treatment, which demonstrated excellent biocompatibility of the membrane-coated nanoparticles. The fabricated nanoparticles also exhibited a dose-dependent cell death in tumor spheroids, which was further corroborated with Calcein AM/ PI dual staining results. Translation of the therapeutic efficacy of the synthesized nanoassembly substantiated the biological relevance of the membrane-tethered protein.

The subsequent endeavor was to develop tmTNFα in its purified form. In this quest, the membrane-tethered moiety, i.e., the full-length tmTNFα, was subcloned and expressed using a bacterial expression vector. The GST tagged tmTNFα was purified to homogeneity using affinity chromatography, and its structural integrity was assessed. The structural characterizations of purified tmTNFα revealed the integrity of the protein, while cell viability assays demonstrated significant antiproliferative effect on HepG2 (IC_{50}: 36 nM) and HeLa (IC_{50}: 23 nM) cells. Mechanistic insights into the mode of cell death unveiled G1 arrest in HepG2 and G2/M arrest in HeLa cells accompanied by disruption of mitochondrial membrane potential and activation of executioner caspases. Subsequent, flow cytometry-based assays resulted in confirmatory evidence of apoptosis after treatment with the recombinant protein. Additionally, recombinant tmTNFα on tumor spheroids also showed a reduction in spheroid's size due to extensive cell death.

The final part of the thesis was to formulate a suitable delivery vehicle for the recombinant protein. This work was aimed to engineer a suitable cargo for stabilization and efficient delivery of functional tmTNFα *in vitro*. The synthesized microcarriers were characterized for the delivery of recombinant tmTNFα. The functionality of the protein-loaded microcarriers was assessed by cell viability studies. The results demonstrated the physical properties of the microparticles, efficient loading of the purified tmTNFα along with retention of its functional integrity. The cell viability assay results elucidated enhanced anti-cell proliferative potential of cargo immobilized tmTNFα.

Conclusion and Future prospects in **Section 4** summarises the key findings of this current thesis. The effectiveness of tmTNFα on monolayer cells, as well as on complex tumor spheroids, demonstrates the therapeutic significance of recombinant tmTNFα as an attractive option in cancer therapeutics. The current work bestows a new lead towards formulating delivery platforms to achieve

effective therapeutic efficacy of tmTNFα. This work provides future scope of testing efficacy of tmTNFα *in vivo* for its translational potential.

List of Abbreviations and Acronyms

AICD	Activation Induced Cell Death
AO/EtBr	Acridine Orange/ Ethidium Bromide
Bax	Bcl-2 Associated X Protein
Bcl2	B-Cell Lymphoma 2
Bcl-xL	B-Cell Lymphoma-extra large
BET	Brunauer Emmett Teller
BJH	Barrett Joyner And Halenda
BSA	Bovine Serum Albumin
CD	Cluster of Differentiation
CD	Circular Dichroism
cFLIP	Cellular FLICE (FADD-Like IL-1β-Converting Enzyme)-Inhibitory Protein
cIAP	Inhibitors of Apoptosis Proteins
Da	Dalton
DD	Death Domain
DISC	Death Induced Silencing Complex
DLS	Dynamic Light Scattering
DMEM	Dulbecco's Modified Eagle's Medium
DMSO	Dimethyl Sulfoxide
DR	Death Receptor
EDTA	Ethylenediaminetetraacetic Acid
EDX	Energy Dispersive X-Ray
ERK 2	Extracellular Signal-Regulated Kinases

FADD	Fas-Associated Death Domain
FasL	Fas Ligand
FDA	Food and Drug Administration
FESEM	Field Emission Scanning Electron Microscopy
FITC	Fluorescein Isothiocyanate
GFP	Green Fluorescent Protein
GST	Glutathione S-Transferase
GST-π	Glutathione S-Transferase -Pi
h	Hour
HCl	Hydro Chloric acid
HepG2	Hepatocyte Carcinoma
HL-60	Human Leukemia-60
IC	Inhibitory Concentration
IFN	Interferon
IL	Interleukin
IPTG	Isopropyl β-D-1-thiogalactopyranoside
JC-1	Tetraethyl-benzimidazolylcarbocyanine Iodide
LB	Luria Bertani Broth
LPS	Lipopolysaccharide
LS	Leader Sequence
MALDI TOF	Matrix Assisted Laser Desorption/Ionization Time of Flight
MCF	Michigan Cancer Foundation
MTT	(3-(4,5-Dimethylthiazol-2-Yl)-2,5-Diphenyltetrazolium Bromide
MHC	Major Histocompatibility Complex

NCCS	National Centre For Cell Science
NEB	New England Biolabs
NF-κB	Nuclear factor kappa-light-chain-enhancer of activated B
NK	Natural Killer
OD	Optical Density
PBS	Phosphate Buffer Saline
PBST	Phosphate Buffer Saline with 0.1% Tween
PCR	Polymerase Chain Reaction
PEG	Poly Ethylene Glycol
PI	Propidium Iodide
PMA	Phorbol 12- Myristate 13-Acetate
PMSF	Phenylmethanesulfonyl fluoride
PVDF	Polyvinylidene Difluoride
RIP	Receptor Interacting Protein
RNA	Ribonucleic Acid
ROS	Reactive Oxygen Species
rpm	Revolutions Per Minute
rTNFα	Recombinant TNFα
SD	Sphingomyelinase Domain
SDS PAGE	Sodium Dodecyl Sulphate Polyacrylamide Gel Electrophoresis
STAT	Signal Transducer and Activator of Transcription
TACE	TNF α Converting Enzyme
TBS	Tris Buffer Saline
TEM	Transmission Electron Microscopy
TNF α	Tumor Necrosis Factor alpha

tmTNFα	Transmembrane TNFα
TNF R	TNF Receptor
TRADD	TNF-Receptor-Associated Death Domain
TRAF	TNF Receptor Associated Factor
TRAIL	TNF-Related Apoptosis-Inducing Ligand
TRID	TNF Receptor Internalization Domain
TRITC	Tetramethyl rhodamine isothiocyanate
X-gal	5-bromo-4-chloro-3-indolyl-β-D-galactopyranoside

List of Schemes

List of Figures

Figure 3.20 (A) SDS-PAGE depicting induction of GST tmTNFα. Lane 2 and 3: Induced supernatant and pellet at 37 °C. Lane 5 and 6: Induced supernatant and pellet at temperature 28 °C. Lane 8 and 9: Induced supernatant and pellet at temperature 22 °C. Lane 1: Uninduced supernatant and pellet at 37 °C. Lane 4: Uninduced supernatant and pellet at temperature 28 °C. Lane 7: Uninduced supernatant and pellet at temperature 22 °C. Lane M: Broad range marker 10-250 kDa Thermo Scientific. (B) Purification of GST-tmTNFα, Lane 1 purified GST -tmTNFα at 52 kDa, Lane 2 shows protein marker

Figure 3.21 Purification of only GST protein- Lane 1 purified GST at 26 kDa, Lane 2 shows protein marker (Thermo Scientific PAGE-Ruler Unstained)

Figure 3.22 Western Blot with anti-TNFα antibody depicting a band at 52 kDa corresponding to monomeric GST-tmTNFα and another band at higher molecular weight (152 kDa) of self-assembled trimeric form of the recombinant protein

Figure 3.23 (A) MALDI TOF analysis of tryptic digested GST-tmTNFα, (B) Circular dichroism spectra depicting secondary structure of GST-tmTNFα

Figure 3.24 (A) PCR amplification of TNF RI for HepG2, HeLa, MCF-7, U87MG and A375 cell lines with beta-actin as an internal control along with ImageJ analysis. Lanes 1,3,5,7,9 denoting internal control for HepG2, HeLa, MCF-7, U87MG and A375 cell lines. Lanes 2,4,6,8,10 indicates PCR amplification of TNF RI for respective cell lines(B) PCR amplification of TNF RII for HepG2, HeLa, MCF-7, U87MG, and A375 cell lines with beta-

carbonate microspheres (i) before and (ii) after protein loading, (D) Hydrodynamic diameter of the microparticles before and after protein loading

Figure 3.48 (A) Assessment of cell viability upon treatment with increasing concentrations of calcium carbonate microparticles and with recombinant tmTNFα loaded calcium carbonate microparticles. The concentration of the recombinant protein loaded on the microparticles were 9 nM, 15 nM, 24 nM, and 36 nM for 0.075, 0.125, 0.2 and 0.3 mg/ml microparticles respectively. (B) Evaluation of the IC_{50} concentration of recombinant tmTNFα loaded calcium carbonate microparticles on HeLa cells

Section 1

Introduction and Review of Literature

Introduction and Review of Literature

1.1. Protein therapeutics: The complex network of signaling cascades play a major role in orchestrating the delicate harmony between cell growth, division, and programmed death of cells [1]. Proteins, either in secreted or in membrane-bound forms, interact with their respective receptors and modulate intricate signaling networks to maintain balance in the overall behavior of the cells [2]. Multiple signaling pathways play roles in replenishing dead cells with new healthy cells [2]. In repertoire, recombinant proteins have revolutionized treatment modality of several diseases, namely, diabetes, cancer, respiratory, cardiovascular, and inflammatory diseases [3]. An array of therapeutic proteins are in clinical use ever since the approval of the first recombinant protein human Insulin - Humulin by the Food and Drug Administration (FDA) in 1982 [4].

Protein therapeutics are armed with several advantages over small molecule-based drugs-

1) Recombinant proteins have very complex and specific functions, which simple chemical compounds fail to achieve.
2) Proteins, in general, tend to target particular signaling pathways, specifically, which decreases the probability of adverse side effects.
3) Humanized recombinant proteins do not elicit immune responses and are well tolerated as the body naturally produces these proteins.
4) Several studies show the clinical development of therapeutic proteins is faster as compared to small molecule drugs [3].

In the case of cell death-related pathways, death signals like Tumor Necrosis Factor (TNF), Cluster of Differentiation (CD) 95L, and TNF-Related Apoptosis-Inducing Ligand (TRAIL) is essential. The binding of these proteins on their corresponding

receptors initiates the death-signaling cascade resulting in cell apoptosis [5]. One class of such signaling entities are the cytokines that orchestrate a plethora of immune responses [6]. This group of glycoprotein messengers has revolutionized the therapeutic paradigm of several diseases, including cancer. Prime examples of cytokines approved for cancer immunotherapy include Interleukin (IL) 2 and Interferon (IFN) α 2 [7,8], which act by harnessing the body's immune system to ablate tumors. Soluble tumor necrosis factor-alpha (TNFα) (17 kDa) is such a pro-inflammatory, multifunctional cytokine, produced from transmembrane TNFα (tmTNFα) (26 kDa) through enzymatic cleavage [9]. rTNFα (recombinant TNFα) has been reported to induce growth inhibition via caspase-dependent apoptosis by interacting with TNF Receptor I (TNF RI) [10]. But, contrary to anti-proliferative properties, several studies indicate the tumor-promoting role of rTNFα, mainly through activation of Nuclear Factor Kappa-Light-Chain-Enhancer Of Activated B cells (NF-κB) [11], which promotes invasion and migration of the cells [12, 13]. Considering the dual nature of rTNFα, now the primary emphasis is to explore tmTNFα [14]. Literature suggests that tmTNFα is not merely a silent precursor of soluble TNFα, but it can also initiate signal transduction cascade [15]. Besides, several reports elucidate, tmTNFα does not trigger the NF-κB signaling cascade, thus negating any possibility of initiating cell proliferation by forward signaling [16]. Therefore, understanding the biological effect of tmTNFα as a ligand in the form of a functional expressed protein could open a new vista in the realm of cancer therapeutics.

1.2. Background: In the year 1890, a New York surgeon William Bradley Coley, repeatedly found spontaneous regression of metastatic sarcoma upon injecting the patients with a Streptococcal concoction [17,18]. These toxins, widely referred to as Coley's toxins, were extensively used for the next 30 years, to treat several inoperable sarcoma cases [19]. Despite obtaining excellent initial responses, these

toxins faced enormous criticisms and disapproval by many leading surgeons at that time, primarily because of the inconsistencies [20]. From the year 1962, the use of Coley's toxin, as a therapeutic, was banned by the FDA, USA [17]. Several years later, Murray Shear and his colleagues unveiled that bacterial lipopolysaccharide is the active component present in the Streptococcal concoction, leading to tumor regression [21,22]. W O' Malley demonstrated that the tumor regressing potency induced by the bacterial lipopolysaccharide was due to an endotoxin in the serum, which was activated upon injection [23]. This endotoxin, responsible for hemorrhagic necrosis of tumors, was named as - tumor necrosis factor-alpha (TNFα) in the year 1975 by E. A. Carswell et al. [24] and a decade later, the 17 kDa functional recombinant TNFα was purified from *Escherichia coli* [25]. In the subsequent year, the protein was purified to homogeneity from the supernatants of Phorbol 12-myristate 13-acetate (PMA) induced Human leukemia (HL)-60 cell line and characterized [26].

1.3. The duality of 17 kDa TNFα: TNFα gene is located on chromosome 6p21.3 inside the major histocompatibility complex (MHC) [27]. Initially, TNFα is expressed as a type II transmembrane protein of 233 aminoacids (26 kDa), which undergoes enzymatic cleavage by a metalloenzyme – TNFα converting enzyme (TACE) between amino acids alanine (76) and valine (77) [28]. This enzymatic cleavage produces the secreted, circulating form of the cytokine- soluble TNFα, consisting of 157 amino acids (17 kDa) [29,30] **(Scheme 1.1)**. The tmTNFα has an N-terminus 76 amino acid leader sequence primarily responsible for membrane anchorage of the full-length protein [31]. Both tmTNFα and soluble TNFα are biologically active, and they initiate the signaling cascade by binding with TNFα receptors, which leads to a spectrum of responses [32]. Since the identification of this multidimensional pleiotropic cytokine- TNFα, a plethora of research and investigations have been carried out to unravel the potential of this molecule [33]. Although primarily TNFα

was known as a tumor-suppressing agent, its dual nature became well evident gradually [34]. Despite initial reports on antiproliferative effects, considerable pieces of evidence started unveiling the tumor-promoting role of the soluble TNFα [35,36], along with the associated systemic toxicity [37]. This pro-tumorigenic function is attributed by the simultaneous activation of the transcription factor NF-κB, which transactivates several genes responsible for cell survival, proliferation, and metastasis [38,39]**.** The soluble TNFα is referred to as a "double-edged sword" due to several orchestrating interplay of signaling molecules [14].

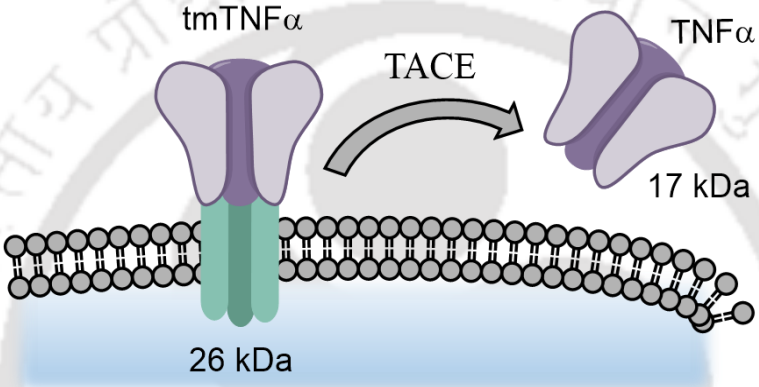

Scheme 1.1: tmTNFα (26 kDa) undergoes enzymatic cleavage by TACE to produce the secreted soluble TNFα (17 kDa).

1.4. Anti-cell proliferative potential of tmTNFα*:* Although the soluble form of TNFα is an enzymatic cleavage product of the full-length membrane-tethered form, these two proteins do not share the exact physiological "precursor-product" relationship [31]. The two proteins differ in their mode of action, though the external ligand-binding portion of both soluble and transmembrane TNFα has the same amino acid residues [40]. The tmTNFα has an extra 76 amino acid leader sequence, which contributes to the differential folding of the transmembrane protein in three-dimensional space [15,41]. The anti-cell proliferative potential ability of the membrane-tethered form of TNFα was discovered in the late 1980s [42]. The amino acid residues of the leader sequence of tmTNFα are mainly responsible for its cytotoxicity. Mutations in the cysteine (-28) and methionine (-71) amino acid of the

leader sequence cause complete loss of apoptosis by the molecule [43]. The intact uncleaved, 26 kDa full-length form of TNFα can ablate target cells by cell-to-cell contact. T Decker et al. initially observed that phorbol 12- myristate 13-acetate (PMA) activated macrophages express a membrane-tethered TNFα on the surface, which is primarily responsible for the killing of target cells, just by contact [27, 29]. The purified cell membranes of the activated macrophages can also induce cell growth inhibition to TNFα-sensitive cells, while the uninduced macrophage membranes do not exhibit such effects. The mechanism of cell growth inhibition of both the soluble and the membrane-tethered TNFα is receptor-dependent; however, the signaling cascades are different [44]. Although the extracellular sequence of soluble TNFα and tmTNFα are the same, the 76 kDa leader sequence substantially influences the mode of action of the two molecules [31]. The difference is so immense that in many cell lines, these two TNF members function in a diametrically opposite manner. Soluble TNFα treatment, in Raji cells, induces proliferation of the cells, whereas treatment with tmTNFα induces cell death [45]. Another study revealed that the tmTNFα had a higher a cytocidal spectrum than the soluble TNFα, where soluble TNFα was cytotoxic against only L929 cells, the tmTNFα was efficient to kill both hepatocyte carcinoma (HepG2) and L929 cells [46].

The mode of cell killing was revealed to be primarily apoptosis for tmTNFα, while it was predominantly necrotic for soluble TNFα. Also, apoptosis induced by tmTNFα, in the two different cell lines, was at two separate phases of the cell cycle. In HepG2 cells, apoptosis took place at the G1 phase, while the apoptosis of L929 cells occurred predominantly at S phase [47]. A separate study elucidated that tmTNFα induced apoptosis in HL-60, Raji, and K562 cell lines mainly took place in the S phase of cell cycle [48]. In HepG2 cells, treatment with recombinant tmTNFα induced cell cycle arrest in the G1 phase, whereas in HeLa, cell cycle progression was arrested at the G2/M phase of cell cycle [49]. Qingfen Li et al. meticulously carried out an extensive study to understand the differences in the mode of action

of the two TNFs, both *in vivo* and *in vitro*. They elucidated that the tumor cells, retrovirally transfected with gene encoding tmTNFα, induced cell death by cell to cell contact.

Moreover, those cells induced Fas ligand-mediated cell death accompanied by the formation of a capsule around the tumor, thus inhibiting tumor metastasis [50]. Murine mouse model, Lewis Lung carcinoma, and B16F10 mouse melanoma cell lines were transduced with retroviral vectors expressing either membrane or soluble isoform of TNFα. In the retrovirally transfected cell lines, there was no observable effect on cell viability, but the same tmTNFα expressing vectors were capable of reduction of tumor volume to 65% in comparison to only vector control tumors when they were transfected subcutaneously in tumor models. Contrastingly, soluble TNFα increased tumor volume to 7-fold with respect to control experimental groups. B16F10 cells expressing tmTNFα induced 60±29% cell death in myeloid cells, compared to less than 1% cytotoxicity induced by recombinant soluble TNFα. Natural killer (NK) cells expressing tmTNFα, can also efficiently kill K562 (immortalized leukemia cell line) cells within 24 h [51].

However, it should be mentioned here that there are reports which show that expression of tmTNFα promotes chemo-resistance in breast cancer [52]. Also, tumor cells of 63.8% of breast cancers express tmTNFα on their surface, whereas, in healthy breast tissue, tmTNFα expression remains undetectable [53]. In several cases of breast cancer, overexpression of tmTNFα is found to be associated with poor prognosis. MDA-MB-231 cell lines, which express high levels of the membrane-tethered form of TNFα, are resistant to the cytotoxicity induced by soluble TNFα, compared to MCF-7 cells that express low levels of tmTNFα [54].

All the aforementioned studies indicate that tmTNFα is cytotoxic to several cancer cells, and at certain times it may be cytotoxic to those cancers that are even resistant to soluble TNFα. Furthermore, the cytotoxicity induced by tmTNFα in different cell lines is associated with growth arrest in different cell cycle phases, which

indicate that there must be more than one underlying mechanism for cell death in the TNFα sensitive cells. Notably, several evidences also show the proliferative property of this full-length type II transmembrane protein, explicitly denoting that an opposing signaling mechanism may come into play in certain instances. Therefore, a detailed insight of the molecular pathways initiated by tmTNFα in several cell lines has been elucidated in the subsequent portion.

1.5. Mechanism of action*:* Although cell death and survival pathways initiated by soluble TNFα have been widely studied for the last two decades, the detailed mode of action of tmTNFα remains elusive. Recent elucidation of the signaling mechanism initiated by tmTNFα uncovered a completely distinct signaling cascade as compared to the soluble counterpart [44]. Moreover, reports suggest, tmTNFα can bind with both the TNF receptors- TNF receptor I (TNF RI) and TNF receptor II (TNF RII), while the soluble counterpart preferentially binds with the receptor I. As a matter of fact, tmTNFα is the primary activating ligand of the TNF RII [55]. Also, similar to other members of TNF superfamily, tmTNFα is capable of initiating bidirectional signaling- Forward signaling and Reverse signaling [56]. This explicitly means that when tmTNFα is expressed on the surface of a cell, it can function as a ligand as well as a receptor [57]. Forward signaling is initiated when the molecule binds as a ligand to the TNF receptors on the surface of other cells. This essentially brings about apoptosis and tumor suppression, primarily by cell-to-cell contact. Whereas, when tmTNFα is expressed on the surface of a cell, the moiety itself can function as a receptor and transduces reverse signaling in that particular cell, which simultaneously activates the tumor proliferation signaling cascade in most of the instances [58]. Molecular events associated with TNFα have been portrayed below.

1.5.1. Reverse signaling of tmTNFα leading to inhibition of apoptosis: Reports suggest that, while acting as a receptor, they induce cancer cell survival, proliferation and make them chemoresistant to a certain extent. Endogenous TNFα in Raji cells brings about the resistance of the cells to soluble TNFα induced cytotoxicity by constitutively activating the NF-κB cell survival pathway. The constitutive activation of NF-κB in Raji cells can be inhibited by creating antisense against tmTNFα [16]. The leader sequence of tmTNFα is only involved in this reverse signaling procedure, but not the extracellular part. Over-expression of tmTNFα on breast cancer cell line- MDA-MB-231 renders them resistant to the cytotoxic effects of soluble TNFα. Moreover, it is noteworthy to mention here that breast cancer cell lines like MCF-7 express deficient levels of tmTNFα and are susceptible to soluble TNFα mediated cytotoxicity. Transfection of TNF leader sequence (TNF-LS) to these TNFα susceptible MCF-7 cell lines makes them resistant. This essentially indicates that the leader sequence of TNFα is responsible for making the cells resistant to the soluble TNFα mediated cytotoxicity [59]. Studies reveal that expression of tmTNFα promotes resistance of the MDA-MB-231 cells towards cytotoxic drug doxorubicin through reverse signaling. This resistance is induced by the phosphorylation of extracellular signal-regulated kinases (ERK) 2 by tmTNFα reverse signaling, which in turn activates the glutathione s-transferase - pi (GST-π), a molecule that mediates detoxification of cells from a large number of xenobiotic and anti-cancer agents. Along with the activation of the GST-π ERK 2 axis, reverse signaling induces constitutive activation of NF-κB, leading to the transcription of anti-apoptotic genes, further employing one extra level of resistance against a well-known chemotherapeutic drug- doxorubicin [52] **(Scheme 1.2)**.

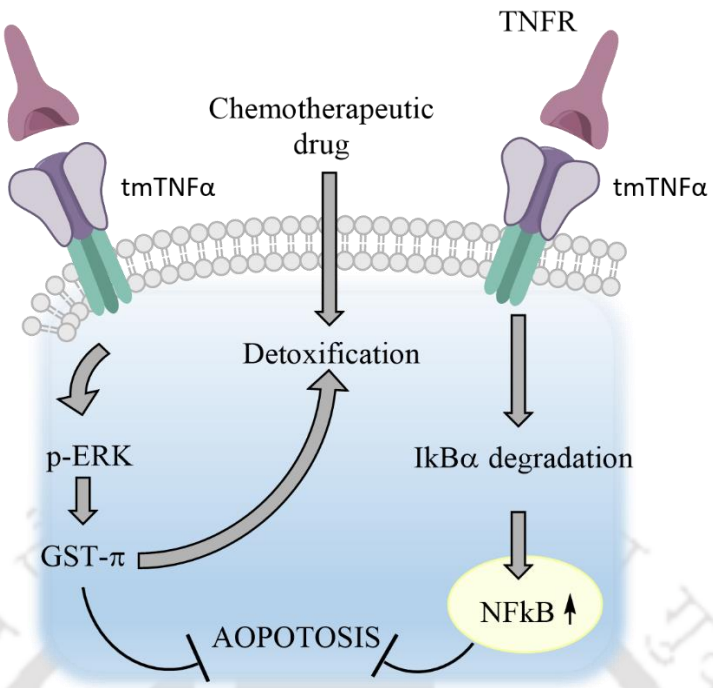

Scheme 1.2: Schematic demonstrating essentially the reverse signaling pathways initiated by tmTNFα. Binding of TNF R induces two separate reverse signaling cascades (i) the degradation of IkBα which leads to the simultaneous activation of NF-kB, (ii) activation of the p-ERK-GST π axis which detoxifies chemotherapeutic drug like doxorubicin. Conceptualized and redrawn based on *Transmembrane TNF-Alpha Promotes Chemoresistance in Breast Cancer Cells ,Zhang Z et al. Oncogene* 37, 3456–3470 (2018).

1.5.2. Induction of apoptosis by binding with TNF RI: tmTNFα initiates forward signaling by binding to TNF RI, which belongs to the family of death receptors. The TNF RI contains three domains, namely- TNF receptor internalization domain (TRID), sphingomyelinase domain (SD), and the death domain (DD) [60]. Binding of TNFα, with TNF RI as a ligand, initiates allosteric changes in the receptor to facilitate attachment of signal transducer and activator of transcription (STAT) 1 to the cytoplasmic portion of TNF RI. STAT1 attaches with the SD region of TNF RI, extending 319 to 337 amino acids, in a death domain-independent manner. This binding of STAT1 to the SD of TNF RI, further recruits the TNF-receptor-associated death domain (TRADD) to form Death induced silencing complex (DISC) in the plasma membrane to initiate apoptosis. Furthermore, tmTNFα does not induce activation of NF-κB, proliferative signal, as

the two prime proteins for NF-κB activation- Receptor interacting protein (RIP) 1 and inhibitors of apoptosis proteins (cIAP) 1, remain undetected. The binding of TRADD to STAT1 completely inhibits binding of TRADD with TNF receptor-associated factor (TRAF) 2 and RIP1, while simultaneously keeping the interaction of TRADD and (Fas-associated death domain) FADD undisturbed. Caspase-8 also gets localized to the plasma membrane **(Scheme 1.3)**. Thus, activation of NF-κB proliferative signaling is wholly suppressed. This might be the mechanistic reason why tmTNFα is capable of killing those cells that are not affected by soluble TNFα. STAT 1 is a crucial player in tmTNFα mediated cytotoxicity, and the reports show that impairment of STAT1 markedly reduces the cytotoxicity of the transmembrane moiety [44].

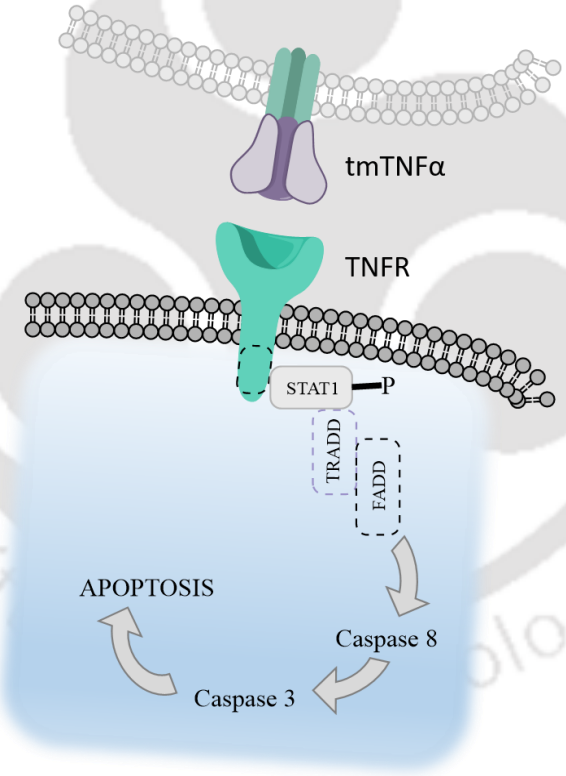

Scheme 1.3: Schematic illustrating tmTNFα induced apoptosis upon binding with TNF RI, involving the interaction of STAT 1, TRADD and FADD. Concept source: *STAT1 mediates transmembrane TNF-alpha-induced formation of death-inducing signaling complex and apoptotic signaling via TNFR1. Jiang*, Y. *et al.. Cell Death Differ.* 24, 660–671 (2017).

1.5.3. Involvement of β-actin in tmTNFα mediated apoptosis: tmTNFα can also bind with TNF RII to initiate a signaling cascade, which promotes apoptosis. This involves the involvement of actin cytoskeleton- precisely β-actin. Primarily, the actin cytoskeleton is responsible for maintaining proper cell morphology and polarity, but increasing pieces of evidence suggest that the cytoskeleton is an integral part of executing apoptosis and necrosis [61]. Activated caspases cleave actin into two fragments f- actin and t- actin, which further triggers apoptosis, indicating that actins serve as an effector molecule and as regulators to carry out apoptosis. A study by Hui Chen et al. showed the involvement of β-actin in tmTNFα mediated apoptosis by carrying out experiments that involve disruption of the actin cytoskeleton's dynamic structure, with specific actin polymerization inhibitors. Disruption of actin polymerization rendered HL-60 leukemia cell line, resistant to the cytotoxicity induced by tmTNFα - explicitly indicating the role of the actin cytoskeleton in facilitating tmTNFα mediated apoptosis. Since the primary ligand for TNF RII is tmTNFα, and treatment of β-actin inhibitor inhibited the binding of TNFα with TNF RII, the precise mechanism behind this might be due to decreased expression of TNF RII on the cell surface [62]. NF-κB is a transcription factor that plays a crucial role in resistance against death ligand-induced apoptosis by activating the translation of several anti-apoptotic genes. NF-κB needs to be translocated in the nucleus from the cytoplasm to transactivate the anti-apoptotic genes, and intact IκB protein inhibits the translocation of this transcription factor, holding it back to the cytoplasm [63]. tmTNFα inhibits the degradation of IκB, thus preventing the induction of anti-apoptotic genes. Binding of tmTNFα with TNF RII induces the dissociation of TRAF2 from TNF RII. It facilitates the translocation of RIP1 from the cytoplasm followed by subsequent binding of RIP1 in the plasma membrane- in turn inhibiting the action of NF-κB. The binding of TRAF with TNF RII is essential for the activation of NF-κB. RIP is a vital adaptor kinase which stands at the crossroads of cell fate decision. While full-

length RIP1 is responsible for activation of NF-κB inducing cell survival, a C terminal caspase-8 cleaved fragment of RIP1 promotes apoptosis. On the other hand, TNFα activates caspase-8, which results in the cleavage of RIP1 simultaneously inactivating NF-κB, thus sensitizing the cells in a pro-apoptotic pathway [64] **(Scheme 1.4)**. Impairment of the actin filaments blocked the caspase-8 activation; therefore, RIP1 remained intact, leading to NF-κB activation, rendering resistance of the cells towards cytotoxicity. Moreover, molecules such as cFLIP and cIAPs bind to TNF RII, negatively regulating the activation of caspase-8. Binding of tmTNFα with the TNF R uncouples these from TNF RII, leading to activation of caspase-8. Disruption of the actin filaments impaired the uncoupling of cellular FLICE (FADD-like IL-1β-converting enzyme)-inhibitory protein (cFLIP) from TNF RII , making the cells resistant to the tmTNFα induced apoptosis, primarily by inactivating caspase-8. In a nutshell, binding of tmTNFα sensitizes the cells towards the apoptotic pathway by inhibiting NF-κB mediated activation of anti-apoptotic genes, which is regulated in several steps by the actin-associated signaling [61,65].

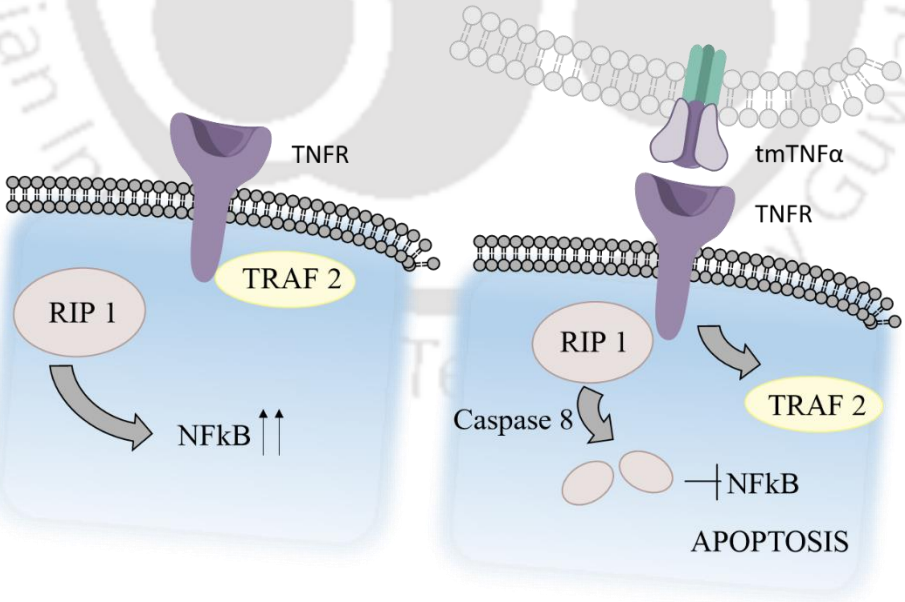

Scheme 1.4: Schematic representation of inhibition of NF-kB upon binding of tmTNFα with TNF RII controlled by the actin cytoskeleton. Conceptualized and

redrawn based on. *The involvement of β-actin in the signaling of transmembrane TNF-α-mediated cytotoxicity. Chen, H. et al "J. Leukoc. Biol.* 89, 917–926 (2011).

1.5.4. tmTNFα activates programmed necrosis- necroptosis*:* While apoptosis is a well-characterized and vastly studied mode of programmed cell death, necrosis is a sudden unprogrammed, unregulated event [66]. Though apoptosis and necrosis have been widely studied for many years, a more regulated form of necrosis has been uncovered recently– termed as necroptosis, which exhibits features similar to necrosis but is initiated by a programmed signaling event [67,68]. Studies reveal that membrane-tethered form of TNFα can induce programmed necrosis, upon binding with TNF RII, in certain cell lines. Target cells like L929 cells and RAW, when treated with effector cells expressing tmTNFα, undergo a remarkable decrease in cell viability without increasing the level of active caspase-3. On the other hand, it was found that tmTNFα treatment leads to the generation of reactive oxygen species (ROS) by the mitochondria. Besides, the ceramide signaling pathway is involved in this case of activating programmed necrosis. A stable interaction of membrane TNFα with TNF RI and TNF RII promotes the formation of receptor clusters in the lipid rafts, which are highly abundant in ceramide precursor, sphingomyelin. The abundance of receptor clusters and the lipid rafts recruit sphingomyelinase, leading to the formation of ceramide from sphingomyelin. Thus, the ceramide signaling pathway is initiated, resulting in decreased mitochondrial membrane integrity causing generation of ROS [69] **(Scheme 1.5)**.

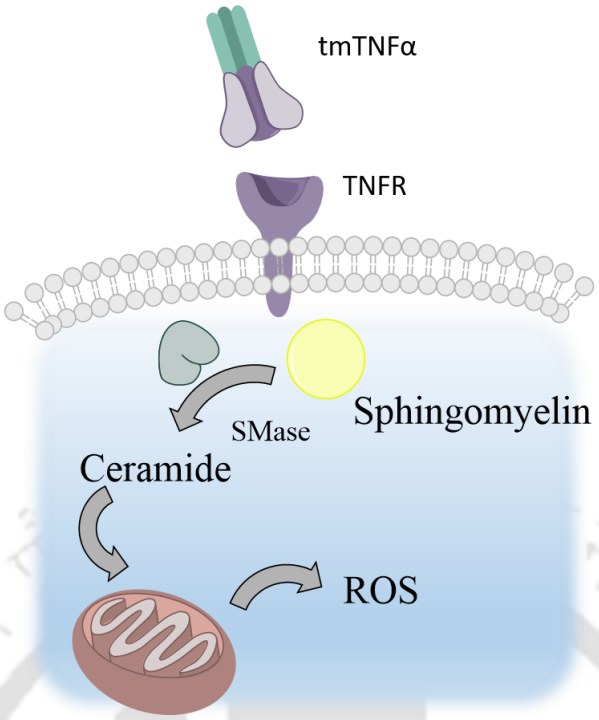

Scheme 1.5: Schematic of the activation of Necroptosis by tmTNFα by activating Ceramide signaling pathway, which leads to the generation of reactive oxygen species. Concept source: Membrane TNF-alpha-activated programmed necrosis is mediated by Ceramide-induced reactive oxygen species. Conceptualized and redrawn based on *Membrane TNF-Alpha-Activated Programmed Necrosis Is Mediated by Ceramide-Induced Reactive Oxygen Species Ardestani, S.; Deskins, D. L.; Young, P. P.. J. Mol. Signal.* 2013, 8 (1).

1.5.5. Induction of Activation induced cell death (AICD) in the T cells*:* To protect self from autoimmune responses, human T lymphocytes undergo programmed cell death, when activated by a ligand on their T cell receptor. This signaling mechanism is known as activation induced cell death (AICD), and tmTNFα plays a chief role in this process [70]. In this regard, it is to be mentioned that tmTNFα, is capable of acting both a ligand as well as a receptor. tmTNFα mediates AICD by both the forward and reverse signaling. When tmTNFα was inhibited by knockdown in human primary T lymphocytes and Jurkat cells (a line of human immortalized T lymphocytes), AICD decreased significantly. Simultaneously, inhibition of the TACE enzyme, which cleaves the precursor membrane-tethered form to the soluble form, rendered an increase in apoptosis of the studied cell lines, remarkably. Thus, undoubtedly establishing the role of this

moiety as a ligand to initiate AICD. It is most probable that forward signaling to induce AICD by tmTNFα takes place by TNF RII, but not by TNF RI. tmTNFα is also involved in increasing the sensitivity of the T cells to AICD by reverse signaling. Upon induction with TNFα receptor I, the sensitivity of tmTNFα expressing Jurkat cells, towards apoptosis, increases. This is established by the upregulation of death ligand-receptor complexes like FasL/Fas and TRAIL/ death receptor (DR) 4 - the key players facilitating AICD [71] **(Scheme 1.6)**.

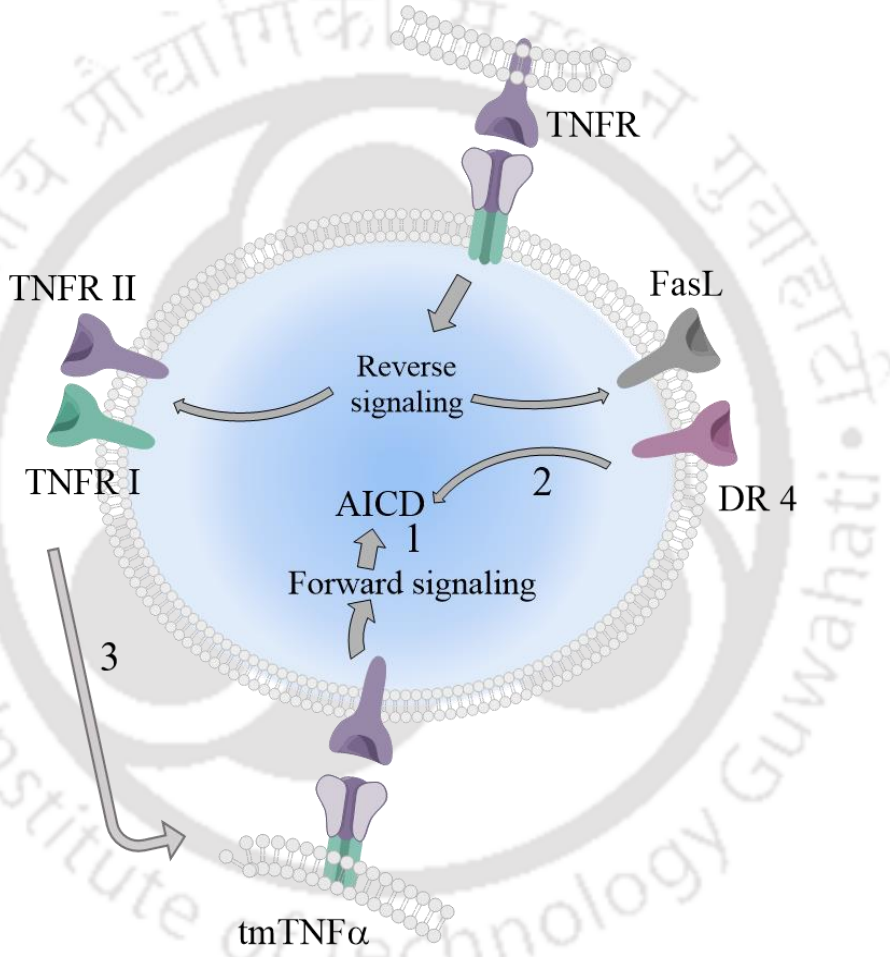

Scheme 1.6: Schematic illustrating induction of activation induced cell death by tmTNFα. More than one pathway is involved in this process- (1) Binding of tmTNF α to TNF R, induces AICD by forward signaling. (2) Reverse signaling also leads to the overexpression of Fas L and DR4, which induces AICD. (3) Overexpression of TNF RI and TNF RII, by reverse signaling, sensitizes the cells towards tmTNFα induced AICD. Concept source: *Transmembrane TNF-α promotes activation-induced cell death by forward and reverse signaling. Zhang, M. et al. Oncotarget* 8, 63799–63812 (2017).

1.5.6. Maintaining the antiproliferative potential of the Natural Killer (NK) cells: The natural killer (NK) cells are a part of the immune system, which directly takes part in protecting the body from cancer. They are the first line of defense mechanism in our body, which primarily helps to combat cancer [72,73]. Low levels of NK cell's activity is directly related to increased susceptibility of cells towards cancer and is associated with high tumor metastasis [74,75,76]. Human NK cells constitutively synthesize tmTNFα, which is primarily responsible for NK cell-mediated cytotoxicity. For the NK cell-mediated cytotoxicity, reverse signaling initiated by the membrane TNFα is mainly involved. The binding of soluble TNFR to the membrane TNFα induces improved exocytosis of perforin and grananzymes that participate in apoptosis of the target cells. Moreover, this binding also causes an increase in the transcription of perforin and grananzyme B. The type II transmembrane protein (tmTNFα) contains a phosphorylated serine residue in the N-terminal cytoplasmic region. Upon binding of soluble TNF R with the tmTNFα, this particular site is dephosphorylated. Although the exact mechanism is still not clear, the increased exocytosis of perforin and grananzymes, might be attributed to this particular dephosphorylation of the specific serine residue. This leads to a rise in Ca^{2+} levels inside the cells culminating in the exocytosis (**Scheme 1.7)**. Additionally, induction of tmTNFα by sTNF R, induces the overexpression of FasL, which further results in increased apoptosis of the target cells. The activation of NF-κB, by reverse signaling of tmTNFα might be responsible for FasL activation [51].

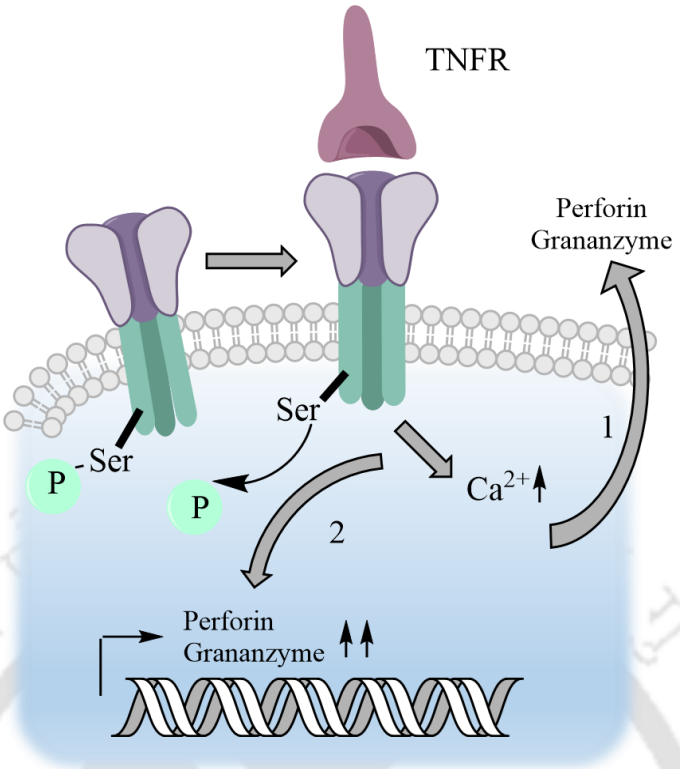

Scheme 1.7: Schematic of induction of antiproliferative potential of NK cells upon binding of TNF R to tmTNFα. (1) The binding, leads to de-phosphorylation of a particular serine residue that increases intracellular calcium levels leading to increased exocytosis of perforin and grananzyme. (2) The transcription of those genes increases upon tmTNFα binding with TNF R. Concept source: *Influence of reverse signaling via membrane TNF-alpha on cytotoxicity of NK92 Cells. Yu, M. et al. Eur. J. Cell Biol.* 88, 181–191 (2009).

In a nutshell, tmTNFα has much better anti-cell proliferative activity than the soluble TNF counterpart. It is well evident from the stated molecular mechanisms that the transmembrane moiety has immense potential to be used as an anti-cancer therapeutic in the future. However, several factors like short half-life, vulnerability to internal proteases, and uncontrolled release are some of the challenges, which limit the acceptance of a recombinant protein as a suitable therapeutic candidate. To surmount the limitations of the recombinant protein, and to maintain proper structural and functional integrity, researchers have fabricated several promising delivery systems like micro and nanocarrier.

In this quest, a diverse array of nanoparticles ranging from metallic, semi-metallic to polymeric particles have emerged [77]. Amongst these, biodegradable

polymeric nanoparticles are the most promising class for delivering biological molecules and drugs. These polymeric nanoparticles are armed with a multitude of advantages such as enhanced stability, higher drug payload, tunable physicochemical properties, homogeneous particle distribution, and controlled drug release [78]. Chitosan, consisting of α-(1-4)-2-amino-2-deoxy-β-D-glucan repeats, is one such FDA approved biopolymer, which has been reported as a drug delivery vehicle in several biological applications [79,80,81]. However, the use of bare nanoparticles often leads to rapid clearance from the bloodstream due to opsonization [82]. Coating nanoparticles with a layer of hydrophilic polyethylene glycol (PEG) has been established to deceit the body's immune system [83]. Yet, rapid clearance of the PEGYlated nanoparticles was reported when the animals were injected with the second dose, owing to the formation of anti-PEG immunoglobulin M antibodies [84]. Hence, a new generation of novel biomimetics could offer an alternative to cloak the synthetic nanocarriers by coating with natural membranes [85,86,87]. The biological membrane coated nanoparticles could escape the body's defense machinery and retained prolonged circulation time in the body [88]. Amidst a multitude of natural membranes, which are used to disguise the nanoparticles from the strict surveillance of the immune system, the macrophage membranes deserve special mention because macrophages are the circulating sentinels of the body having innate characteristics of homing towards the inflammation-affected area [89,90]. Interestingly, the homing property of the whole macrophage cells has shown the accumulation of the drug-carrying macrophage cells near cancer cells.

For efficient delivery of recombinant proteins to the target site, several delivery vehicles have also been engineered, having unique advantages. In this regard, calcium carbonate deserves special mention as a promising protein delivery system. Series of benefits like ease of synthesis, abundant availability, biocompatibility, biodegradability makes calcium carbonate very suitable as an efficient drug carrier [91,92].

Moreover, the porous nature and pH sensitivity impart calcium carbonate with desirable virtues to be a perfect cancer therapeutic delivery vehicle [93]. The porous structure of the calcium carbonate microparticles endows them to have a higher loading efficiency. At the same time, the pH sensitivity facilitates the release of the therapeutic payload, specifically at the mildly acidic tumor microenvironment.

The benefits of therapeutic proteins over small-molecule drugs have facilitated their dominance in the worldwide pharmaceutical market. Protein therapeutics can also be used in combination with chemotherapeutic drugs to augment their therapeutic effects and to reduce the intolerable side effects. In order to unleash the full therapeutic potential of the membrane-tethered TNFα, the tumor proliferative property of the tmTNFα should be nullified. This can be achieved just by negating the reverse signaling of this transmembrane protein.

This thesis aims to fabricate a suitable nanocarrier cloaked with macrophage membrane-tethered TNFα and to understand its therapeutic efficacy. Furthermore, to obtain tmTNFα in a pure form, a venture to produce recombinant tmTNFα from *Escherichia coli* has been carried out. Since the recombinant proteins have a very short half-life and tend to be degraded easily in a biological system, the purified functional recombinant tmTNFα has been loaded successfully on calcium carbonate microparticles, and its therapeutic efficacy has been evaluated.

1.6. Objectives of the Thesis: The following objectives were framed based on the lead of protein therapeutics and the intriguing nature of tmTNFα -

1. To understand the role of tmTNFα on cell growth inhibition using TNFα overexpressed macrophage membrane coated nanocarrier.
2. Finding anti-cell proliferative role of recombinant tmTNFα by cloning, expression, purification, and functional characterization.
3. Finally, development of an efficient delivery system for recombinant tmTNFα.

1.7. Salient outcome of the current thesis work:

- LPS induced transmembrane TNFα overexpressed macrophage membrane nanoassembly, was fabricated, having innate therapeutic potential.
- The nanoassembly was found to be non-immunogenic to macrophage cells and non-hemolytic to RBC.
- Cytotoxicity and mode of cell death on cancer monolayers and tumor spheroids was evaluated upon treatment with nanoassembly.
- Recombinant transmembrane TNFα demonstrated significant anti-proliferative potential by tweaking cell cycle progression along with the alteration of pro & anti-apoptotic signals.
- Mechanistic insights of cell death revealed membrane blebbing, nuclear pyknosis, activation of executioner caspases, and disruption of membrane potential leading to apoptosis.
- Synthesis and characterization of calcium carbonate microparticles for efficient delivery of recombinant protein.
- Reduction of cell viability of cancer cell lines, upon treatment with recombinant tmTNFα loaded calcium carbonate microparticles, has established the biomedical application potential of tmTNFα.

Section 2

Materials and Methods

Materials and Methods

2.1. Materials:

Avanti Polar Lipids- Mini Extruder Set and Accessories

Bio-rad -PCR Master mix, SYBR Green, cDNA synthesis kit

Borosil- Glasswares

Cell Signaling Technology- Anti-TNFα antibody

Corning – Spin X concentrator (Cut off- 20 kDa)

Eppendorf - Cell culture plates

GE Healthcare- Thrombin, Anti GST-antibody, pGEX-4T-2 vector, Gel running apparatus

Gibco- Antibiotic-Antimycotic solution

HiMedia India – Bovine serum albumin (BSA), ampicillin, IPTG, Luria Bertani Broth (LB), polyethylene glycol (PEG), X-gal (5-bromo-4-chloro-3-indolyl-β-D-galactopyranoside)

Merk (Germany)- ammonium hydroxide, ethanol

NEB (USA) - Restriction enzymes - BamHI, XhoI, EcoRI, Cut smart buffer

Promega – pGEM-T easy vector kit, Quick Ligation Kit

Sigma-Aldrich (USA) – Agarose, Dulbecco's modified eagle's medium (DMEM), Fetal bovine serum (FBS), gel extraction kit, Plasmid miniprep kit, Glutathione-agarose beads, Hydroxycinnamic acid, Lysozyme (from chicken egg white), ponceau S, propidium iodide (PI), reduced Glutathione, RNA Isolation Kit ,RIPA Buffer, Triton-X-100, Trizma base (Tris) , Tween -20, Tetra methyl ethylene diamine (TEMED), Tri reagent, ammonium persulphate (APS) Trypsin-EDTA, Trypsin Profile IGD kit dimethylsulphoxide (DMSO),3-(4,5-dimethylthiazol-2-Yl)-2,5diphenyltetrazolium bromide (MTT), chitosan, starch, lipopolysaccharide (LPS), phorbol 12-myristate 13-acetate (PMA), resazurin disodium salt

Tarsons- Plasticware

Thermo Scientific- DNA and Protein ladder, Trypan blue *(Invitrogen),* Caspase-3/7 Green Detection Reagent

Integrated DNA Technologies (IDT)- Primers for all PCR reactions have been listed below:

β Actin	Fwd: 5' CTGTCTGGCGGCACCACCAT 3'
	Rev: 5' GCAACTAAGTCATAGTCCGC 3'
Bax	Fwd: 5' AAGCTGAGCGAGTGTCTCAAGCGC 3'
	Rev: 5' TCCCGCCACAAAGATGGTCACG 3'
Bcl-xL	Fwd: 5' ATGGCAGCAGTAAAGCAAGCGC 3'
	Rev: 5' TTCTCCTGGTGGCAATGGCG 3'
Bcl 2	Fwd: 5' GATTGTGGCCTTCTTTGAG 3'
	Rev: 5' CAAACTGAGCAGAGTCTTC 3'
TNF RI	Fwd: 5'- TGCCTACCCCAGATTGAGAA -3'
	Rev: 5'- ATTTCCCACAAACAATGGAGTAG -3'
TNF RII	Fwd: 5'- CTCACAGTGCTCCTCCCAAG -3'
	Rev: 5'- GTCTCCAGCTGTGACCGAAA -3'
Cyclin A	Fwd: 5'-TCAGCTGGGAAGGACCGGGG -3'
	Rev: 5'-GGGGGCTCTTGGACCCCACA -3'

2.2. Cell lines and cell culture conditions:

Human embryonic kidney cells (HEK-293), cervical cancer cells (HeLa), hepatic carcinoma cells (HepG2), breast cancer cells (MCF-7, MDA-MB-231), human glioblastoma cells (U87MG), human malignant melanoma cells (A375) were obtained from the repository of National Centre for Cell Science (NCCS), Pune. Cells were maintained in Dulbecco's modified Eagle's medium (DMEM) supplemented with 10% (v/v) fetal bovine serum (FBS) and 1% penicillin and streptomycin in humidified air containing 5% CO_2 at 37 °C.

2.3. Method Sections:

2.3.1. Methods related to development and evaluation of bioactivity of transmembrane TNFα-expressed macrophage membrane-coated chitosan nanoparticles

2.3.1.1. Monocyte Differentiation: THP-1 cells (monocytes) were differentiated into macrophages by treating them with 100 µM of phorbol 12-myristate 13-acetate (PMA) for 24 h. The PMA concentration used for differentiation was optimized using increasing concentrations of PMA (0-100 µM), and the conversion of monocytes into macrophages was confirmed by microscopy and flow cytometry.

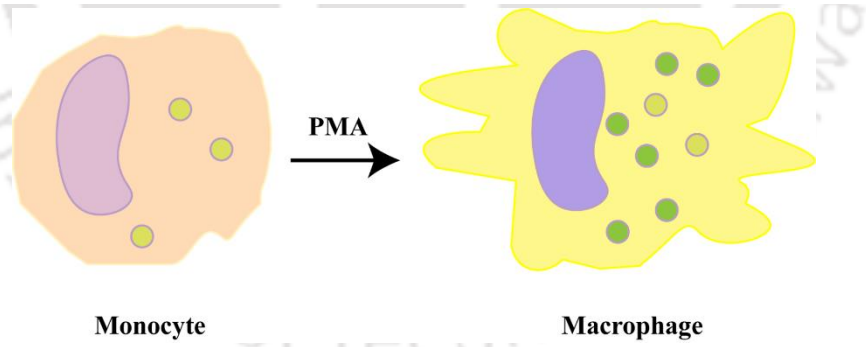

Scheme 2.1: Schematic representation of differentiation of Monocytes into Macrophages

2.3.1.2. Optimization of LPS concentration: The macrophages were challenged with varying concentrations (0-500 ng) of bacterial lipopolysaccharide (LPS) to produce TNFα. Literature suggests the time of secretion of soluble TNFα by the

macrophages is 4-5 h. To obtain transmembrane TNFα, the time was reduced to 2.5 to 3 h and the LPS concentration was optimized for maximum induction of TNFα.

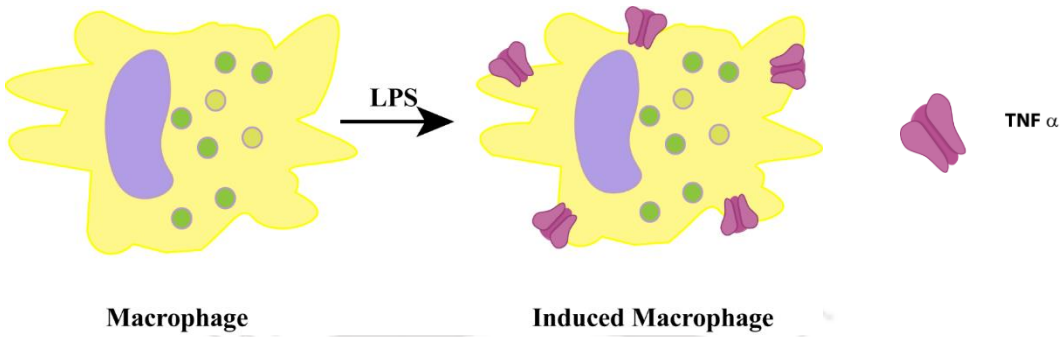

Scheme 2.2: Schematic representation of induction of Macrophages with LPS to produce TNFα on the membrane

2.3.1.3. Isolation of TNFα expressed macrophage membrane: The macrophages were harvested by scraping and were kept overnight in a hypotonic lysis buffer containing sodium bicarbonate, ethylene diamine tetra acetic acid (EDTA), phenylmethane sulfonyl fluoride (PMSF). Following overnight incubation, the cell suspension was loaded into hand held Dounce Homogeniser and disrupted with 30 passes. The suspension was centrifuged at 3500 g to remove the larger debris, the supernatant was again centrifuged at 15000 g for 40 min, and pellet was obtained containing the plasma membrane of the macrophages. The pellet was washed 4-5 times with PBS by repeated centrifugation, to remove any other contaminants. To evaluate the expression of TNFα in the isolated membrane of the macrophages, Western blotting with anti-TNFα antibody was performed. The expression on TNFα after adding 100 ng/ml LPS was also confirmed by semiquantative polymerase chain reaction (PCR) using TNFα specific primers. β-actin was used as an internal positive control.

2.3.1.4. Preliminary cell viability assay with the membrane fractions: In order to study the therapeutic potential of the TNFα expressing macrophage membrane, HeLa, MCF-7, MDA-MB-231 cells were seeded in 96 well plates and treated with increasing concentration of the LPS induced macrophage membrane. After 48 h, cell viability was evaluated using MTT assay by recording the absorbance at 570 nm and 630 nm as background.

2.3.1.5. Synthesis of chitosan nanoparticles: Chitosan nanoparticles were synthesized using the well-established protocol of ionic gelation method using 0.5 mg/ml chitosan and 0.75 mg/ml TPP, the chemical recation of which have been mentioned below :

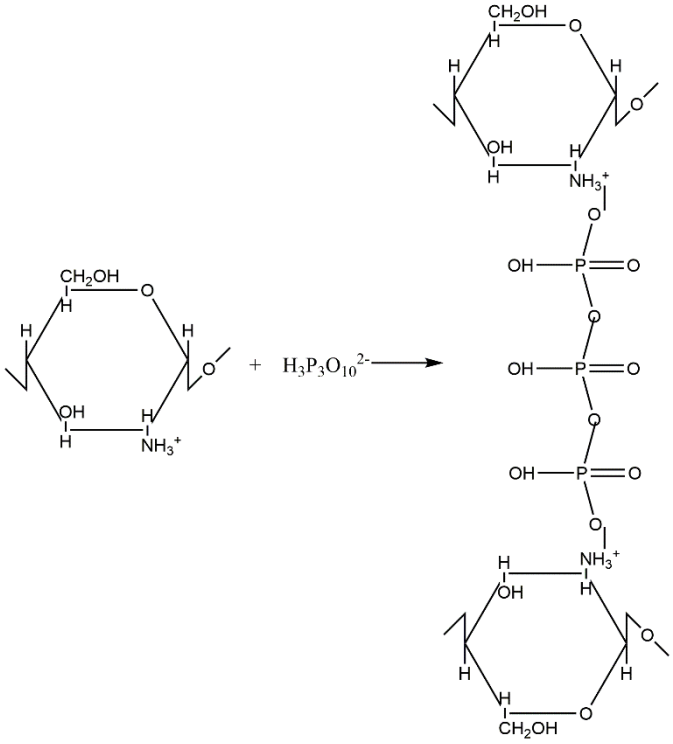

Chemical reaction of the synthesis procedure using chitosan and TPP

The solution was stirred for 24 h at 600 rpm. After synthesis, the solution was centrifuged at 15,000 rpm for 30 min to pellet down the nanoparticles and washed 4-5 times with water by repeated centrifugation to remove any unreacted

components. Zeta potential and hydrodynamic diameter were measured by Malvern Zeta Sizer Nano ZS.

2.3.1.6. Imaging of the chitosan nanoparticles: The chitosan nanoparticles were characterized by Field emission scanning electron microscopy (FESEM) and Transmission electron microscopy (TEM). For FESEM, the nanoparticles were drop cast on an aluminium-coated piece of glass coverslip and allowed to dry overnight followed by imaging using FESEM (ZEISS Sigma 300) . For TEM imaging, 10 µl nanoparticle suspension was drop-cast on a carbon coated copper grid, air dried and observed using TEM (JEM 2100 Jeol, Peabody, MA,USA).

2.3.1.7. Macrophage membrane coating around the chitosan nanoparticles: Macrophage membranes were serially extruded through 0.8 µm, 0.4 µm pore size membrane in the extruder (Avanti Polar Lipids). To prepare macrophage membrane-coated chitosan nanoparticles (nanoassembly), chitosan nanoparticles and macrophage membrane vesicles were combined and extruded through 0.2 µm pore sized membrane.

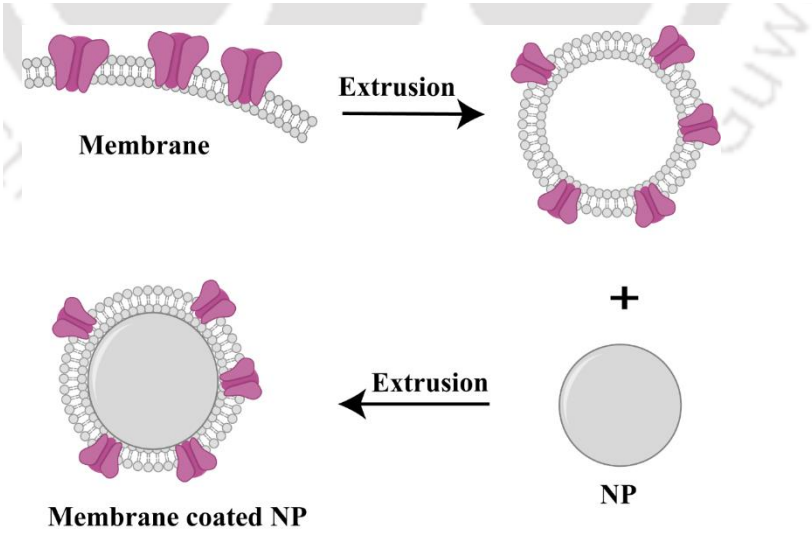

Scheme 2.3: Schematic representation of the extrusion process

2.3.1.8. Confirmation of membrane coating: Membrane coating over the chitosan nanoparticle core was confirmed by TEM imaging, sodium dodecyl sulphate polyacrylamide gel electrophoresis (SDS PAGE) and Western blotting with anti-TNFα antibody. For TEM analysis, 10 µl of as-synthesized nanoparticle were drop-cast on a carbon-coated copper grid, air dried overnight and observed under TEM (JEM 2100 Jeol, Peabody, MA,USA). In order to ensure successful coating of the macrophage membranes over the chitosan nanoparticle, SDS PAGE was carried out. Proteins from uninduced macrophage, LPS induced cell membrane and LPS induced macrophage membrane coated nanoparticles were electrophoresed in 12% SDS PAGE. Silver staining was performed to visualise and compare the proteins in the gel. Furthermore, Western blotting was also performed to validate successful membrane coating over the chitosan nanoparticles. For this, equal amount of proteins from uninduced macrophage, LPS induced cell membrane and induced macrophage membrane coated nanoparticles were electrophoresed in 12% SDS PAGE for separation according to molecular weight. Subsequently, the proteins were transferred from the gel to the polyvinylidene difluoride (PVDF) membrane followed by blocking for 2 h with 4% bovine serum albumin (BSA). The protein containing membrane was then incubated with anti-TNFα primary antibody overnight followed by incubation with horseradish peroxidase tagged secondary antibody. The blots were developed using chemiluminiscent peroxidase substrate (Sigma) and visualised under ChemiDoc transilluminator (Bio-Rad). The hydrodynamic diameter of the membrane coated nanoparticles were recorded by Malvern Zeta Sizer Nano ZS.

2.3.1.9. Biocompatibility study: Biocompatibility of the THP-1 membrane coated nanoparticle was studied before evaluating therapeutic potential of the system on cancer cells. For this, the expression of several interleukins were studied by real time PCR. For this purpose, human monocytes (THP-1 cells) were differentiated into macrophages using PMA (100 ng/ml) for 24 h. Following

differentiation the cells were treated with membrane coated nanoparticles. Bacterial lipopolysaccharide (500 ng/ml) was used as a positive control for the experiment. Following treatment, RNA was isolated using TRI Reagent (Sigma) and cDNA was synthesized using BioRad cDNA synthesis kit. Real time PCR was performed (Rotor, GeneQ, Qiagen, R0115115) using GAPDH as an internal control and the expression of interleukins- IL6 and IL1β was studied with quantitative PCR.

2.3.1.10. Hemocompatibility study: For hemocompatibility testing, 1 ml blood was centrifuged at 1000 RCF for 5 min and the supernatant was discarded. To the pellet, 1 ml phosphate buffer saline (PBS) was added and centrifuged again. Finally, the freshly isolated RBCs were incubated on ice for 3 h with the macrophage membrane coated nanoparticle, 0.1% Triton (Positive Control) and with PBS (negative control). Percentage hemolysis was measured by recording the absorbance at 550 nm, considering 100% hemolysis with the Triton X sample.

2.3.1.11. Stability study of nanoassembly: The stability of the nanoassembly was studied by recording dynamic light scattering (DLS) by Malvern Zeta Sizer Nano ZS over a period of consecutive 7 days.

2.3.1.12. Cytotoxicity studies: In order to study the therapeutic potential of the fabricated module, HeLa, MCF-7 and MDA-MB-231 cells were seeded in 96 well plates and treated with increasing concentration of macrophage membrane coated nanoparticles. After 48 h, cell viability was assessed using colorimetric MTT assay. For this, the treated cells were incubated with 0.5 mg/ml MTT in Dulbecco's Modified Eagle's Medium (DMEM) for 2 h. Subsequently, MTT was removed and 150 µl of organic solvent dimethyl sulfoxide (DMSO) was added followed by 10 min of incubation. Absorbance was recorded using multiplate reader (Tecan, Infinite M200 Pro) at 570 nm and 630 nm as background. Cell viability percentage

was calculated. To understand whether the nanoassembly retained its activity, the membrane coated nanoparticles were stored for 7 days in 4 °C. After 7 days, cytotoxicity assay was performed on HeLa cells. To ascertain specific role of transmembrane TNFα, the nanoassembly was also preincubated for 1 h in rocking condition at room temperature in presence of anti-TNFα antibody. Thereafter, HeLa cells, seeded at a density of 5 X 10^3 cells/well, were treated with only nanoassembly and with antibody treated nanoassembly for a period of 48 h. Subsequently, MTT assay was performed for both of the treatment groups and absorbance was recorded at 570 nm.

2.3.1.13. Calcein AM/ PI dual staining: To qualitatively evaluate the mode of cell death differential staining was performed. HeLa cells were treated with the nanoassembly for 48 h. Following treatment, the media was removed and the cells were gently washed with 100 µl of PBS. Thereafter, Calcein AM/ propidium iodide (PI) solution was added in the final concentrations of 2 µM and 4 µM followed by a 30 min incubation in dark. The cells were then visualized by Confocal microscope (Zeiss LSM 880).

2.3.1.14. Caspase 3/caspase 7 assay: Activation of effector caspases after treatment was studied with Cell Event Caspase-3/7 Green Detection Reagent (Thermo Fisher Scientific). For this, HeLa cells were seeded at a density of 5X10^3 cells/well in a 96 well plate. Following 24 h of treatment, 100 µl of diluted reagent solution (4 µM) was added and incubated for 30 min. Subsequently, the cells were imaged using confocal microscope (Zeiss LSM 880).

2.3.1.15. Generation of 3D tumor spheroids of HeLa cells: To create three-dimensional spheroids, 96 well plates were pre-coated with serum free media containing 1.5 % (w/v) agarose. HeLa cells were seeded at a density of 2 x10^4

cells/well in agarose pre-coated plate with a final media volume of 200 µl. Subsequently, the plates were centrifuged at 1500 g for 10 min to form aggregates and incubated at 37 °C with 5% CO_2 in humidified atmosphere.

2.3.1.16. Assessment of viability of the spheroids: Three days old spheroids were treated with increasing concentrations of the nanoassembly. Following 72 h of treatment, Resazurin disodium salt was added to each well and incubated for 4 h in CO_2 incubator at 37 °C. Thereafter, absorbance at 570 nm was measured using multiplate reader. Live/dead cell imaging of the treated spheroids were carried out with 2 µM of Calcein-AM and 4 µM of PI, respectively. Following 30 min of incubation, the spheroids were washed with PBS and imaged using confocal microscope (Zeiss LSM 880).

2.3.2. Methods related to functional studies of recombinant transmembrane TNFα

2.3.2.1. Cloning of GST-tmTNFα: The pMD18 vector harbouring tmTNFα gene was obtained from Sino Biologicals plasmid repository ID: HG10602-M G07NO11M14. The open reading frame was PCR amplified from the clone obtained using gene specific Forward primer: 5'-C ACCATGAGCACTGAAAGCAT GATCC-3' and a Reverse Primer: 5'-GTTCGTCCTCC TCACAGGGCAATGAT-3′ using Taq polymerase (Bio-rad PCR Master mix). Gene-specific forward and reverse primer having BamHI and XhoI overhangs were introduced to perform TA cloning. Double digestion with - BamHI and XhoI (New England Biolabs (NEB)) released insert of the desired length accomplishing clone confirmation. The gene was further cloned in bacterial expression vector pGEX-4T-2, for which the TA clone containing the gene flanked by restriction sites as well as the bacterial expression vector pGEX 4T-2 (Amersham) was double digested with BamHI and XhoI. The released insert along

with the vector was eluted and ligated using the Quick Ligation Kit (NEB). The ligated product was transformed into *E.coli* DH5α competent cells. Double digestion with the aforementioned restriction enzymes confirmed the recombinant clone.

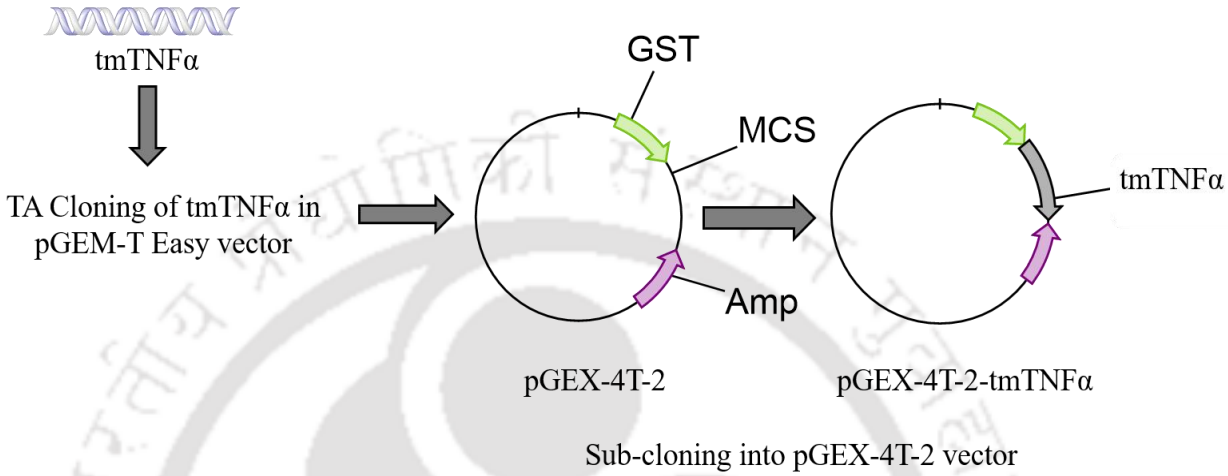

Scheme 2.4: Schematic representation of the cloning process

2.3.2.2. Expression and Purification of GST-tmTNFα: *Escherichia coli* BL21 (DE3) strain (Institute of Microbial Technology, India) was transformed with the recombinant pGEX-4T-2 GST-tmTNFα plasmid construct. This was used as inoculum for small-scale primary culture in 5 ml Luria- Bertani media containing 100 mg/ml ampicillin. Following overnight incubation of primary culture at 37 °C and 180 rpm, 5 µl culture was used as inoculum for secondary culture in 1:100 dilution. This was allowed to reach mid-log phase to optical density (OD) of 0.6 when isopropyl β-D-1-thiogalactopyranoside (IPTG) of varying concentrations ranging from 1 mM to 2 mM was added as an inducing agent. The induced secondary culture was kept at varying temperature ranging from 22 °C to 37 °C to standardize the temperature optima. Induction time was also varied from 6 to 12 h to obtain the best suitable induction time (data not shown). Thereafter, the cells were pelleted down at 7000 rpm under chilled conditions for 5 min. The pellets were lysed in lysis buffer, which composed of 50 mM Tris-HCl (pH-8), 150 mM

NaCl, 0.1% β mercaptoethanol, 1.4 mM PMSF after discarding the supernatant. Sonicated samples were centrifuged at 12000 rpm and were electrophoresed on a 12 % sodium dodecyl sulfate-polyacrylamide gel to optimize favorable condition for the protein expression. Temperature of 22 °C, IPTG concentration of 1 mM, and induction time of 10 h was found to be most suitable for the expression of our protein in the soluble fraction. For all subsequent protein purifications, these induction conditions were maintained. Following induction, pelleted cells were sonicated in probe sonicator followed by centrifugation at 12,000 g for 20 min. After filtering the supernatant with 0.45 μm syringe filter, protein solution was loaded onto the glutathione-agarose affinity column (Sigma) and incubated for 1 h for efficient binding with the glutathione-agarose beads followed by sixteen washes with chilled 50 mM Tris-HCl (pH 8) to remove any nonspecific binding before elution. Elution buffer composed of 15 mM L-reduced glutathione in 50 mM Tris–HCl (pH 8). All steps were performed under chilled conditions and the samples were analyzed on 12 % SDS-PAGE. For the purification of GST protein, 500 ml of secondary culture of pGEX-4T-2 vector containing inherent GST tag was induced with 0.5 mM IPTG for 8 h at 28 °C. Following induction, GST protein was purified using glutathione agarose (Sigma) affinity chromatography after lysing the bacterial pellet by sonication. The protein purification process followed have been illustrated in **Scheme 2.5**.

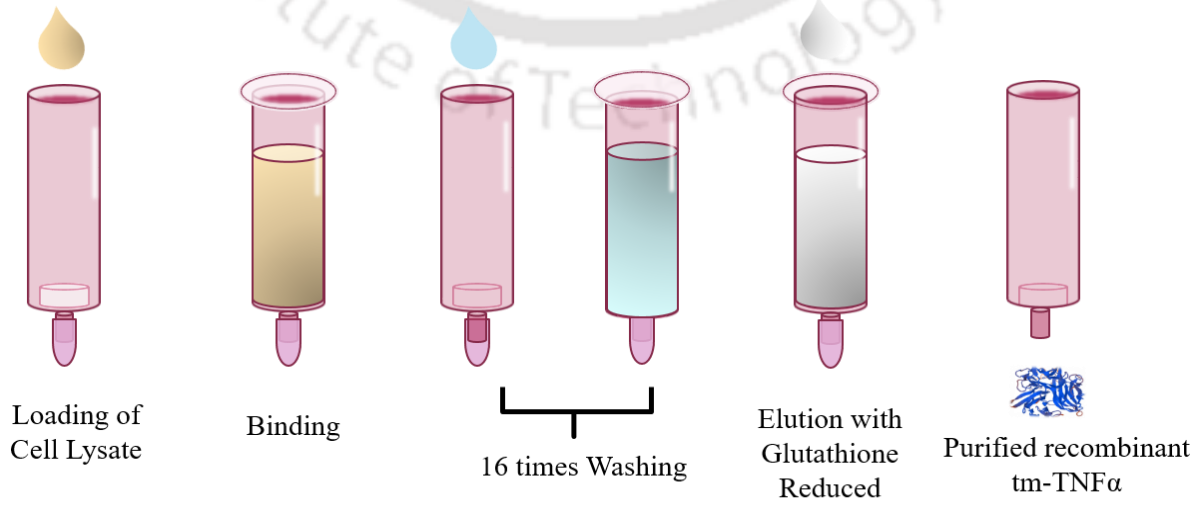

Scheme 2.5: Representation of purification of recombinant tmTNFα by affinity chromatography

2.3.2.3. Characterization:

MALDI analysis: To confirm the identity of the protein MALDI MS-MS analysis was carried out. Protein band was digested *in situ* using Trypsin Profile IGD kit (Sigma) according to manufacturer's protocol. Following digestion, the sample was mixed with matrix α-cyano-4-hydroxycinnamic acid in a 5:3 ratio and spotted on analyzer plate. 4800 Proteomics Analyzer having TOF/TOF Optics (Applied Biosystems) was used to perform the analysis. Automatic mode was used to acquire the data.

Recording of Circular dichroism: JASCO-815 spectrophotometer was used to record the circular dichroism spectrum to evaluate the secondary structure of GST-tmTNFα. For this, concentrated protein sample were dialyzed against 10 mM Tris pH 7.4. For all the measurements, cuvette of path length 1 mm was used. Scanning from 190 nm to 280 nm wavelength was done under constant nitrogen gas purging at a temperature of 25°C for four accumulations. Following the accumulations, background spectrum of only buffer sample was subtracted from the experimental data.

Western Blotting: Western blotting was performed with anti-TNFα antibody (Cell Signaling Technology) to confirm the presence of GST tagged tmTNFα. Sample was loaded on a 12 % SDS gel and electrophoresed at a constant voltage of 120 V, followed by transfer of the samples onto polyvinylidene difluoride (PVDF, Millipore USA) membrane. A constant voltage of 25 V for 3 h was maintained for the protein transfer on membrane. After confirming the transfer with Ponceau S (reversible staining), the membrane was washed with Phosphate Buffer Saline with 0.1% Tween-20 (PBST), followed by blocking with 3 % BSA, 1X with TBS, 0.1% Tween-20 for 2 h. Thereafter, the membrane was incubated with 1:5000 diluted primary antibody in blocking solution at 4 °C with gentle shaking overnight.

Secondary anti-rabbit IgG grown in rabbit was added and incubated for 2 h, after thoroughly washing the membrane with PBST. The blot was developed using chemiluminescent peroxidase substrate and the reaction buffer in 1:2 ratio.

2.3.2.4. Performing PCR to check receptor expression: tmTNFα is reported to bind to both the TNF receptors-TNF RI and TNF RII to initiate signaling cascade. To check the receptor expression, semi-quantitative PCR for both of the receptors keeping β-actin as an internal control, was performed. Around $1x10^5$ cells (HepG2, HeLa, MCF-7, U87MG, A375) were seeded in 96 well cell culture plate. RNA was isolated from the cells after 3 days using RNA Isolation Kit (Sigma). Synthesized RNA was quantified and 1 μg was used to prepare cDNA for all 5 cell lines using Bio-Rad cDNA synthesis kit. As template for the PCR reaction, equal amounts of cDNA were used for each of the cell lines. Following PCR, the results were analyzed with ImageJ software.

2.3.2.5. Labeling of tmTNFα and confocal microscopy: Purified tmTNFα was conjugated with fluorescein isothiocyanate (FITC) by using EDC conjugation protocol. EDC forms an amide bond between COOH and NH_2 groups; thus, amine containing amino acids were calculated. Each tmTNFα has 55 amine side chain containing amino acids. The conjugation reaction was performed at 1:1.5:5 molar concentrations of NH_2: EDC: FITC. tmTNFα in conjugation buffer (MES, 0.1M, pH 5) was mixed with EDC followed by the addition of FITC. Following 6 h incubation with the labeled protein, the cells were washed gently and counterstained with Hoechst for nuclei staining. The localization of the FITC labeled recombinant TNFα was tracked using confocal microscopy.

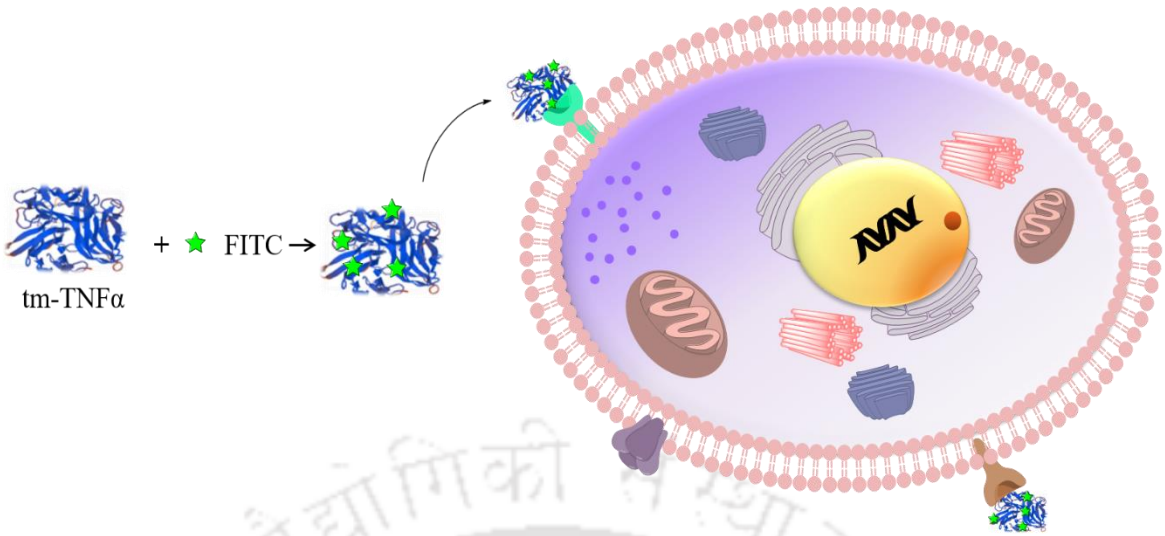

Scheme 2.6: Schematic representation of labeling and binding of tmTNFα

2.3.2.6. Cell viability assays:

MTT assay: Briefly, HepG2, HeLa, MCF-7, A375, HEK cells were seeded in a 96 well plate having a density of $5X10^3$ cells/well in serum media. After attachment, the cells were treated with increasing concentrations of recombinant GST tagged tmTNFα. Cell viability was determined by MTT assay after 48 h. MTT (0.5 mg/mL) in DMEM was added to the cells and incubated for 2 h. Thereafter, MTT was removed and 150 µl of dimethyl sulfoxide (DMSO) was added for the dissolution of formazan crystals. Multiplate reader (Tecan Infinite M200 Pro) was used to measure the absorbance of the dissolved formazan crystals at 570 nm having a reference of 630 nm. Tris-HCl of pH 7.4, 10 mM was also added in triplicates in increasing amounts to rule out any cytotoxic effect of the buffer. As a control experiment, the effect of only GST protein alone in increasing concentrations was also studied on those cell lines for 48 h as a control. Anti-cell proliferative effects of recombinant soluble TNFα (procured from Sigma) was examined on HepG2 and HeLa after 48 h of treatment.

Trypan Blue assay: To quantitatively validate the results of MTT assay, trypan blue dye exclusion assay was carried out. Cells were seeded on a 6 well plate at a density of $2x10^5$ cells/well. After attachment, the cells were treated with IC_{50}

concentration of recombinant GST-tmTNFα for 48 h. Following completion of treatment, cells were harvested by trypsinization and trypan blue dye (10 µl) was added to equal volume of cell suspension. The percentage of live cells was counted by Countess automated cell counter (Invitrogen) by loading the dye mixed cell suspension on counting chamber and imaged.

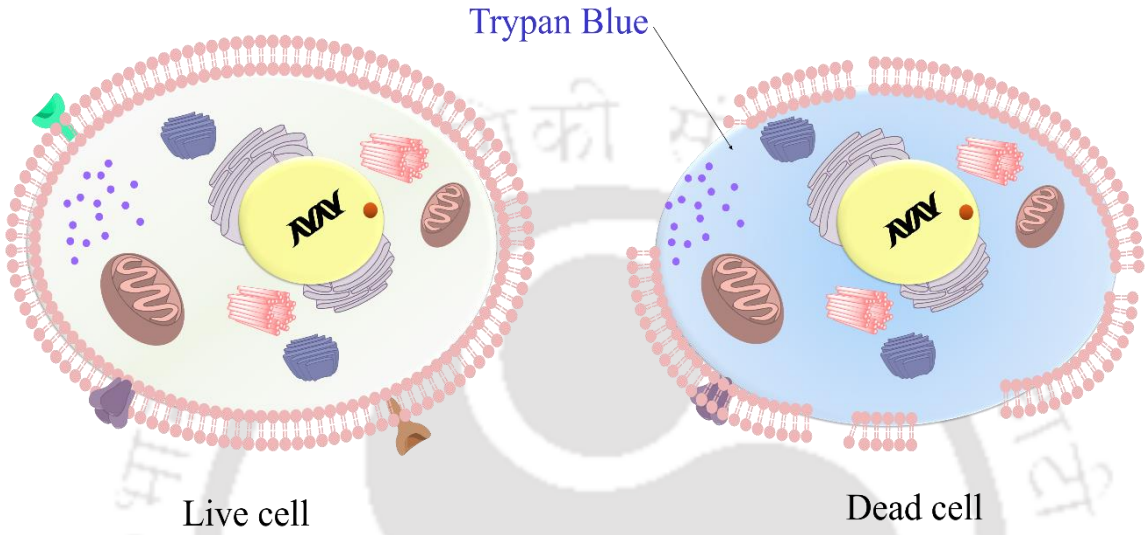

Scheme 2.7: Illustration of the principle of Trypan blue assay for determining cell viability

2.3.2.7. Cell cycle analysis: HepG2 and HeLa cells were seeded in a six well plate at a density of 10^5 cells/well and incubated overnight. After attachment, the cells were synchronized by incubating them with serum free media for 24 h. Following synchronization, the cells were treated with IC_{50} concentrations of the recombinant protein for 48 h. Subsequently, the cells were harvested by trypsinization, fixed with 70% chilled ethanol and incubated overnight at -20 °C. The cells were then centrifuged, washed with chilled PBS and treated with 0.2 mg/mL RNase A at 37 ° C for 1 h. Thereafter, propidium iodide (10 µg/ml) was added, incubated for 20 min at 4 °C and analyzed with FACSCalibur (BD Biosciences).

2.3.2.8. Studies to analyze mode of cell death:

AO/EtBr Dual staining: To qualitatively evaluate the mode of cell death we performed dual staining with Acridine orange/ Ethidium bromide (AO/EtBr). AO is a membrane permeable dye which stains both live and dead cells while EtBr is a DNA intercalating agent which can only penetrate the of membrane-compromised cells and fluoresces red. HepG2 cells were treated with recombinant TNFα for 48 h. Media was removed and the cells were gently washed with 100 µl of PBS. Thereafter, 10 µl of AO/ETBR solution was added in the ratio of 1:1 and incubated for 5 min. The cells were visualized by fluorescence microscope (Nikon Eclipse Ti-U, Tokyo, Japan) under green fluorescent (GFP) filter & tetramethyl rhodamine isothiocyanate (TRITC) filters.

Morphology study by Confocal microscopy: To observe the morphology, cells were treated and fixed with 4% formaldehyde and observed under Confocal Microscope (Zeiss LSM 880).

Nuclear staining: Following treatment, the cells were fixed and stained with 0.2 µg/ml Hoescht-33423 solution. Thereafter, the cells were washed with PBS to remove the residual dye and observed under Confocal Microscope.

Apoptosis assay: FITC tagged Annexin V and PI (BD pharmingen) was used to determine the extent of apoptosis in the treated cells. Subsequent to 48 h treatment, the cells were harvested by trypsinization and stained with equal amounts of Annexin V and PI according to manufacturer's protocol. Finally, the stained cells were analyzed by flow cytometer (CytoFLEX, Beckman Coulter).

2.3.2.9. JC-1 staining: Disruption of mitochondrial membrane potential, a significant feature of apoptosis was probed using JC-1 (tetraethylbenzimidazolylcarbocyanine iodide) staining. After completion of treatment, the cells were washed twice with PBS followed by the addition of JC-1 (10 µM) in DMEM and incubated for 20 min. The cells were immediately visualized under fluorescence microscope (Nikon Eclipse Ti-U, Tokyo, Japan).

2.3.2.10. Caspase 3/caspase 7 assay: Activation of effector caspases after treatment was studied with Cell Event™ Caspase-3/7 Green Detection Reagent (Thermo Fisher Scientific). HepG2 and HeLa cells were seeded at a density of 5 X 10^3 cells/well in a 96 well plate. Following treatment for 12 h, media was removed from the wells and 100 µl of diluted reagent solution (4 µM) was added and incubated for 30 min. Nucleus was counterstained using Hoechst and the cells were imaged using confocal microscope.

2.3.2.11. Semi quantitative PCR to check the expression of apoptotic markers: RNA of treated and untreated samples were isolated using RNA isolation kit (Sigma) and cDNA was synthesized by first strand cDNA synthesis kit (Biorad). Expression of Bcl-2 associated x protein (Bax), B-cell lymphoma (Bcl) 2, B-cell lymphoma extra-large (Bcl-xL) were checked with gene specific primers keeping β- actin as an internal control.

2.3.2.12. Effect of recombinant tmTNFα on growth, viability of HeLa spheroids: Three-dimensional spheroids were generated using facile forced floatation method [94,95]. For surface area measurement, the spheroids were treated with the recombinant protein for 72 h, thereafter confocal microscope was used to capture brightfield images of the spheroids. ImageJ software was used for calculation of area and diameter of the spheroids. After 4 days they were treated with increasing concentrations GST tagged tmTNFα. Following 72 h of treatment, Resazurin disodium salt was added to each well and incubated for 4 h in CO_2 incubator at 37 ° C. Thereafter, absorbance at 570 nm was measured using Tecan multiplate reader. 30 min staining with Calcein-AM (2 µM) and PI (4 µM) was performed for live dead imaging of the spheroids, followed by confocal microscopy (Zeiss LSM 880).

2.3.3. Methods related to immobilization of recombinant transmembrane TNFα on a suitable delivery cargo

2.3.3.1. Synthesis of calcium carbonate microspheres and characterization: Calcium carbonate ($CaCO_3$) microspheres were synthesized by modification of the process described by Wu et al [96]. Briefly, 100 mg of soluble starch (Extra pure soluble starch, Merck) was added under the stirring condition to 10 ml of deionized water. The solution was heated at 80 ° C for an hour. After the complete dissolution of starch, calcium chloride was added and stirred for one hour. To it, an aqueous solution of 10 ml sodium carbonate (0.1 mole/L) was added and kept stirring overnight. Calcium carbonate microparticles were obtained by centrifugation at 5000 rpm for 10 min. The as-synthesized microparticles were thoroughly washed five times with deionized water by repeated centrifugation at 5000 rpm. The microparticles were air dried at 60 °C for 4 h. Zeta potential and hydrodynamic diameter were measured by Malvern Zeta Sizer Nano ZS. The microparticles were characterized by FESEM and energy dispersive X-ray (EDX) Analysis. For this, the microparticles were drop cast on an aluminum-coated piece of glass side and allowed to dry overnight. X-ray diffraction analysis was performed to decipher the composition of molecules in the microparticles in the atomic scale. The obtained peaks were analysed using Match! (Phase identification from Powder Diffraction software). Brunauer Emmett Teller (BET) pore size analysis was carried out to ascertain the pore size and surface area of the microparticles. The thermal decomposition of the synthesized calcium carbonate microparticles was also performed using thermo gravimetric analyser (NETZSCH STA 449F3A-0232-M) . For TGA analysis, 15.851 mg of synthesised calcium carbonate microparticles were heated at 20 °C to 900 °C under constant Argon gas purging with simultaneous recording of the spectra.

2.3.3.2. Purification of the recombinant protein and loading on the microcarrier: tmTNFα was cloned, expressed, and purified using the protocol already described in the previous work [49]. Following purification, the recombinant protein was concentrated using a Corning MINI column concentrator (cut off 20 kDa). The amount of recombinant tmTNFα loaded in the microcarriers was evaluated by incubating both for 4 h, at room temperature followed by centrifugation at 5000 rpm for 10 min. The amount of protein loaded in the microparticle was calculated by probing the amount of free protein present in the supernatant by Bradford assay. Absorbance was recorded with (Tecan Infinite 200 pro) multiwell plate reader at 595 nm. The loading percentage was calculated by subtracting the amount of free protein in the supernatant from the initial amount of protein present.

Zeta potential and hydrodynamic diameter of the microparticles before and after protein loading were measured using Malvern Zeta Sizer Nano ZS.

2.3.3.3. Evaluation of the therapeutic potential of the protein-loaded microcarrier: To study the therapeutic potential of the protein-loaded microcarrier, HeLa cells were seeded in 96 well plates and treated with increasing concentrations of bare calcium carbonate microparticles, and with protein loaded calcium carbonate microparticles. After 48 h, cell viability was assessed using colorimetric MTT Assay by recording the absorbance at 570 nm and 630 nm as a background with multiplate reader (Tecan Infinite M200 Pro).

Section 3

Results and Discussion

3.1. Generation of transmembrane TNFα-expressed macrophage membrane-coated chitosan nanoparticles and evaluation of their anti-cell proliferative activities

ACS Omega 5, 3, 1572–1580, 2020.

Results and Discussion

Abstract: Transmembrane TNFα, a crucial signaling cytokine, holds anti-cell proliferative potential. The successful delivery of this intact transmembrane protein to the target site is quite intriguing. Amidst numerous nanocarriers, a novel class of new generation macrophage membrane coated nanocarriers are endowed with innate tumor homing abilities and inherent capacity of escaping the body's defense machinery. In this perspective, a novel therapeutic module has been fabricated by coating nontoxic, biodegradable chitosan nanoparticle core with engineered macrophage membrane-tethered TNFα. Herein, the expression of membrane-bound TNFα was induced by challenging PMA differentiated THP-1 cells with bacterial lipopolysaccharide. Subsequently, the as-synthesized chitosan nanoparticle core was coated with TNFα expressed macrophage membrane through the extrusion process. While transmission electron microscopy (TEM) imaging, SDS PAGE, and Western blotting results demonstrated successful coating of the chitosan nanoparticles with TNFα induced membrane, cytotoxicity assays on several cancer cells like - HeLa, MDA-MB-231, and MCF-7 unveiled the innate anti-cell proliferative property of the membrane coated nanoparticles. Furthermore, evaluation of the expression of several interleukins following treatment demonstrated the biocompatibility of the membrane-coated nanoparticles. These fabricated nanoparticles also showed dose-dependent cell death in tumor spheroids, which was further corroborated with Calcein AM/ PI dual staining results. Translation of the therapeutic efficacy of the synthesized nanoparticles from monolayer to tumor spheroids augments its potential in cancer therapy.

A three-step procedure was followed for the preparation of transmembrane TNFα expressed macrophage membrane coated chitosan nanoparticles. Initially, THP-1 monocytes were differentiated into macrophages using varying concentrations of PMA. Concentration-dependent conversion of floating monocytes into adherent macrophages was visualized using microscope, as shown in **Figure 3.1.** It was observed that with increasing concentrations of PMA (0-100 μM), the monocytes became larger, granular, and less refractive.

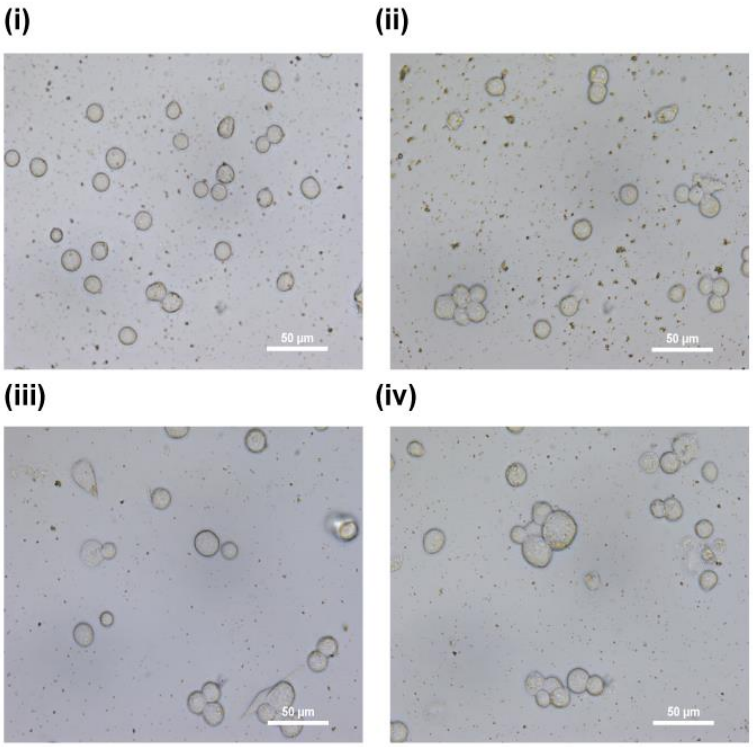

Figure 3.1: Microscopic assessment of monocytes differentiating into macrophages with increasing concentrations of PMA, (i) 0 µM (ii) 40 µM (iii) 80 µM (iv) 100 µM. [Scale bar: 50 µm]

The successful conversion of monocytes into macrophages was further confirmed by flow cytometry-based studies **(Figure 3.2)**, which also depicted an increase in the granularity of the cells with a higher concentration of PMA.

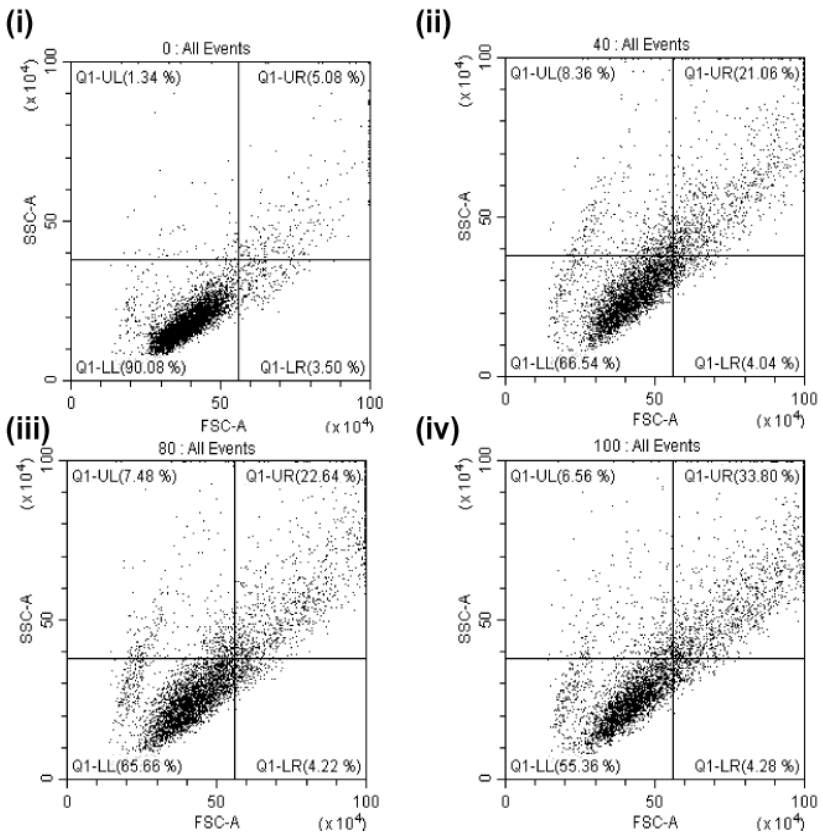

Figure 3.2: Flow cytometry-based assessment of monocytes differentiating into macrophages with increasing concentrations of PMA, (i) 0 μM (ii) 40 μM (iii) 80 μM (iv) 100 μM, respectively.

Synthesis of soluble TNFα by the macrophages is known to be driven by the interaction of LPS with TLR on the macrophage surface as early as 4 h post stimulation [97]. Therefore, to obtain membrane expressed TNFα, the time duration of LPS stimulation was initially optimized. It was found that 2.5 h of LPS stimulation was most suitable for maximum transmembrane-TNFα expression. The amount of LPS required for maximum induction of transmembrane-TNFα was also optimized by using varying concentrations of LPS. Western blot analysis **(Figure 3.3**) with the anti-TNFα antibody on the isolated membrane showed a gradual rise in the transmembrane-TNFα concentration up to 100 ng/ml.

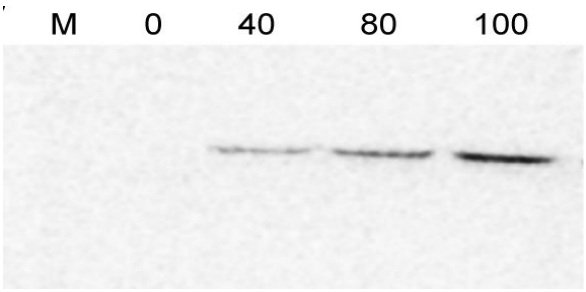

Figure 3.3: Western blot of the macrophage membrane induced with increasing concentrations (ng/ml) of LPS.

Therefore, in order to induce the expression of transmembrane-TNFα in THP-1 monocytes, the above stated concentrations of PMA and LPS were used for the subsequent experiments. The expression of TNFα by the differentiated macrophages upon LPS stimulation was also confirmed by semiquantitative PCR using TNFα specific primers. The gel image (**Figure 3.4**) revealed a distinct band corresponding to transmembrane-TNFα around 750 bp in 100 ng/ml LPS treated macrophages, while there was no amplification in the untreated ones.

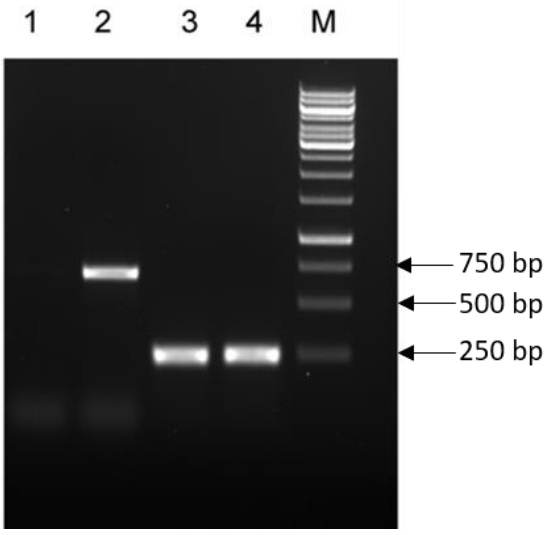

Figure 3.4: Semi-quantitative PCR using TNFα specific primers- Lane 1: Untreated, Lane 2: 100 ng/ml LPS treated. Lane 3 and Lane 4: β actin controls for the samples. M: 1 kb GeneRuler DNA Ladder (Thermo Scientific)

The LPS induced macrophage membranes were isolated by hypotonic lysis buffer, and the homogenized suspension was centrifuged to remove cell debris.

Subsequently, the lysate was centrifuged to obtain the plasma membrane fractions of the macrophages. Following successful isolation of the TNFα expressed macrophage membrane fraction, its therapeutic potential was studied. HeLa, MCF-7, and MDA-MB-231 cells were treated with varying concentrations (protein) of the membrane fractions for 48 h, following which cell viability was assessed using MTT assay. Cell viability percentage was calculated, and as shown in **Figure 3.5, t**he results demonstrated a dose-dependent decrease in proliferation of the cells treated with membrane fractions expressing transmembrane-TNFα. It is noteworthy to mention that there was no substantial decrease in cell viability for the uninduced membrane treated control group (**Figure 3.6**). Therefore, the inherent anti-cell proliferative potential of the transmembrane TNFα expressed membrane fraction was validated, which paved the way for the subsequent experiments.

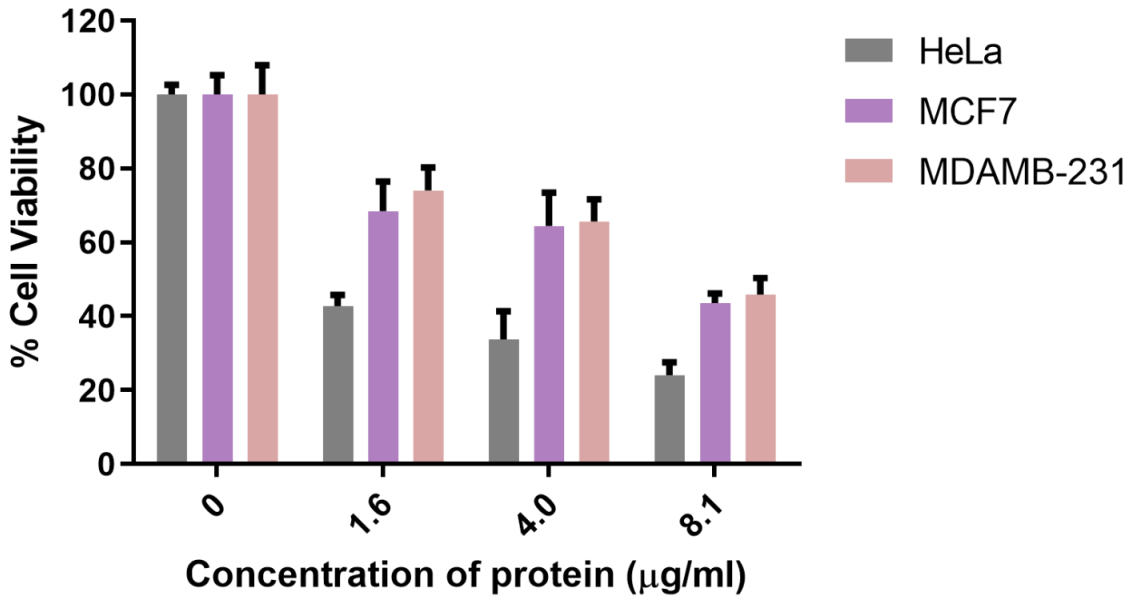

Figure 3.5: Cytotoxicity assay of induced membrane fractions on HeLa, MCF-7 and MDA-MB-231 cells demonstrating a dose dependent decrease in cell viability.

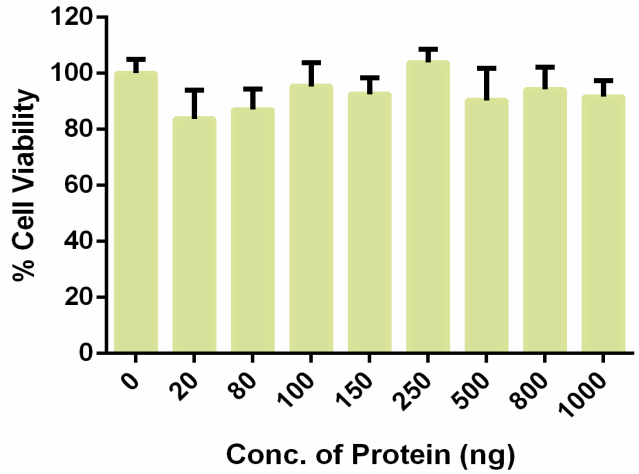

Figure 3.6: Cytotoxicity assay of uninduced membrane fractions on HeLa cells illustrating no noticeable decrease in cell viability.

Hence, capitalizing on the inherent anti-proliferative potential of the macrophage membrane, we proceeded to fabricate this engineered membrane into a stable nanocarrier having innate therapeutic potential. In this regard, the design of a steady framework for the therapeutic membrane was imperative. Therefore, polymeric chitosan nanoparticle core was synthesized using a well-established ionic gelation method. The chitosan nanoparticles had a slight negative charge (-0.7 mV) as determined by Zeta potential analysis **Figure 3.7 A**. The hydrodynamic diameter of the nanoparticles was recorded as 237.5 nm **Figure 3.7 B**.

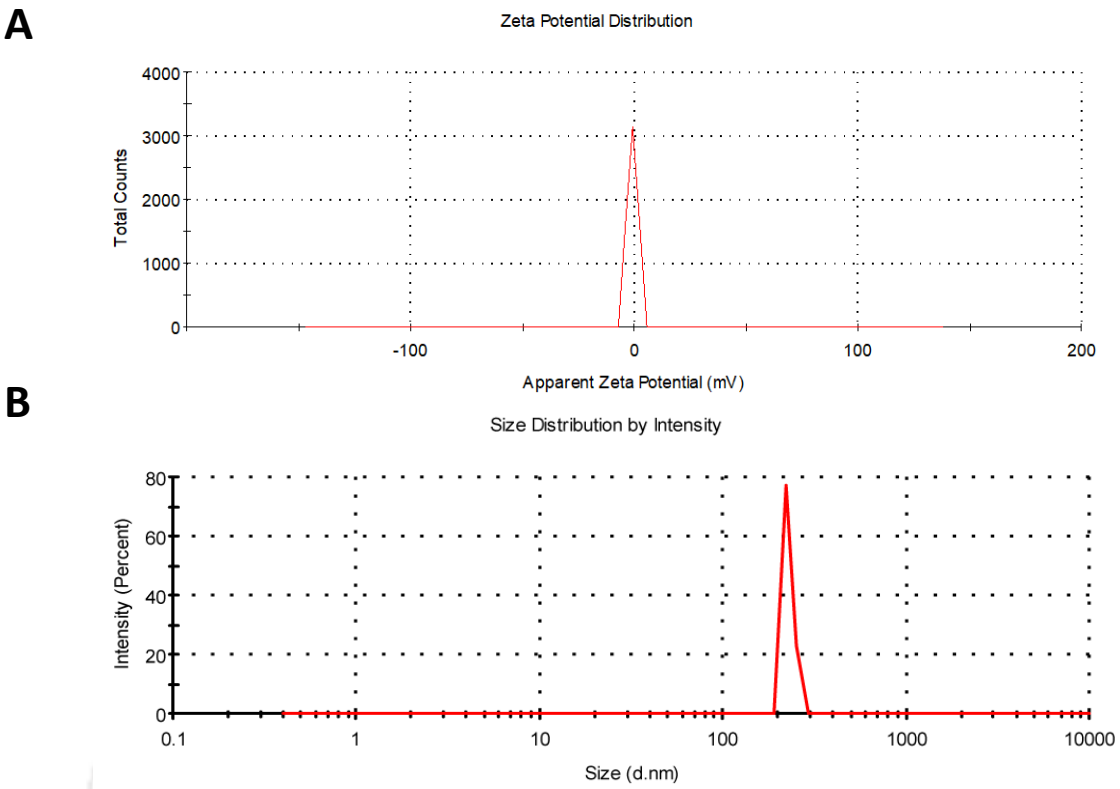

Figure 3.7: Characterization of the chitosan nanoparticles (A) Zeta potential distribution of chitosan nanoparticles having average Zeta potential of -0.7 mV. (B) Hydrodynamic diameter of the chitosan nanoparticles as evident from DLS measurement.

Further, the synthesized chitosan nanoparticles were characterized by FESEM and TEM, which established the successful synthesis of uniform spherical chitosan nanoparticles having roughly 200 nm diameter as evident from **Figure 3.8**.

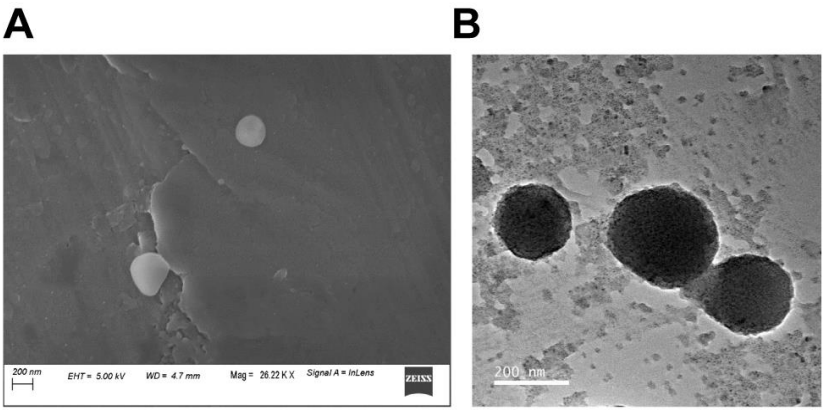

Figure 3.8: (A) FESEM image of the synthesised chitosan nanoparticles (B) TEM analysis of the nanoparticles.

Upon successful synthesis of the chitosan nanoparticles, cytotoxicity of the bare nanoparticles on several cancer cell lines was evaluated. Results of the MTT assay revealed no apparent cytotoxicity of chitosan nanoparticle alone (**Figure 3.9).** Therefore, the chitosan nanoparticles were coated with the engineered TNFα expressing therapeutic macrophage membrane.

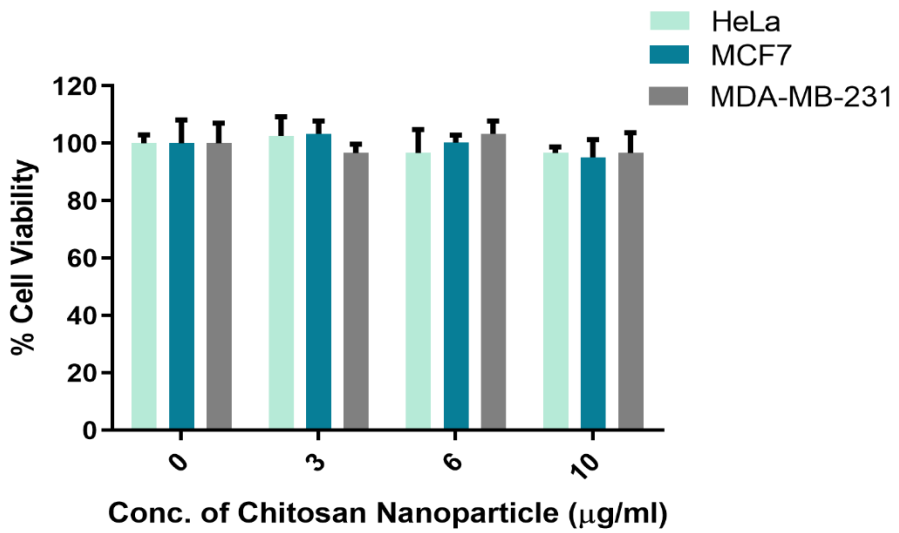

Figure 3.9: Cell viability study with chitosan nanoparticle alone.

For this, a process of serial extrusion of the membranes through 0.8 μm, 0.4 μm pore sized membrane was followed by combined extrusion of both the membrane and the nanoparticles with 0.2 μm pore size membrane. Successful membrane coating over the chitosan nanoparticles was investigated by TEM imaging, sodium dodecyl sulfate polyacrylamide gel electrophoresis (SDS PAGE) and by Western blotting using an anti-TNFα antibody. As evident from the TEM image (**Figure 3.10 B**), distinct halos around the inner chitosan nanoparticle cores denoted successful membrane coating around the chitosan nanoparticles. Furthermore, SDS PAGE (**Figure 3.10 C**) was also performed, where similar protein profiles of the induced macrophage membrane and the membrane coated nanoparticles were

observed, which reconfirmed efficacious membrane coating over the chitosan nanoparticles. Hereafter, for subsequent studies, the transmembrane TNFα expressed membrane coated nanoparticle was termed as "nanoassembly". Western blotting of nanoassembly with anti-TNFα antibody was further carried out, which revealed (**Figure 3.10 D)** distinct band (lane 3) corresponding to TNFα in the nanoassembly. Upon successful coating of the membrane over the chitosan nanoparticle, an increase in size of the nanoassembly as compared to the bare chitosan nanoparticles, owing to the membrane, was also evident from the dynamic light scattering (DLS) data as shown in **Figure 3.10 E.**

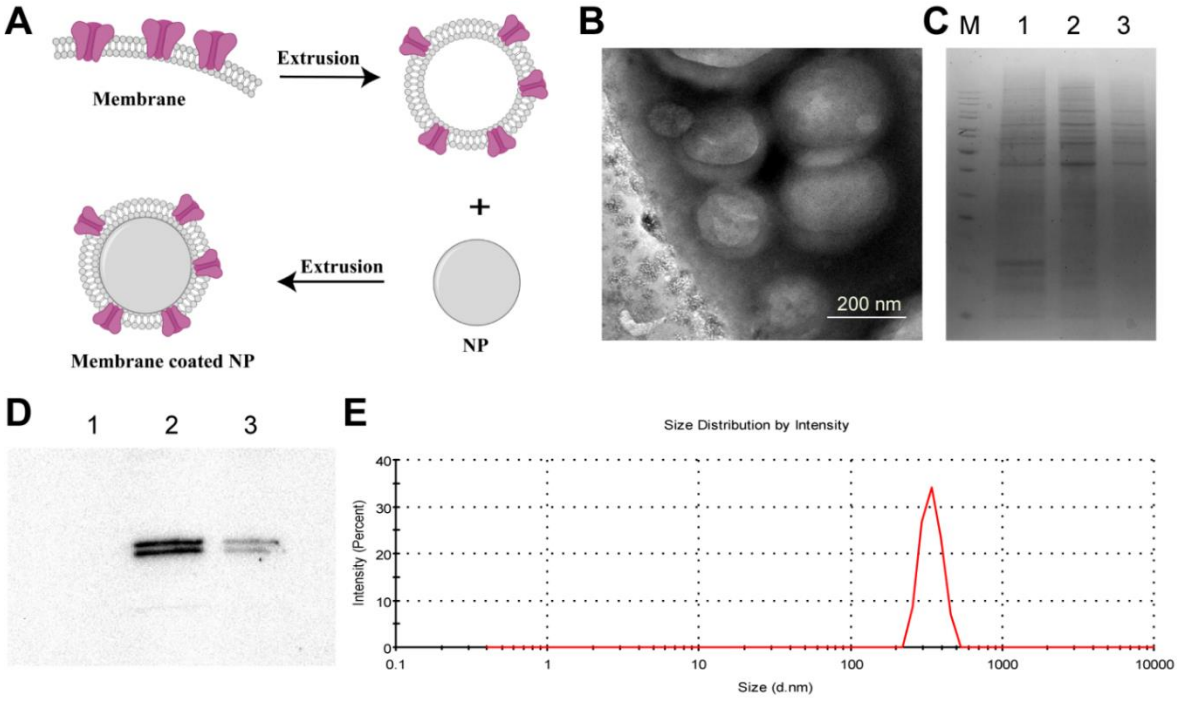

Figure 3.10: (A) Schematic: Extrusion process. (B) TEM image demonstrating successful membrane coating over chitosan nanoparticle (C) SDS PAGE image confirming successful membrane coating. Lane 1: Uninduced cell lysate, Lane 2: LPS induced cell membrane, Lane 3: Induced macrophage membrane coated nanoparticles. Lane M: Thermo Fisher Scientific PAGE Ruler unstained, Size (10-200 kDa) (D) Western Blotting of the membrane coated chitosan nanoparticles with anti-TNFα antibody. Lane 1: Uninduced cell lysate, Lane 2: LPS induced cell membrane, Lane 3: Induced macrophage membrane coated nanoparticles. (E) DLS of the nanoassembly.

Before evaluating the therapeutic potential of the system on cancer cells, it was crucial to ensure the safety of the designed nanoassembly for further biological application. Hence, the biocompatibility of the THP-1 membrane was examined. For biocompatibility evaluation, the expression of several interleukins was assessed that play a role in inflammation and the generation of an immunogenic response. [98]. Since macrophages are the key mediators of immunity, human monocytes (THP-1 cells) were differentiated into macrophages, and the cells were treated with the nanoassembly. Subsequently, the expression of several interleukins- IL6 and IL1β was investigated with quantitative PCR keeping LPS treated macrophages as a positive control. The fold changes in expression of the genes were calculated, and as evident from **Figure 3.11 A**, the membrane-coated nanoparticles did not elicit any immune response since the expression of IL6 and IL1β was quite low in comparison to LPS (0.5 μg/ml) treated positive control samples. Simultaneously, the hemocompatibility of the designed nanoassembly was evaluated by incubating them with intact human RBCs for 3 h on ice [98]. The samples treated with 1% Triton-X 100 was considered to have undergone 100% hemolysis, while PBS treated RBCs were kept as a negative control. From the **Figure 3.11 B**, it was evident that the designed nanoassembly did not induce any hemolysis, whereas a visible hemolysis was observed in the Triton X -100 treated positive control. In order to accomplish appropriate biomedical potential, stability is crucial for any nanocarrier. Hence, the stability of the nanoassembly was assessed over a period of 7 days by recording DLS measurements. It is noteworthy to mention that, there was negligible difference in size of the nanoassembly over a period of 7 days **(Figure 3.11 C)**, which offers an additional advantage to the designed therapeutic module.

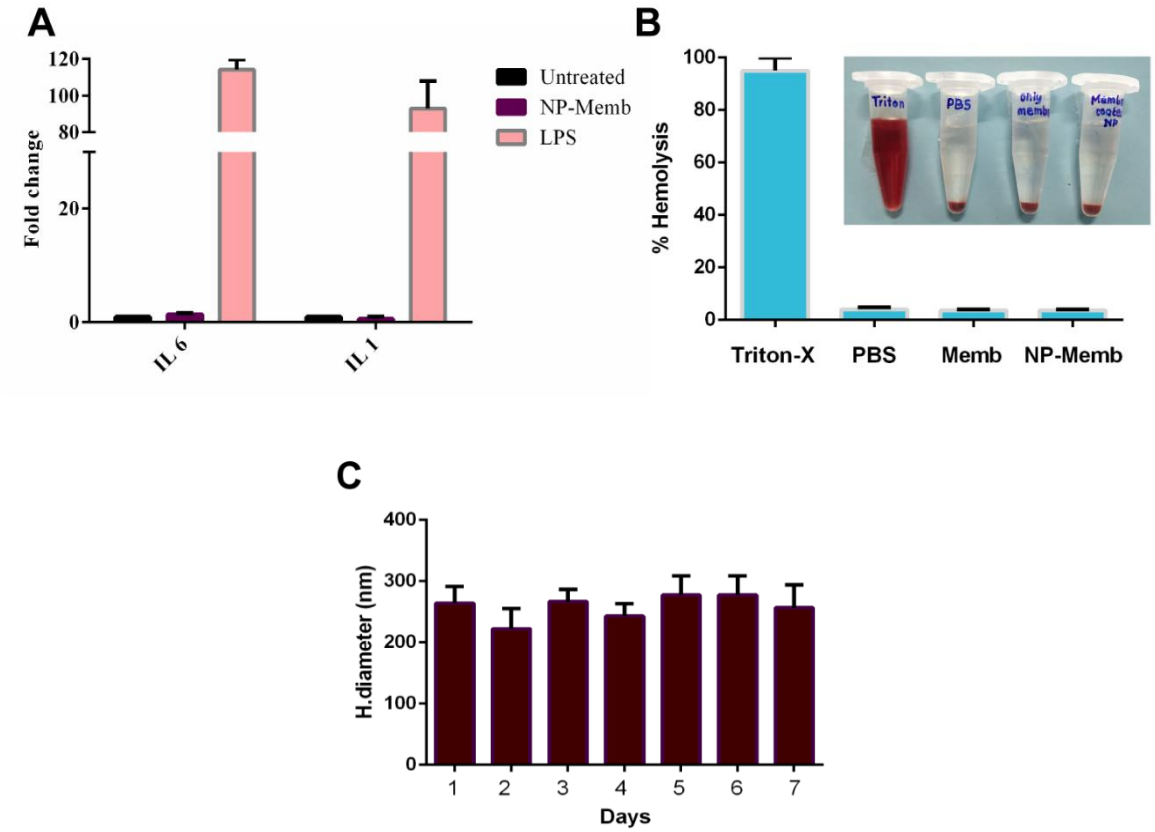

Figure 3.11: (A) Assessment of biocompatibility after treatment with the nanoassembly. (B) Assessment of hemocompatibility (C) Evaluation of hydrodynamic diameters of the nanoassembly by DLS for consecutive 7 days.

Upon completion of evaluation of safety and stability of the nanoassembly, the functional integrity of the fabricated therapeutic module was assessed. Hence, MTT cell survival assay was performed on several cell lines, viz- HeLa, MCF-7 and MDA-MB-231 to evaluate the therapeutic potential of nanoassembly. For this, cells were incubated with increasing concentrations of the nanoassembly and MTT assay was performed after 48 h of treatment. The MTT assay results (**Figure 3.12**) depicted a dose dependent decrease in cell viability with increase in concentration of the nanoassembly, implying that the TNFα expressing membrane retained its functionality even after serial extrusion. It should be mentioned here that there was negligible cell death in the samples treated with chitosan nanoparticles alone, essentially indicating the superior biocompatibility of chitosan and thereby re-

establishing the innate therapeutic potential of TNFα expressed membrane coating over the chitosan nanoparticle core.

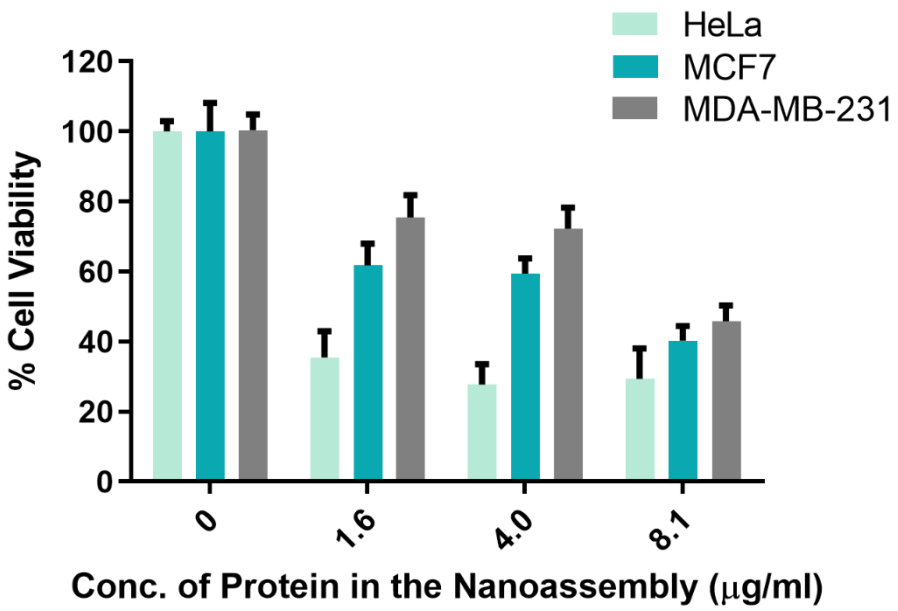

Figure 3.12: Assessment of cell viability upon treatment with increasing concentrations of nanoassembly.

It was observed that the amount of nanoassembly required to bring about IC_{50} in the HeLa cells (IC_{50}:1.317 μg/ml) was much lower than MDA-MB-231 (IC_{50}:7.525 μg/ml) and MCF-7 (IC_{50}:5.9 μg/ml) cells. This can be attributed to the differential expression of TNFα receptors on the surface of these cell lines.

In order to affirm that the anti-proliferative activity of the nanoassembly was ascribed by the transmembrane TNFα component, and not by other proteins present in the membrane after PMA induction, the nanoassembly was pre-incubated for 1 h in the presence of anti-TNFα antibody. It was observed that the anti-cell proliferative effect of tmTNFα was reduced when the nanoassembly was pre-incubated for 1 h in presence of anti-TNFα antibody (**Figure 3.13)**, thus confirming the specific role of transmembrane TNFα in reducing the cell viability.

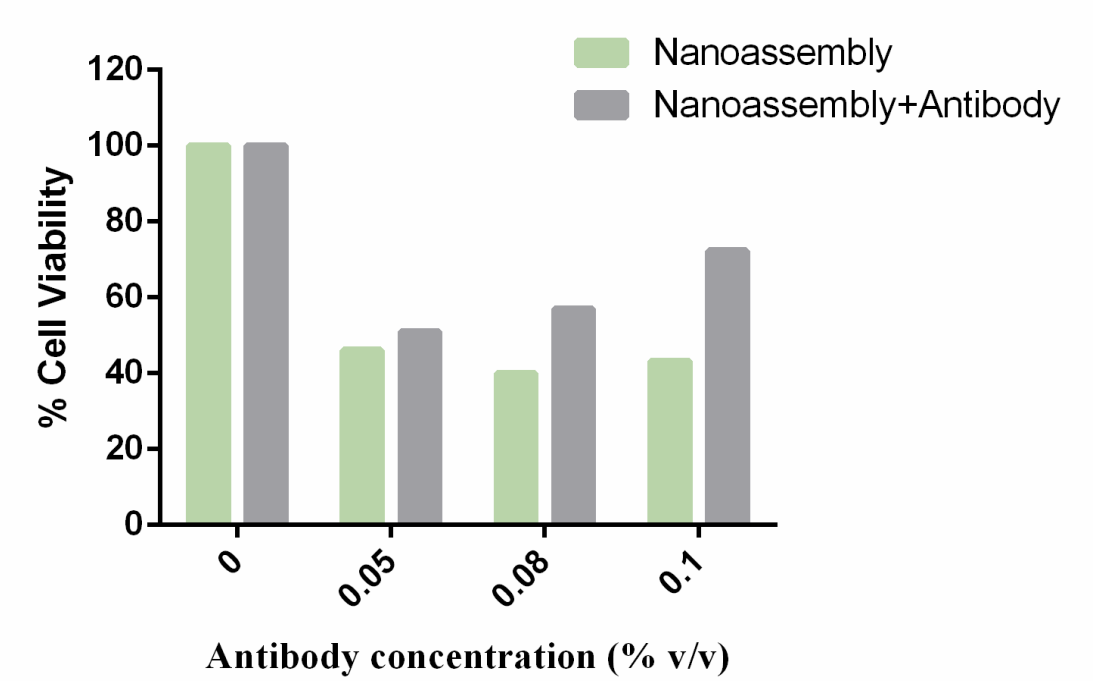

Figure 3.13: Anti-TNFα antibody blocking experiment to decipher the role of transmembrane TNFα in nanoassembly demonstrating the specific contribution of transmembrane TNFα in reducing cell viability. The data represented here are the average of three experiments.

Retention of the activity was assessed by measuring the anti-cell proliferative potential of the nanoassembly on HeLa cells following 7 days of storage. MTT based cytotoxicity assay was performed, which demonstrated a dose-dependent decrease in cell viability (**Figure 3.14**), essentially indicating that the nanoassembly retained activity even after storage for 7 days. Although it should be mentioned here that there was around a two-fold reduction in efficiency after storage as compared to the freshly prepared nanoassembly.

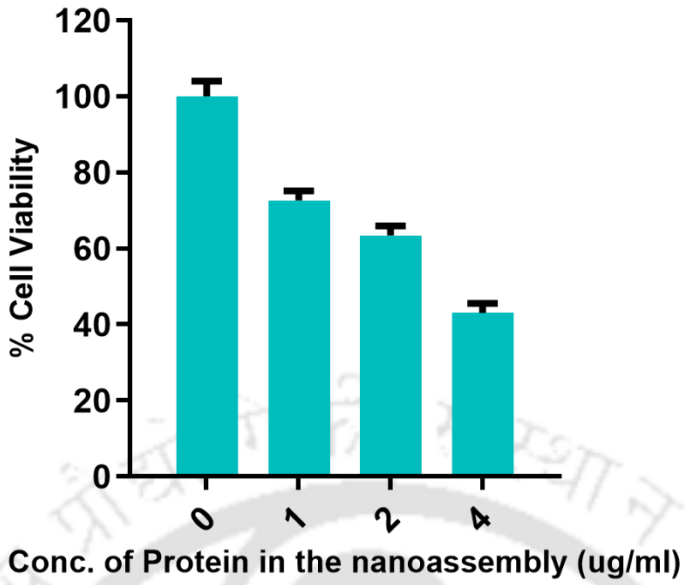

Figure 3.14: Cell viability study with the nanoassembly on HeLa cells after 7 days of storage at 4 °C.

Cell death occurs by two mechanisms - either apoptosis or necrosis. While necrosis is a sudden unprogrammed event, apoptosis is fundamentally a plan of programmed cell death involving a series of regulated events [99]. Therefore, the mode of cell death induced by the designed nanoassembly was investigated by dual staining of treated HeLa cells with Calcein AM and PI. Calcein AM is a vital dye, which is converted to a membrane-impermeable fluorescent analogue by the cellular esterases. Hence, Calcein AM only stains live cells, and the fluorescence leaks out in case of membrane compromised cells [100]. Whereas, PI is a DNA intercalating agent, which is selectively permeable to the membrane compromised cells. Exploiting the differential behavior of the two dyes, both treated and untreated HeLa cells were stained for 30 min and visualized under a confocal microscope. Confocal microscopy images (**Figure 3.15)** illustrated the presence of bright green or yellowish bodies, which essentially denoted the cells that were undergoing early apoptosis; whereas, cells with red nuclei were indicative of late

apoptotic cells. The abundance of apoptotic cells was observed in the cells treated with IC_{50} concentration of the nanoassembly.

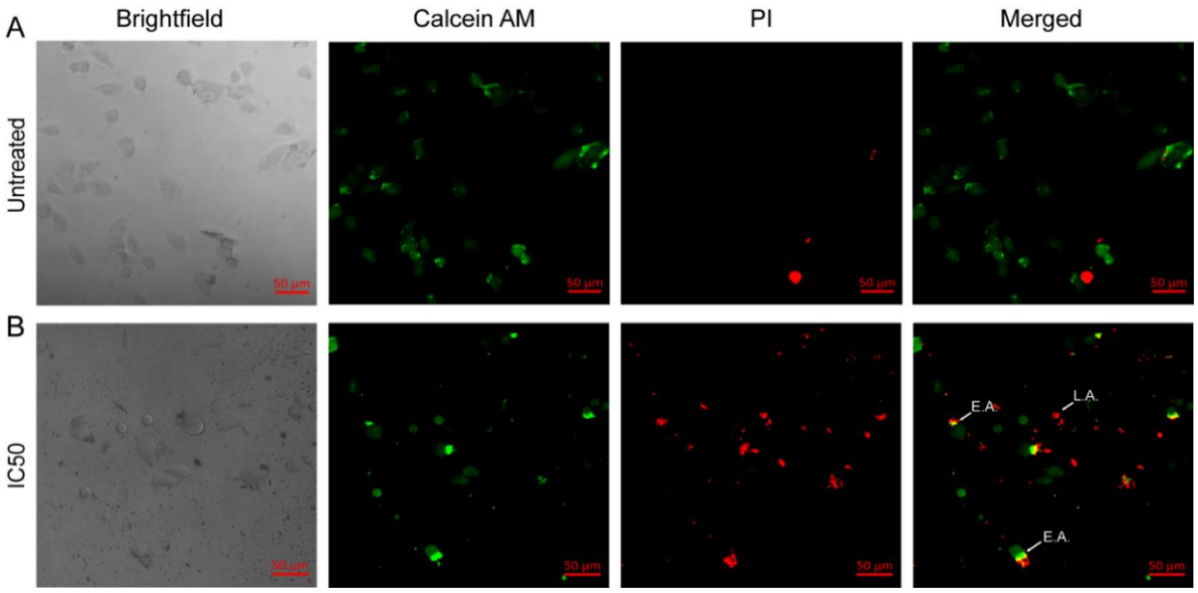

Figure 3.15: Assessment of the mode of cell death using Calcein AM and PI dual staining of HeLa cells. (A) Untreated (B) treated with nanoassembly. E.A and L.A. indicate early apoptotic and late apoptotic cells, respectively.

During apoptosis, initiator caspase cleave and activate downstream executioner caspases, which in turn cleave subsequent proteins [101]. Thus, activation of executioner caspases is considered as a signature of apoptotic cells. So, the expression of executioner caspases - caspase 3 and 7 were studied using an executioner caspase detection kit. For this, the cells were treated with the nanoassembly for 12 h and incubated with the florigenic substrate for 30 min followed by visualization under confocal microscope. The confocal microscopic images (**Figure 3.16**) displayed appearance of intense bright green fluorescence in the treated cells indicative of the executioner caspases activation.

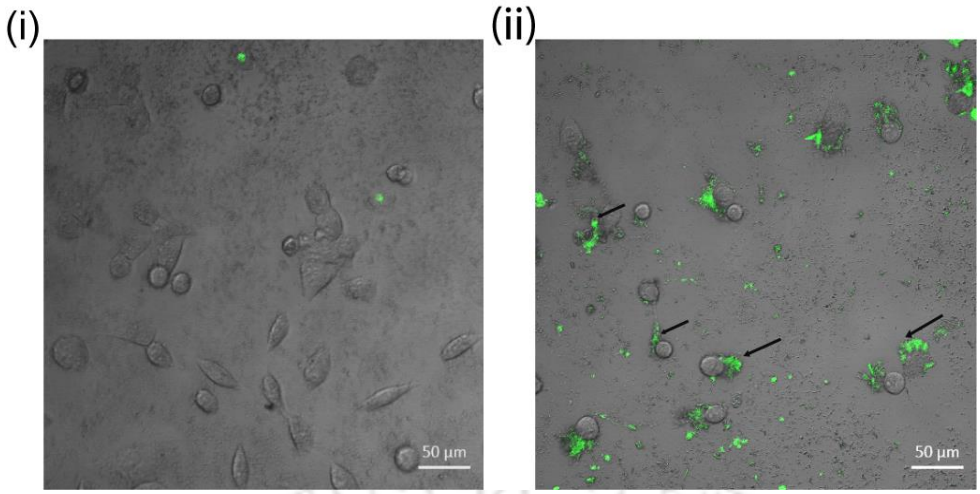

Figure 3.16: Assessment of activation of executioner caspases 3/7 in HeLa cells after treatment with nanoassembly, demonstrating activated executioner caspases. (i) Untreated cells, (ii) treated cells illustrating the activation of executioner caspases (green) denoted with arrows.

The therapeutic efficacy of the engineered system was validated on 3D tumor spheroids. For this, tumor spheroids of HeLa cells were generated by the facile forced floatation method, as discussed in the materials and methods section [94]. The spheroid growth was monitored after every 24 h, and 3-day old compact spheroids were used for experimental purposes. For quantitative evaluation of the therapeutic effect of the fabricated nanoassembly on the spheroids, the spheroids were treated with increasing concentrations of the nanoassembly. The results **Figure 3.17** demonstrated a dose-dependent decrease in cell viability of the spheroids with an increase in the concentration of the nanoassembly. However, the amount of the nanoassembly required for attainment of IC_{50} in HeLa spheroids was higher than IC_{50} of the corresponding monolayer culture.

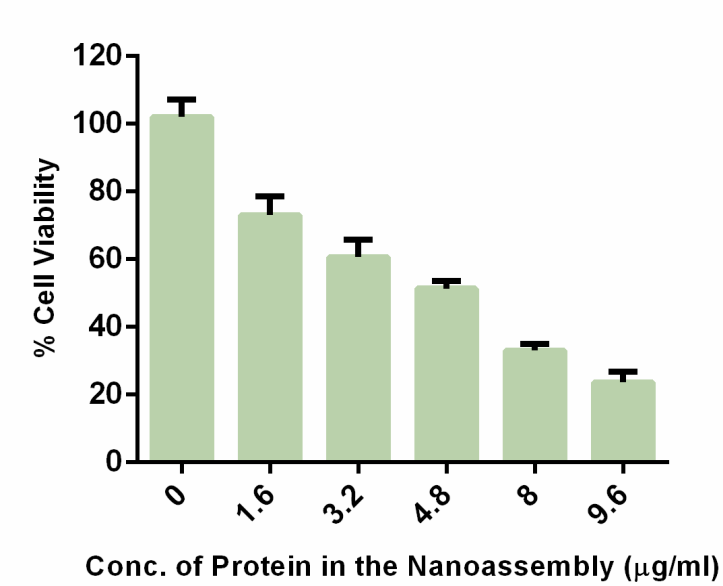

Figure 3.17: Cell viability study with the nanoassembly on HeLa spheroids demonstrating a dose-dependent decrease in cell viability.

For visual evaluation of live and dead cells, the spheroids treated with IC_{50} (7.1 μg/ml) and IC_{75} (10 μg/ml) concentrations of the nanoassembly were further subjected to Calcein AM/PI dual staining procedure. The dual stained spheroids **(Figure 3.18)** imaged using a Confocal microscope (Zeiss LSM 880), illustrated an increase in dead (PI stained) cells after treatment as compared to the untreated spheroids. Dual staining results on treated spheroids visually corroborated the findings of the cell viability assay by Alamar blue.

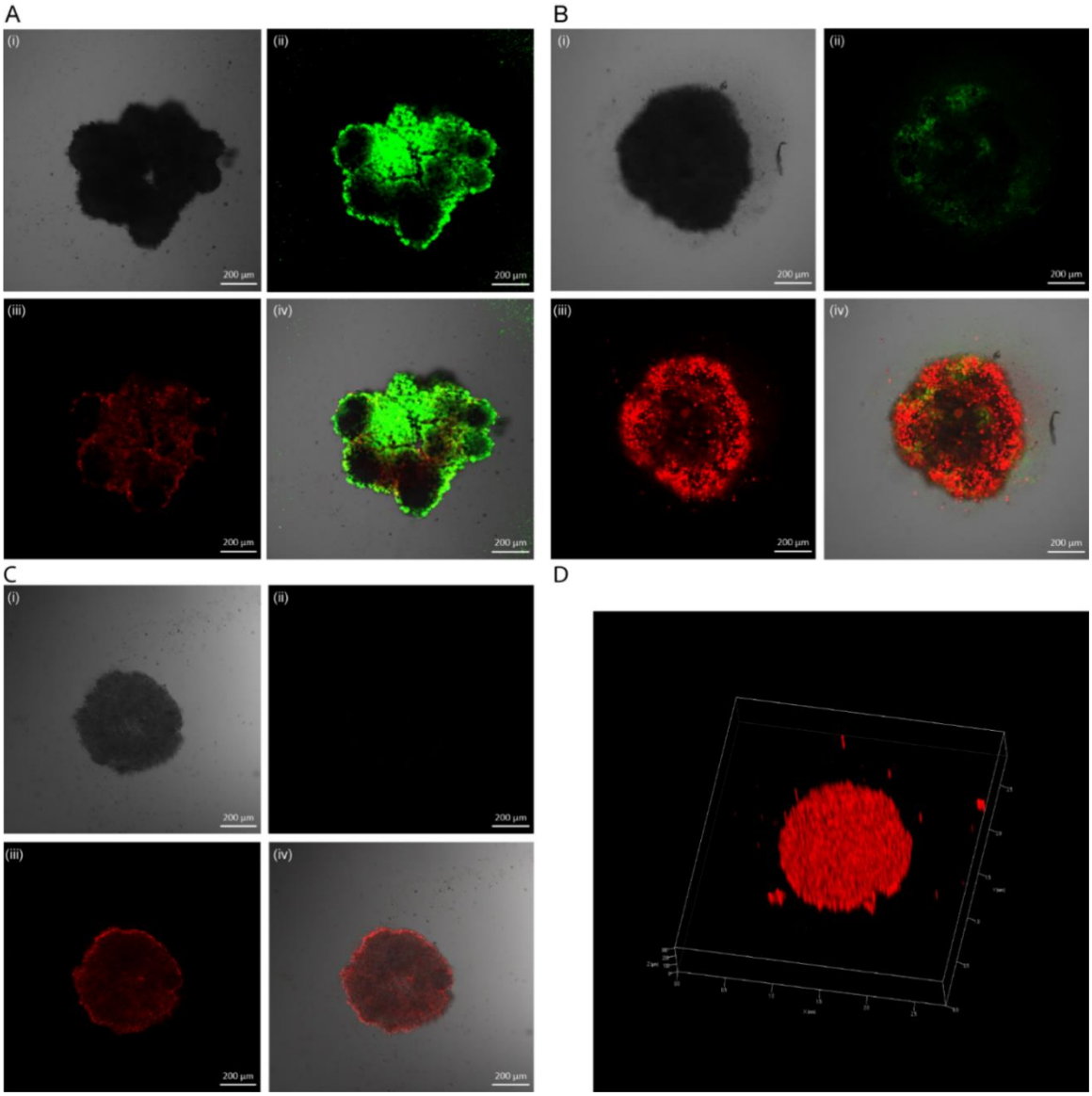

Figure 3.18: Calcein AM/EtBr dual staining study. In A, (i) phase contrast, (ii) Calcein AM stained (iii) PI stained and (iv) merged images of untreated HeLa spheroids, In B, (i) phase contrast, (ii) Calcein AM stained (iii) PI stained and (iv) merged images HeLa spheroids incubated with IC_{50} concentration of nanoassembly, C, (i) phase contrast, (ii) Calcein AM stained (iii) PI stained and (iv) merged images of HeLa spheroid incubated with IC_{75} concentration of nanoassembly, D represents Z-stack projection of HeLa spheroid incubated with IC_{75} concentration of the nanoassembly [Scale bar: 200 µm].

The outcome of the membrane coated nanoparticle work has been illustrated in the scheme below :

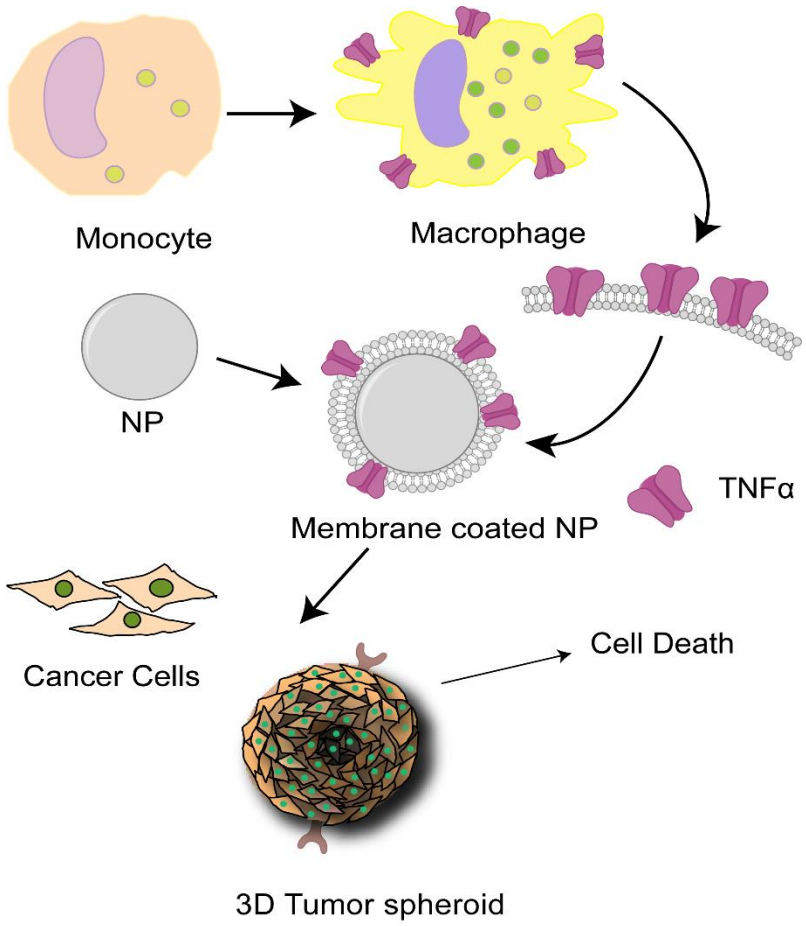

Scheme 3.1: Schematic representation of the design of a therapeutic membrane coated nanocarrier and its effect on 2D monolayer cells and 3D spheroids.

3.2 Generation of recombinant tmTNFα and evaluation of its functional effects

Molecular Biology Reports, 47, 3949–3961, 2020.

Results and Discussion

Abstract: Soluble TNFα, a member of the TNF superfamily, attributes dual roles in apoptosis and cell proliferation, whereas its precursor *transmembrane* TNFα (tmTNFα), has the potential for tumor reduction without initiating proliferation. In this perspective, we recombinantly expressed functional tmTNFα and explored its potential in cell growth inhibition. While structural characterizations of purified tmTNFα revealed the integrity of the protein, cell viability assays demonstrated a remarkable antiproliferative effect on HepG2 (IC_{50}: 36nM) and HeLa (IC_{50}: 23nM) cells. Insights into the mechanism of cell death unveiled G1 arrest in HepG2 and G2/M arrest in HeLa cells along with the disruption of mitochondrial membrane potential and executioner caspase activation. Flow cytometry-based assays provided confirmatory evidence of apoptosis following treatment with recombinant tmTNFα. Furthermore, the effect of the recombinant protein on 3D tumor spheroids was explored, which rendered a reduction in tumor size due to cell death, as evident from confocal microscopy studies. Effectiveness of the tmTNFα in 2D monolayer as well as in complex 3D spheroids demonstrate the therapeutic significance of the protein, featuring recombinant tmTNFα as an attractive option for cancer therapeutics in days to come.

A 702 bp full-length tmTNFα coding region (source: Sino Biologicals) was PCR amplified (**Figure 3.19 A)** with the gene-specific primers and initially cloned into pGEM-T easy vector. As evident from **Figure 3. 19 B**, the release of the TNFα gene (702 bp) upon digestion with EcoRI confirmed successful cloning in the TA vector. Subsequently, the gene was further amplified with a second set of gene-specific primers with restriction enzyme overhangs (BamHI and XhoI) and cloned into the pGEX-4T-2 bacterial expression vector at downstream of N-terminal GST. The GST tag is crucial for affinity-based purification as well as in assisting proper protein folding [102]. The recombinant clone was confirmed by restriction digestion with both BamHI and XhoI, where the release of the full-length 702 bp tmTNFα fragment was observed upon gel electrophoresis **(Figure 3. 19 C).**

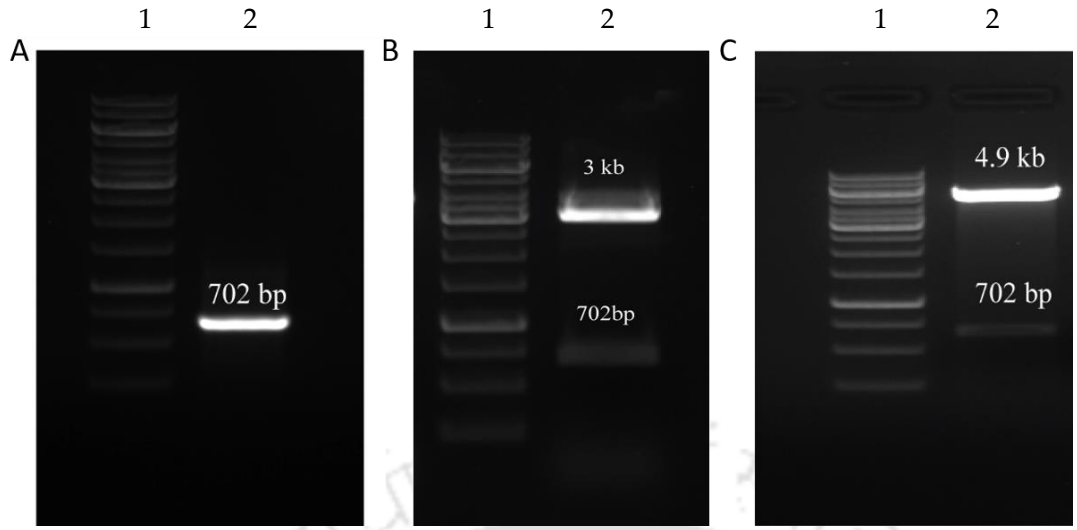

Figure 3.19: (A) Lane 1 displays 1 kb marker, Lane 2 displays PCR amplification of 702 bp tmTNFα gene, (B) Lane 1 is 1 kb ladder, Lane 2 shows digestion of pGEMT-tmTNFα by EcoRI (C) Lane 1 displays 1 kb marker, Lane 2 shows restriction digestion of pGEX-4-T2-tmTNFα with BamH and XhoI.

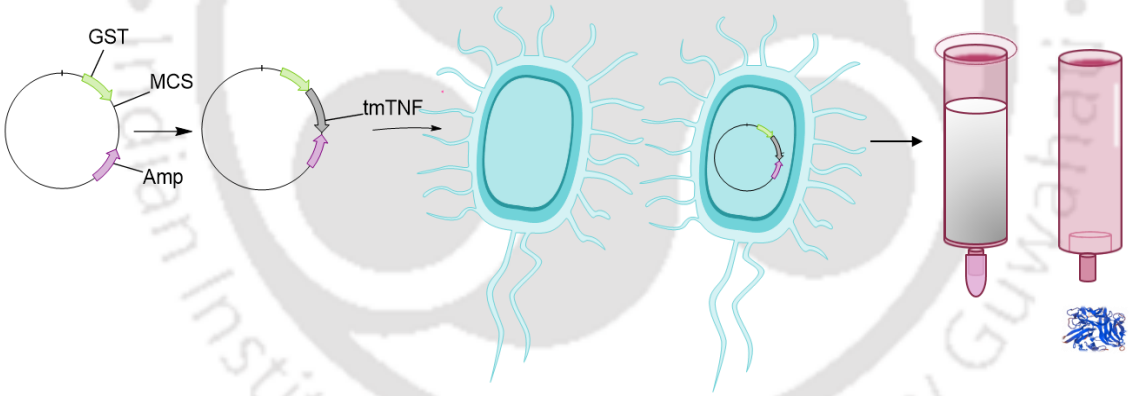

Scheme 3.2: Schematic illustration of cloning, transformation, and purification of recombinant tmTNFα using affinity chromatography.

The recombinant plasmid clone was transformed into *E. coli* BL21 (DE3) strain, a known nonpathogenic host without proteolytic activities [103]. Maximum induction of tmTNFα was obtained with 1 mM IPTG for 10 h at 28 °C (**Figure 3.20 A)**. However majority of the protein was found in the insoluble fraction, so the induction temperature was reduced to 22 °C, and the culture volume was scaled-up to 2 L to obtain a considerable amount of recombinant protein in soluble

fraction [104]. The use of detergent or chaotropic agents was avoided in this process of purification, to retain the functionality. Using the aforementioned induction parameters, the GST-tmTNFα protein was expressed and purified by glutathione agarose affinity chromatography at ice-chilled conditions. A single band of 52 kDa corresponding to MW of GST-tmTNFα was observed upon SDS PAGE analysis. **(Figure 3.20 B)**. To examine the oligomerisation state of the GST tagged tmTNFα, we carefully inspected the SDS-PAGE image of the purified protein, where a faint band around 156 kDa was visible, possibly due to the trimeric state of the protein**.** The purified protein (~20 µg/ml) was quantified by Bradford assay.

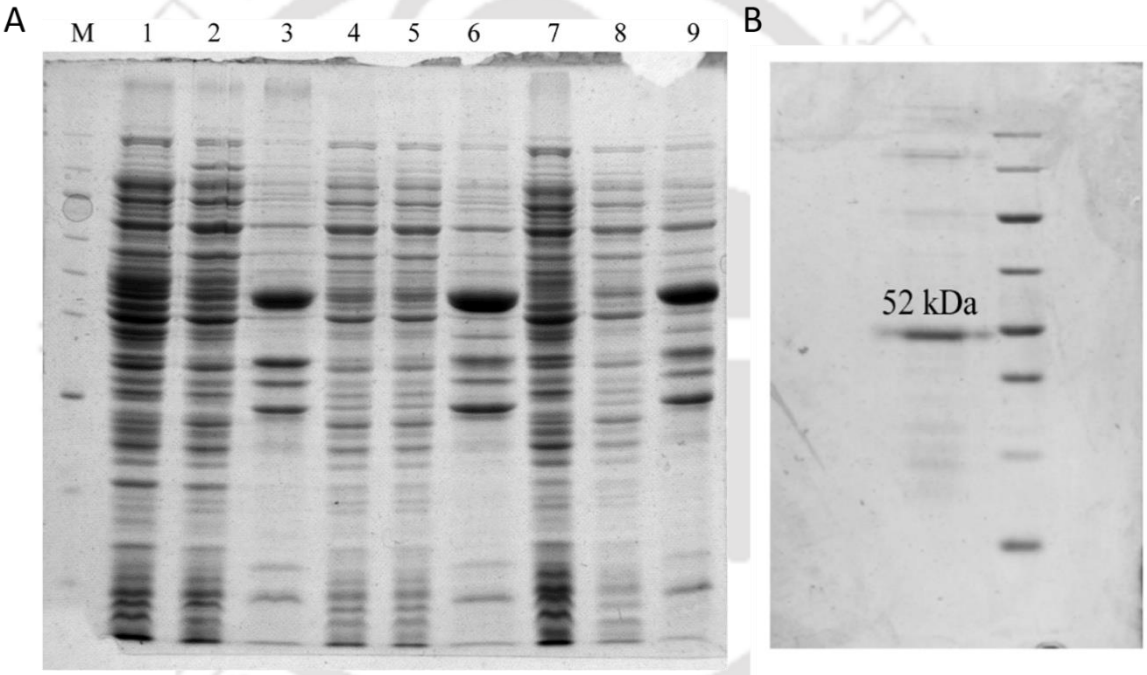

Figure 3.20: (A) SDS-PAGE depicting induction of GST tmTNFα. Lane 2 and 3: Induced supernatant and pellet at 37 °C. Lane 5 and 6: Induced supernatant and pellet at temperature 28 °C. Lane 8 and 9: Induced supernatant and pellet at temperature 22 °C. Lane 1: Uninduced supernatant and pellet at 37 °C. Lane 4: Uninduced supernatant and pellet at temperature 28 °C. Lane 7: Uninduced supernatant and pellet at temperature 22 °C. Lane M: Broad range marker 10-250 kDa Thermo Scientific. (B) Purification of GST-tmTNFα, Lane 1 purified GST - tmTNFα at 52 kDa, Lane 2 shows protein marker.

Since the recombinant protein was GST tagged, the GST protein of 26 kDa **(Figure 3.21)** was also purified using an affinity chromatography column, which

was used for subsequent control experiments.

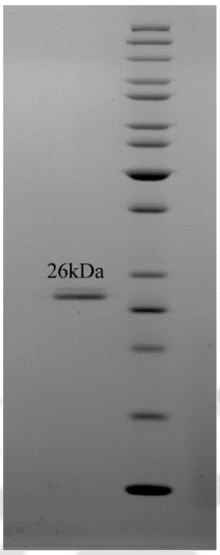

Figure 3.21: Purification of only GST protein- Lane 1 purified GST at 26 kDa, Lane 2 shows protein marker (Thermo Scientific PAGE-Ruler Unstained).

After successful cloning and purification of tmTNFα, the integrity of the recombinant protein was investigated by Western blot, matrix assisted laser desorption/ionization time of flight (MALDI TOF), and circular dichroism (CD) analysis. Western blot with anti-TNFα antibody detected a 52 kDa recombinant GST-tmTNFα band of legitimate size **(Figure 3.22)**. Another band at the higher molecular weight (156 kDa) was also visible, corresponding to the trimeric assembly of the purified GST-tmTNFα protein.

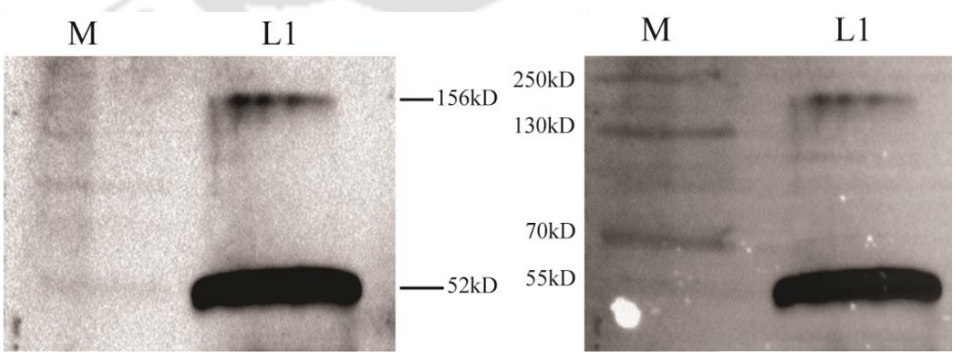

Figure 3.22: Western Blot with anti-TNFα antibody depicting a band at 52 kDa corresponding to monomeric GST-tmTNFα and another band at the higher molecular weight (152 kDa) of self-assembled trimeric form of the recombinant protein.

Further, the tryptic digested recombinant GST tagged tmTNFα was subjected to MALDI analysis to identify peptide fragments accurately [105]. Thereafter, mass profile of each fragment was examined using Findpept, which generated a peptide sequence match of 208 amino acids with sequence query coverage of 45%, confirming the identity of the desired protein. **Figure 3.23 A** illustrates the mass analysis profile of the tryptic-digested fragments where the desired peaks have been marked. The secondary structural integrity of the protein was assessed by CD, (**Figure 3.23 B)**, which demonstrated 5% alpha-helix and 77% beta-sheet, suggesting that GST-tmTNFα belongs to a class of beta-sheet containing proteins. The structure displayed a certain amount of similarity with the soluble TNFα [106].

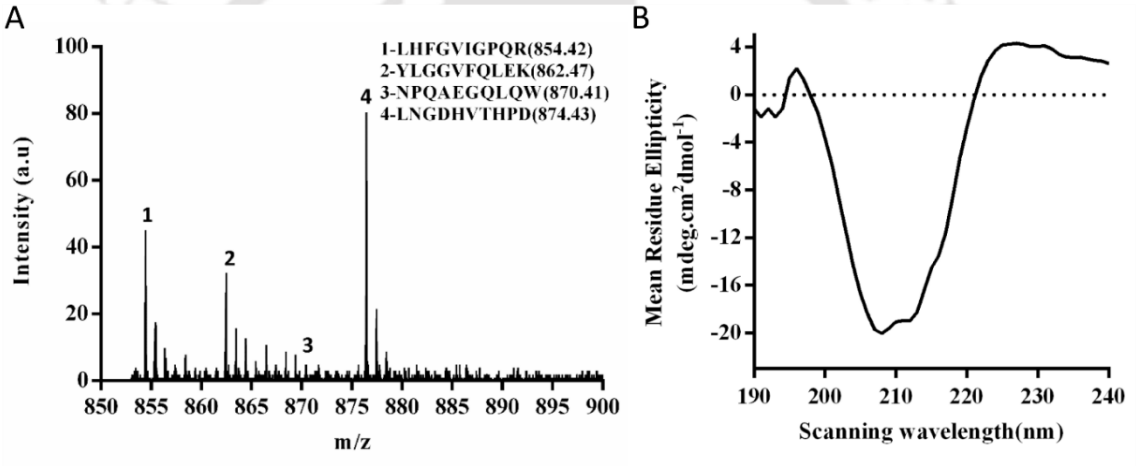

Figure 3.23: (A) MALDI TOF analysis of tryptic digested GST-tmTNFα, (B) Circular dichroism spectra depicting the secondary structure of GST-tmTNFα.

According to reports, tmTNFα can bind with both TNFα receptors: Receptor I (TNF RI) and Receptor II (TNF RII) [44]. Therefore, TNF receptor expression was examined in various cell lines prior to treating the cells with recombinant protein. Semi-quantitative PCR and quantification of amplicons using ImageJ software showed higher expression of TNF RI and TNF RII in HepG2 and HeLa (**Figure 3.24)** among the five cell lines tested. So, efficacy of the recombinant protein was evaluated on these two cancer cells.

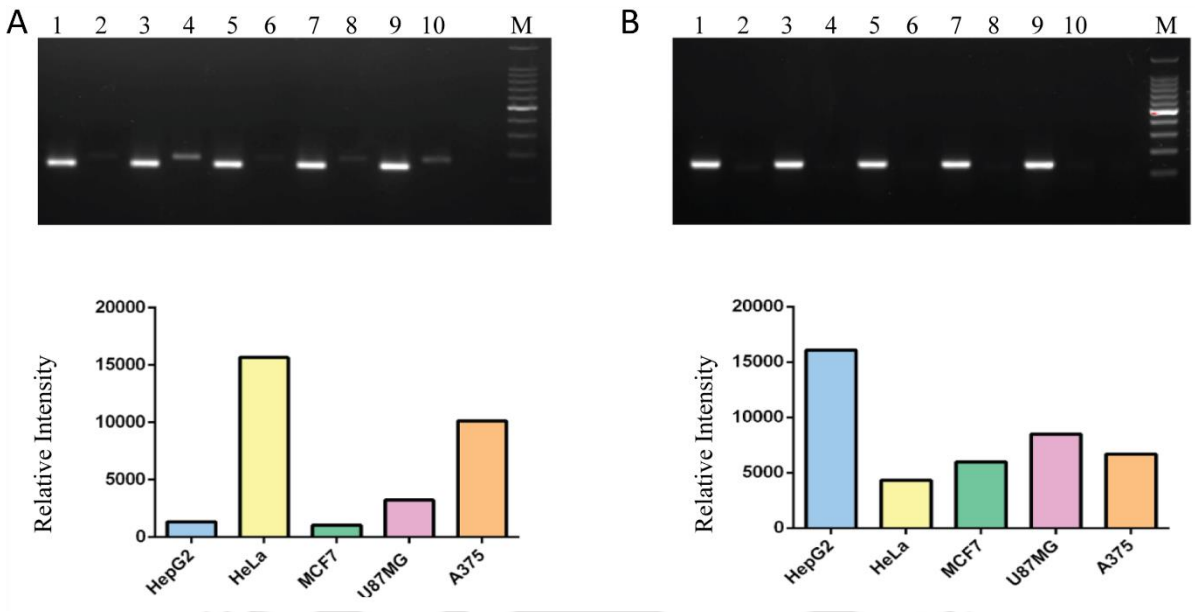

Figure 3.24: (A) PCR amplification of TNF RI for HepG2, HeLa, MCF-7, U87MG and A375 cell lines with beta-actin as an internal control along with ImageJ analysis. Lanes 1,3,5,7,9 denoting internal control for HepG2, HeLa, MCF-7, U87MG and A375 cell lines. Lanes 2,4,6,8,10 indicates PCR amplification of TNF RI for respective cell lines (B) PCR amplification of TNF RII for HepG2, HeLa, MCF-7, U87MG, and A375 cell lines with beta-actin as an internal control along with ImageJ analysis. Lanes 1,3,5,7,9 denotes internal control for respective cell lines. Lanes 2,4,6,8,10 indicates PCR amplification of TNF RII for the above-mentioned cell lines.

To study whether the GST-tmTNFα was internalized or modulated cell signaling from outside, the recombinant protein was fluorescently labeled using the EDC conjugation protocol as described in the materials and methods section. A fluorescent band at 52 kDa **(Figure 3.25 B)** after electrophoretic separation confirmed successful labeling of the protein, subsequent to which, HepG2 cells were incubated for 6 h with the labeled protein. Confocal microscope images **(Figure 3.25 A)** of the treated cells (counterstained with DAPI) demonstrated localization of fluorescently tagged TNFα on the cell surface which was substantiated by fluorescence intensity profile **(Figure 3.25 C)** analysis, illustrating sharp green fluorescence peak on the cell surface with no observable fluorescence from inside of the cells even after 6 h of treatment. Thus, tmTNFα was shown to

mediate signaling from outside of the cells as opposed to its soluble form.

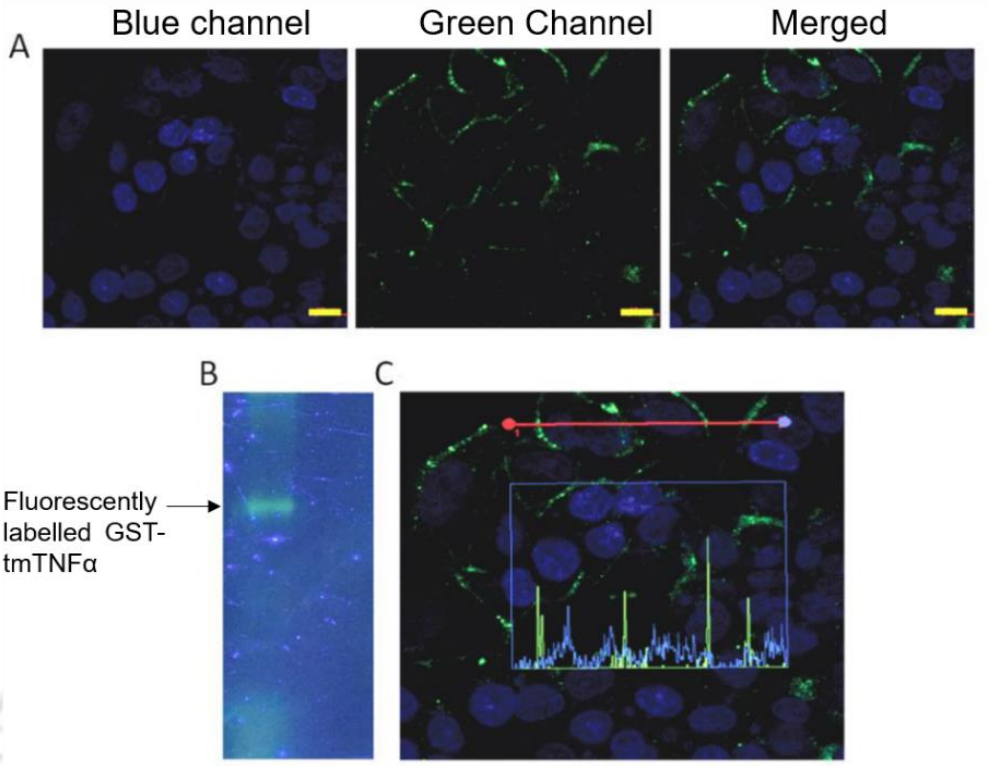

Figure 3.25: (A) Confocal microscope images of the distribution of tmTNFα (B) Fluorescent labeling of tmTNFα. (C) Fluorescence intensity profile depicting green fluorescence from outside of the cells.

Although soluble TNFα and tmTNFα share a somewhat similar structure, their bioactivity is distinctly different [44]. While soluble TNFα can initiate signaling mainly by binding to only TNF RI[107], transmembrane TNFα can execute its antiproliferative action regardless of the expression of TNF RI or TNF RII on the cell surface. Several studies demonstrated a greater cytocidal span of tmTNFα as compared to soluble TNFα [46], as it is capable of efficiently destroying the cells that are resistant to the effect of soluble TNFα. Recent research into the mechanism of action of the two TNFα, have unveiled separate signaling cascades, engaged by the molecules [44]. Moreover, when soluble TNFα binds to TNF RI, it initiates a signaling dichotomy, which culminates into a pro-apoptotic signal on the one hand, and cell proliferation on the other. In contrast, several reports demonstrate that transmembrane TNFα is engaged solely in apoptotic signal transduction when

it is involved in forward signaling as a ligand [16] [44]. However, when the moiety is expressed on the surface of a cell, it can initiate a reverse signaling cascade, which culminates in a pro-tumorigenic response in that particular cell. Therefore, we have engineered a recombinant functional tmTNFα, where tmTNFα binds as a ligand to the TNF receptors on the surface of the cells, and essentially brings about apoptosis and tumor suppression by the forward signaling only. In the current study, we have purified recombinant tmTNFα, focusing on the ligand function of the moiety, using GST affinity chromatography, and evaluated its cytotoxic potential in 2D monolayer as well as in 3D tumor spheroids. Hence, the effect of recombinant tmTNFα on TNF receptor-expressing HepG2 and HeLa cells was examined. The cells were treated with increasing concentrations of recombinant protein. Following 48 h treatment, the anticancer effect of GST-tmTNFα was evaluated by MTT and trypan blue dye exclusion assays. Results of the MTT assay (**Figure 3.26 A, B)** demonstrated a gradual decrease in the viability of the treated cells in a dose-dependent manner, and the corresponding IC_{50} values were 36 nM and 23 nM for HepG2 and HeLa, respectively.

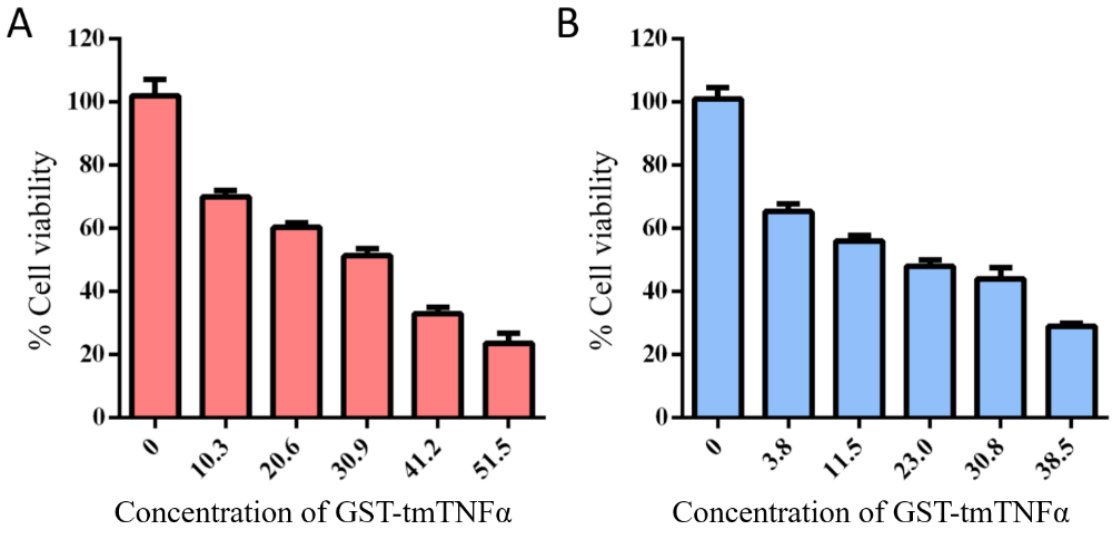

Figure 3.26: MTT assay for assessment of cell viability of (A) HepG2 and (B) HeLa cells, depicting dose-dependent anti-proliferative effect of GST-tmTNFα.

Results of the MTT assay were further corroborated with trypan blue dye exclusion assay, which provided a direct count of live and dead cells. A decrease in the live cell population of the treated cells was observed with an IC_{50} concentration of the recombinant protein as compared to the untreated cells. Countess Images **(Figure 3.27)** illustrated blue encircled cells denoting live population and red denoting dead cells.

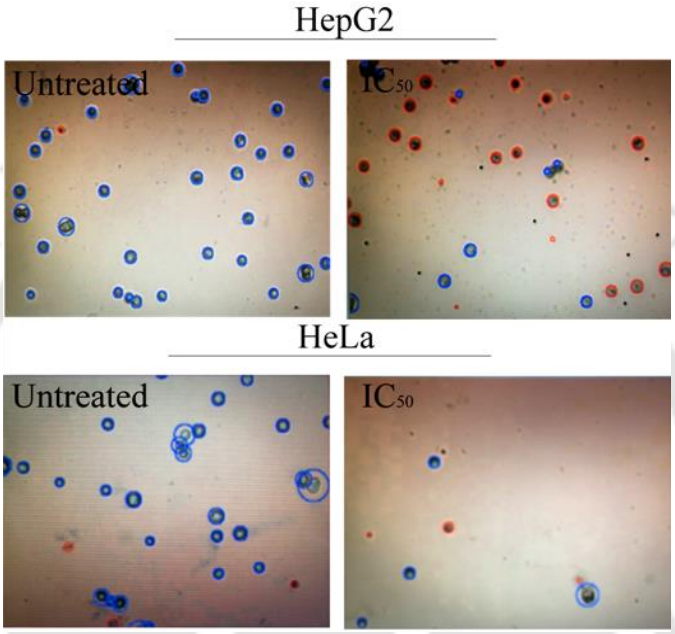

Figure 3.27: Countess Images of untreated cells and cells treated with IC_{50} concentration of recombinant protein. (IC_{50} for HepG2- 36nM, HeLa-23 nM)

To study the effect of recombinant tmTNFα on other cell lines, MCF-7, A375, and HEK cells were also tested, which showed a dose-dependent decrease in cell viability **(Figure 3.28)**. However, the reduction in cell viability was less than HepG2 or HeLa, which might be due to lower expression of TNF Rs in those cells.

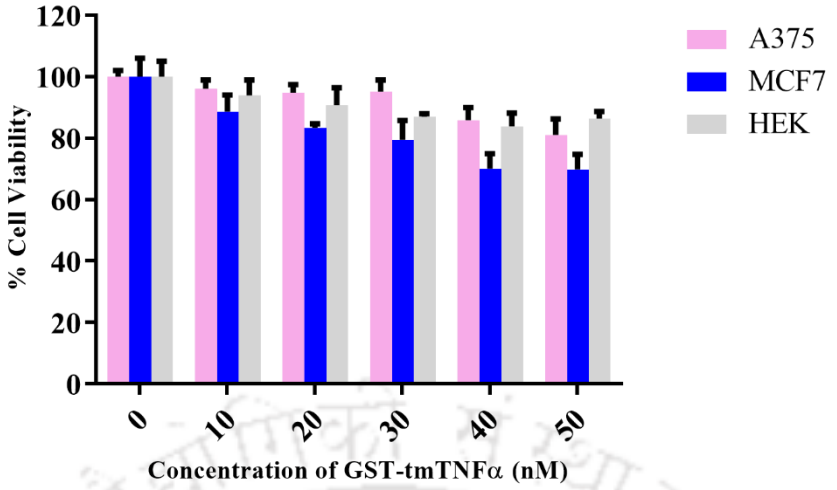

Figure 3.28: MTT assay for assessment of cell viability of A375, MCF-7 and HEK cells, depicting the dose-dependent antiproliferative effect of GST-tmTNFα.

As the TNFα was fused to GST, another set of MTT assay was performed to study any toxic effect of the GST. Results revealed no apparent impact on the cell viability upon the addition of increasing concentrations of protein (5 to 100 nM) (**Figure 3.29)**. This suggests that the reduction in viability of the cell lines upon treatment with GST-tmTNFα is the sole result of the anti-proliferative activity of recombinant tmTNFα. Cytotoxicity study on HeLa and HepG2 was also performed using soluble TNFα.

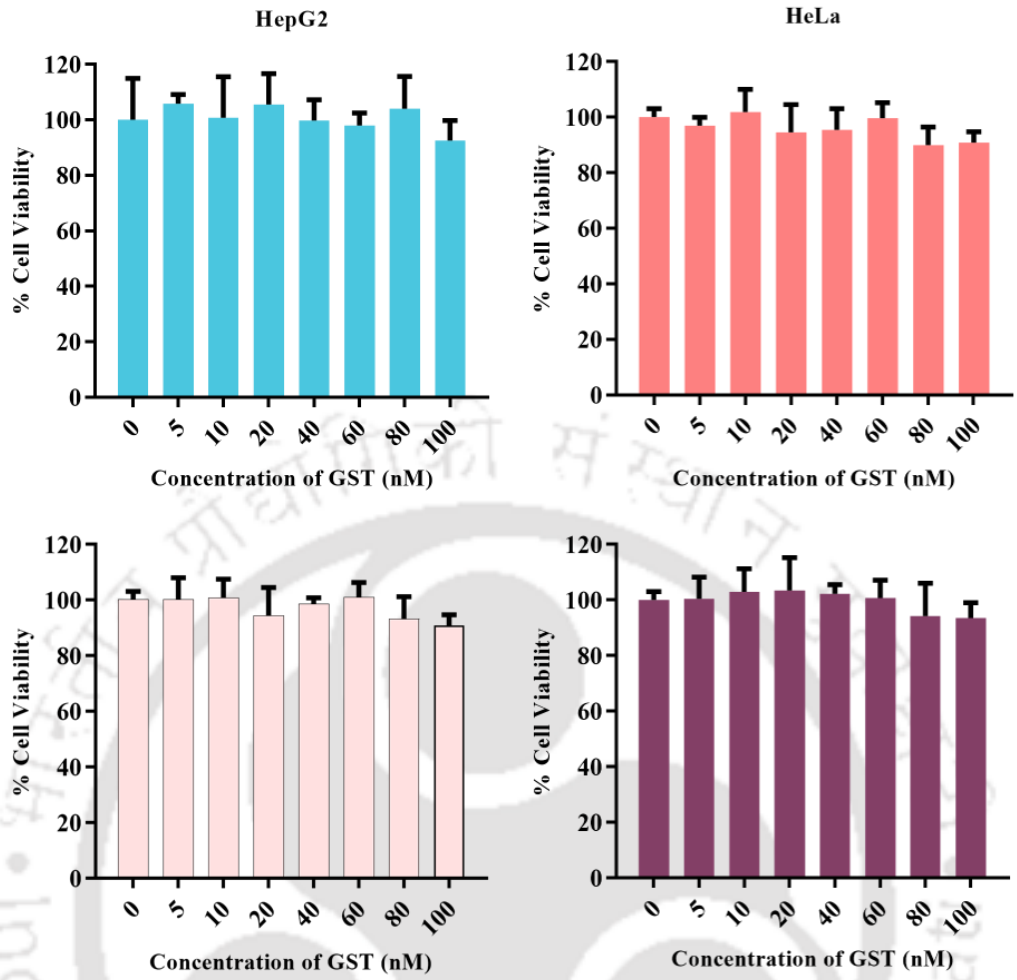

Figure 3.29: MTT assay for assessment of cell viability in (A) HepG2, (B) HeLa, (C) A375 and (D) MCF-7 cells, upon treatment with increasing concentrations of only GST protein, depicting no apparent decrease in viability of the cells.

It is noteworthy to mention that both HeLa and HepG2 cells were almost resistant to the effect of soluble TNFα, as evident from **Figure 3.30.** The results are in accordance with the reports of LI Zuoya et al. [46] and MA Costas et al. [108], where they also demonstrated that soluble TNFα hardly had any cytotoxic effect on HepG2 and HeLa cells.

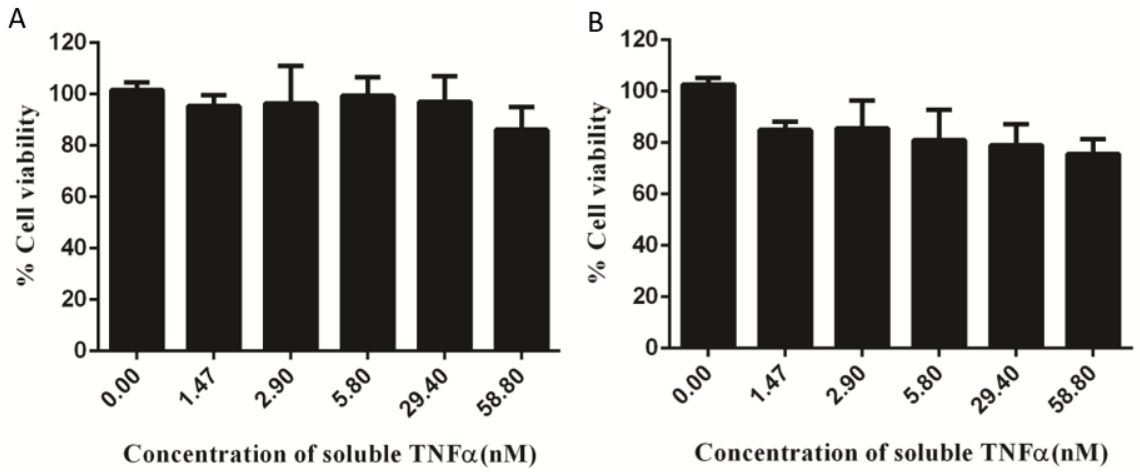

Figure 3.30: MTT assay for assessment of cell viability in (A) HepG2, (B) HeLa cells, upon treatment with increasing concentrations of soluble TNFα, demonstrating no apparent decrease in viability of the cells.

Overall, cell viability assay and trypan blue dye exclusion results demonstrated the anti-proliferative activity of the recombinantly synthesized tmTNFα.

To decipher whether GST-tmTNFα played a role in rewiring the cell cycle progression, flow cytometric cell cycle analysis was performed upon GST-tmTNFα treatment. As evident from the graphical representation, the percentage of G1 cells increased from 57% (untreated) to 70% (treated) in HepG2 cells **(Figure 3.31 A)**, while around 12% G2/M phase arrest was noted in treated HeLa cells **(Figure 3.31 B)**. The difference in response could be due to the differential expression of TNF RI and TNF RII on the two cell lines studied.

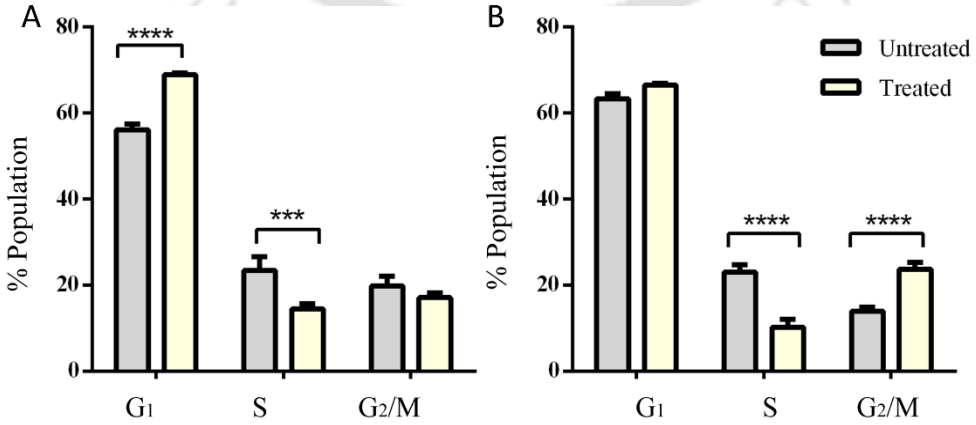

Figure 3.31: Graphical representation of flow cytometry-based assay in (A) HepG2 cells demonstrating a G1 arrest and (B) HeLa cells indicating G2/M phase arrest.

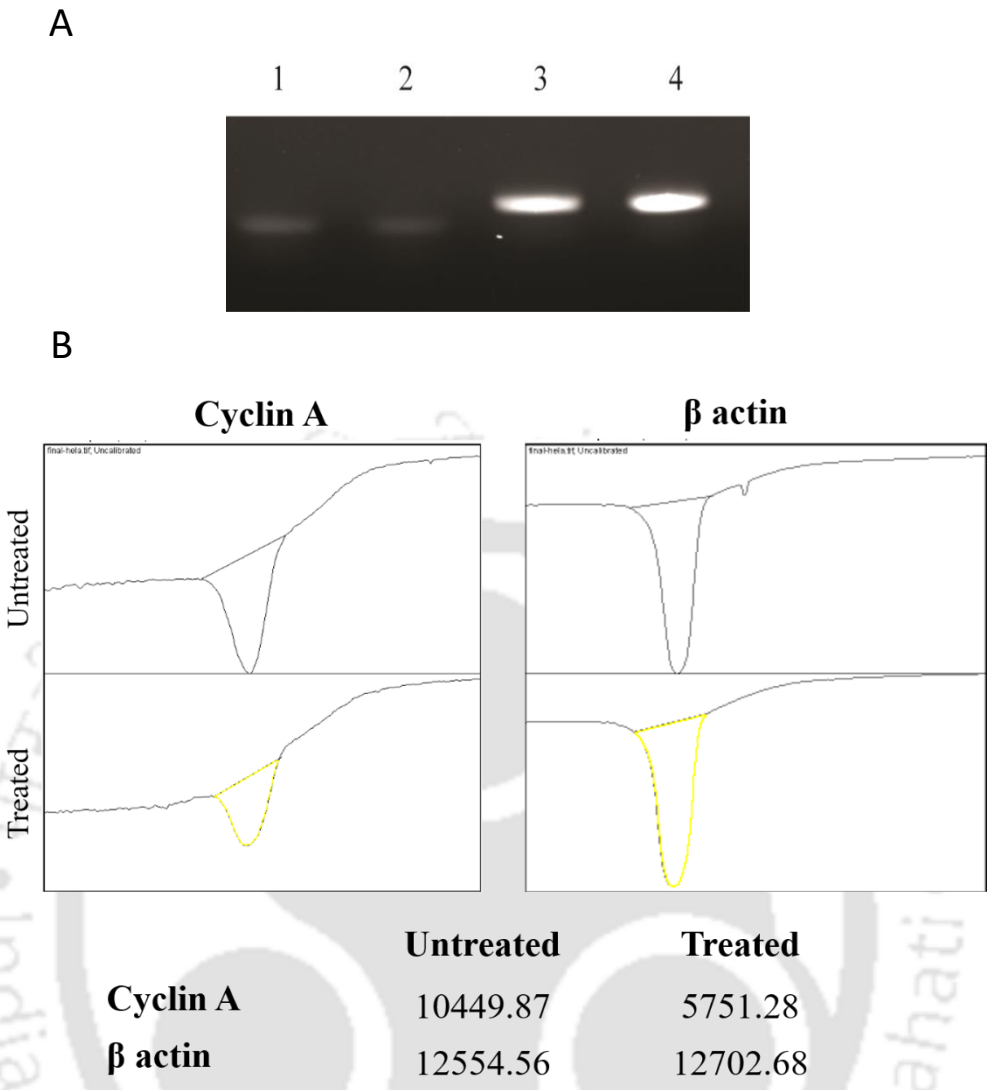

	Untreated	Treated
Cyclin A	10449.87	5751.28
β actin	12554.56	12702.68

Figure 3.32: (A) PCR amplification of Cyclin A (Lane 1,2) on HeLa cell line with beta-actin (Lane 3,4) as an internal control. Lane 1 represents untreated sample, and Lane 2 indicates recombinant protein treated sample. (B) ImageJ analysis for the quantification of the cyclin A and β-actin bands of treated and untreated samples.

Evaluation of the expression of internal cyclins, following treatment with IC_{50} concentration of the recombinant protein, revealed downregulation of cyclin A2, which upon quantification by ImageJ software, unveiled around 1.8-fold decrease in the level of cyclin A2 **(Figure 3.32)**. Analysis of cell cycle progression demonstrated a G1 arrest in Hep G2 cells and G2/M arrest in HeLa cells. At the same time, insight into the molecular mechanism of cell cycle rewiring revealed

around a 1.8-fold reduction in the expression of cyclin A2, which is a core component of mitotic cell cycle progression contributing to the nuclear envelope breakdown [109].

To explore the mode of cell death, dual staining using AO/EtBr solution was performed on HepG2 and HeLa cells, treated with IC_{50} concentration of GST-tmTNFα. AO/EtBr dual staining is a reliable one-step process for visual evaluation of the mode of cell death [110], where, AO being a membrane-permeable dye, can stain both live as well as dead cells, while EtBr being non-permeable, stains membrane compromised cells. Fluorescence microscopy images of the treated samples **(Figure 3.33)** illustrated the presence of apoptotic nuclei with condensed or fragmented chromatin, which appeared orange in color due to EtBr staining. Untreated image panels showed intact nuclei suggesting the occurrence of apoptosis only in treated cells.

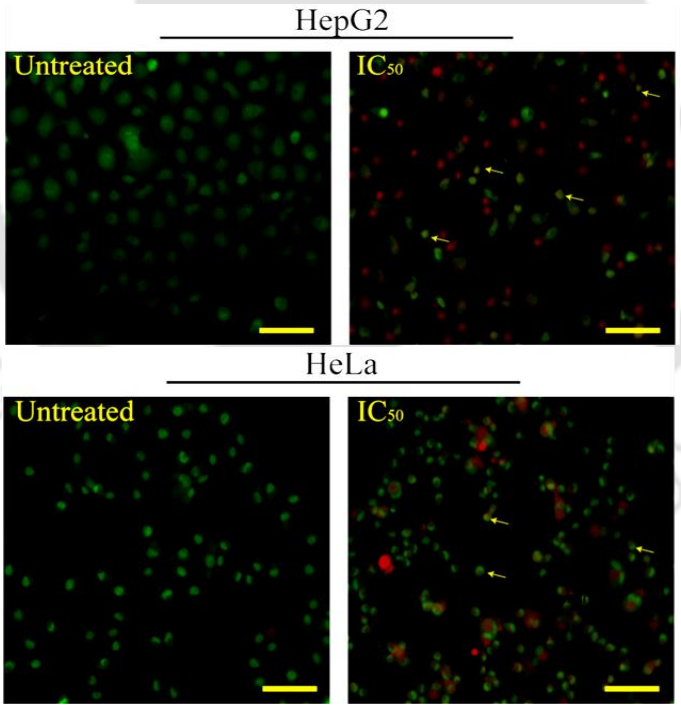

Figure 3.33: Representative image of AO/EtBr dual staining in HepG2 and HeLa cells: Individual panels were merged to distinguish live (green) and apoptotic (orange-red) cells.

Morphological hallmarks of apoptosis include nuclear condensation followed by

DNA fragmentation, cell shrinkage, and membrane blebbing [110]. Hence, change in morphology of the HepG2 and HeLa cells after treatment with GST-tmTNFα was observed by confocal microscopy. As evident from the microscopic images (**Figure 3.34**), the IC_{50} treated cells demonstrated shrinkage and membrane blebs – the signature of apoptosis.

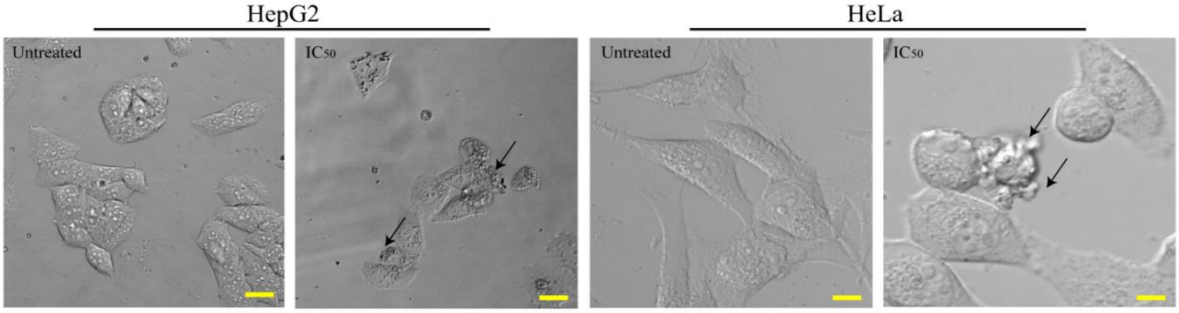

Figure 3.34: Microscopic images of untreated and treated HepG2 and HeLa cells demonstrating the onset of apoptosis.

Furthermore, the changes in the nucleus were observed by staining with Hoechst 33423, which (**Figure 3.35)** illustrated the untreated cells having round uniform nuclei. Whereas, the treated cells had condensed nuclei along with fragmented DNA, essentially indicating the onset of apoptosis. The fluorescence intensity profile of both treated and untreated nuclei, as measured with ImageJ software, corroborated that the untreated nuclei had a uniform fluorescence profile. In contrast, the treated nuclei had uneven fluorescence, denoting a hallmark of programmed cell death.

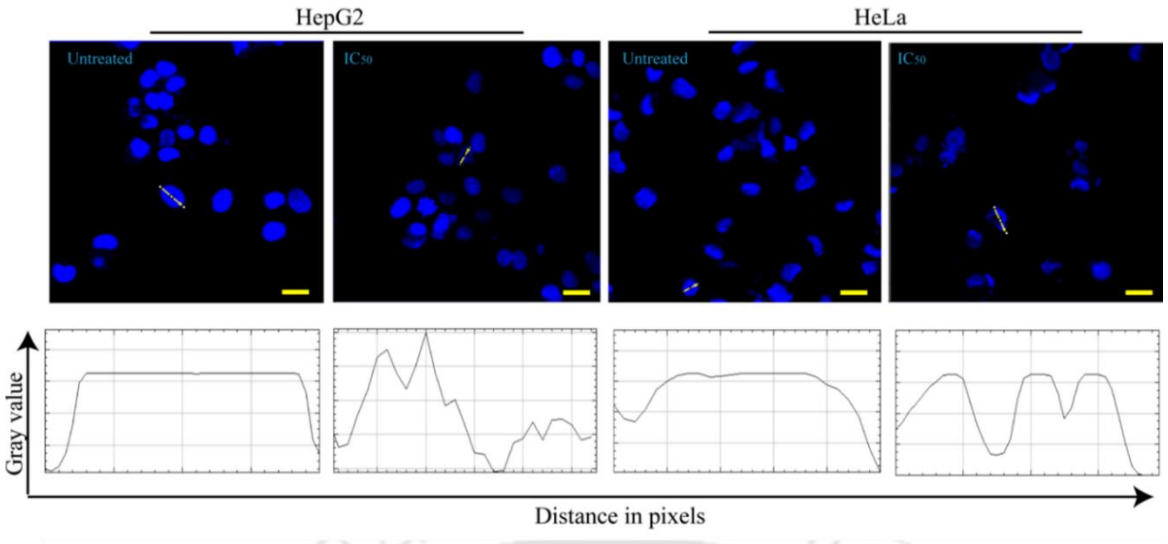

Figure 3.35: Confocal images demonstrating Hoechst stained nuclei of both HepG2 and HeLa cells accompanied with fluorescence intensity profile as measured with ImageJ software.

Flow cytometry-based Annexin V-FITC PI assay was performed to validate the extent of apoptosis induction upon treatment. Results of flow cytometric analysis (**Figure 3.36**) revealed, treatment with IC_{50} concentrations of GST-tmTNFα induced apoptosis in both the cells, with the apoptotic population being 19.8% and 24.2% for HepG2 and HeLa cells, respectively. Moreover, it may be worth mentioning here that the necrotic population was less than 2% for both the treated cells, essentially indicating the onset of apoptotic events without deleterious effects of necrotic death [99]. Subsequent experiments were performed to understand the detailed insight of apoptosis.

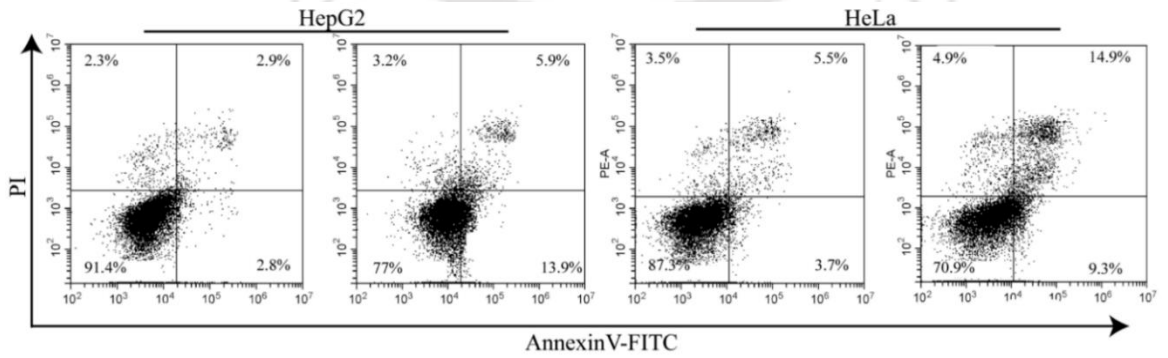

Figure 3.36: Flow-cytometric assessment of early apoptotic late apoptotic and necrotic cells with Annexin V-FITC PI.

To unveil the mechanism of apoptosis, MMP was inspected using tetraethyl-benzimidazolylcarbocyanine iodide (JC-1) dye, which aggregates and fluoresces orange-red in healthy mitochondria,while in damaged mitochondria, the dye yields green fluorescence, indicative of depolarized mitochondrial membrane potential [99]. As evident from the fluorescence microscope images **(Figure 3.37)**, treated cells displayed green fluorescence suggesting membrane depolarisation, while the untreated cells retained healthy mitochondria exhibiting a predominance of orange red fluorescence denoting JC-1 aggregates.

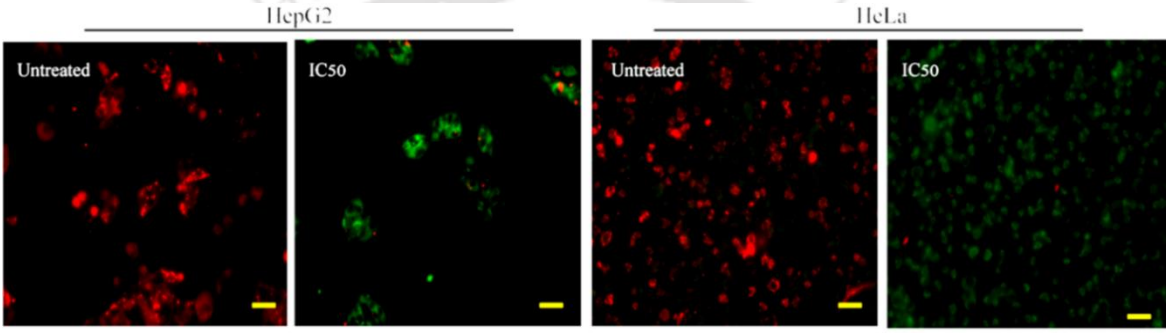

Figure 3.37: Assessment of mitochondrial membrane integrity in GST-tmTNFα treated HepG2 and HeLa cells**.**

Disruption of MMP leads to the activation of executioner caspases- the crucial regulators of apoptosis [101]**.** In apoptosis, initiator caspases cleave executioner caspases, including caspases 3 and 7, which in turn, cleaves cellular proteins, ultimately leading to cell death. Therefore, the presence of activated caspase 3/7 in the treated cells was assessed by confocal microscopy. The assay includes a fluorophore-labeled substrate for caspase 3/7, which fluoresces green upon cleavage. Following 24 h treatment, confocal microscope images of treated samples **(Figure 3.38)** exhibited green fluorescence, which indicated the presence of cleaved and active form of caspase 3/7 in both HepG2 and HeLa cells. However, there was no detectable green fluorescence observed from the untreated cells, denoting the absence of active caspase 3/7, thereby illustrating the involvement of active caspase 3/7 in apoptosis after GST-tmTNFα treatment.

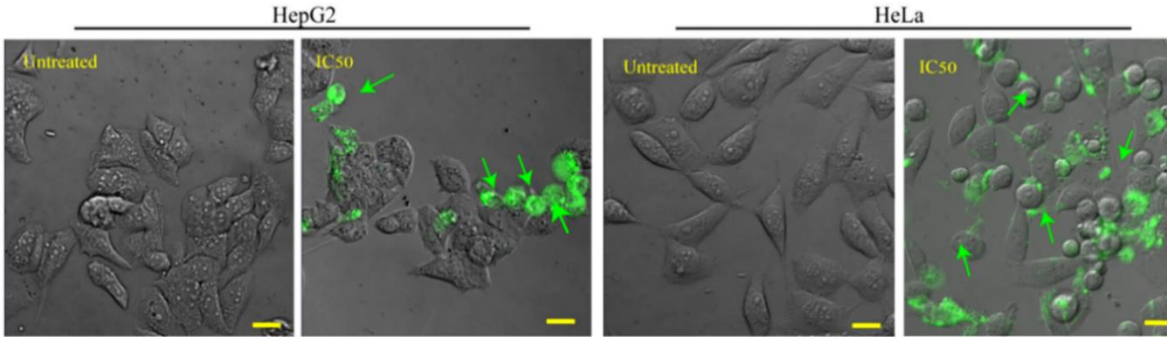

Figure 3.38: Assessment of activation of executioner caspases 3/7 in HepG2 and HeLa cells after treatment with GST-tmTNFα, demonstrating activated executioner caspases.

The molecular events underlying the mechanism of apoptosis was studied by checking the expression of pro and anti-apoptotic genes. During apoptosis, the expression of Bax and Bak increases, which controls the mitochondrial permeability while that of Bcl2 and Bcl-xL decreases, resulting in the release of cytochrome c leading to the formation of apoptosome [111]. Semi-quantitative PCR results revealed **(Figure 3.39)** an increase in the expression of Bax with simultaneous downregulation of Bcl2 and Bcl-xL in the GST-tmTNFα treated HeLa cells. The expression of the β-actin gene, which was used as an internal control, remained unchanged for both treated and untreated samples. Results from gene expression suggested the onset of apoptotic signaling upon tmTNFα treatment.

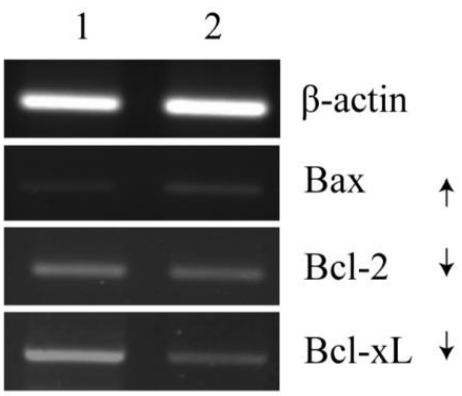

Figure 3.39: Assessment of apoptotic markers by semi-quantitative PCR. Lane 1 represents untreated samples; Lane 2 represents samples treated with IC_{50} concentration of tmTNFα.

Although monolayer cultures are considered as the initial platforms for evaluating the effectiveness of therapeutic protein, several limitations, like lack of cell-to-cell and cell-to-extracellular matrix signaling, make monolayer cultures often unsuitable for recreating *in vivo* microenvironment. Hence, three-dimensional cell culture provides a relevant *in vitro* representative platform for drug screening, as it efficiently mimics the complex and heterogeneous tumor environment [112]. Therefore, the efficacy of GST-tmTNFα was further screened on 3D tumor spheroids as a connecting link between 2D monolayer culture and *in vivo* conditions. Tumor spheroids of HeLa cells were developed in 96 well plates using the forced flotation method. The effect of recombinant GST-tmTNFα on the spheroids was assessed by treating them with increasing concentrations of the recombinant protein. Following treatment, viability was estimated by using Alamar Blue assay, which culminated in the reduction of cell viability with increasing protein concentrations **(Figure 3.40)**. Although, it should be mentioned here that a higher concentration of recombinant protein was required to achieve IC_{50} in spheroid than that of the monolayers. This could be due to less penetrability of the recombinant protein to the core of the spheroids as well as the high initial seeding density. The IC_{50} of the 2D monolayer was 23 nM, while that of the spheroids was 41 nM.

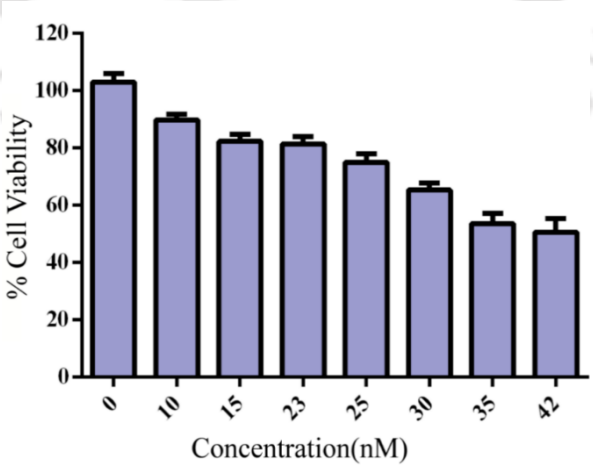

Figure 3.40: Viability determination of HeLa spheroids with resazurin disodium salt, upon treatment with increasing concentrations of GST-tmTNFα.

Furthermore, the effect of recombinant GST-tmTNFα in restricting the growth of 3D spheroids was also evaluated. The average area of the spheroids calculated from corresponding microscopic images **(Figure 3.41)** using ImageJ software was found to reduce by 48% for the treated samples as compared to the untreated spheroids, and the average diameter of the spheroids was reduced to 33% in the treated group, thereby again highlighting the significant antitumor potential of recombinant tmTNFα

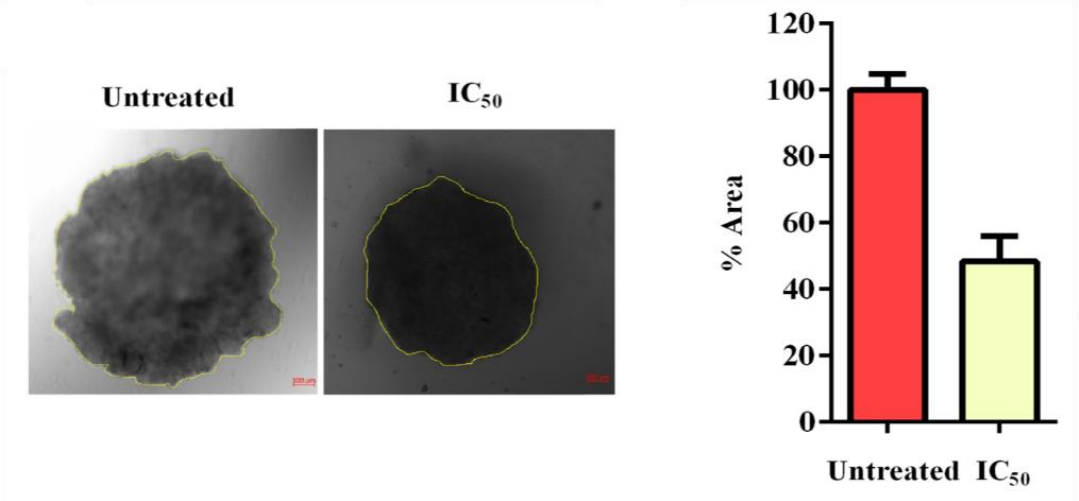

Figure 3.41: Confocal microscope images of HeLa spheroids demonstrating size reduction upon treatment with IC_{50} concentration of recombinant protein.

The effect of recombinant tmTNFα was further assessed by staining the spheroids with fluorescent dyes, namely Calcein-AM and PI. Dual stained spheroids imaged using confocal microscopy displayed higher PI staining in the treated spheroids indicating the presence of dead and apoptotic population **(Figure 3.42)**. In contrast, the untreated spheroids illustrated more green fluorescence representing live cells.

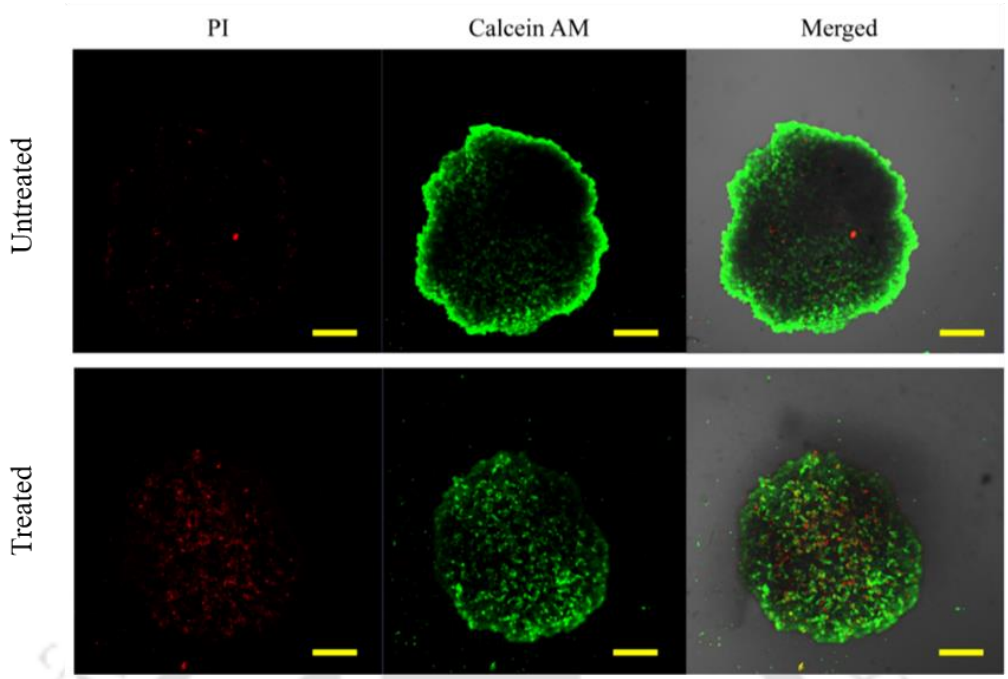

Figure 3.42: Calcein-AM/PI staining revealing visual evidence of cell death in the treated group

The outcome of the evaluation of the functional implications of recombinant tmTNFα in cancer therapeutics, has been illustrated in the scheme below:

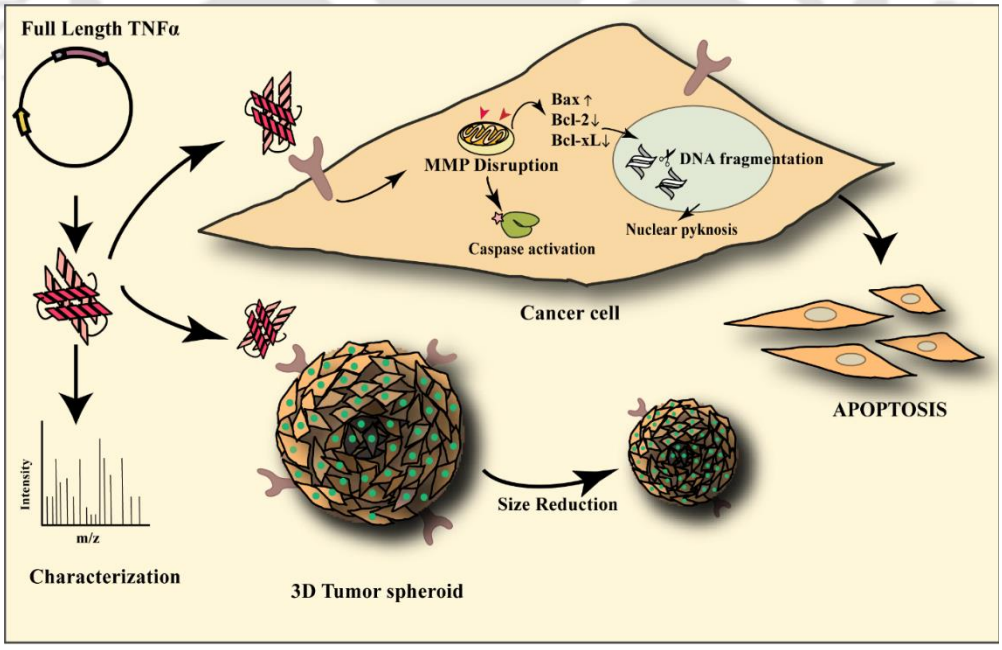

Scheme 3.3: Schematic representation of cloning, purification of recombinant GST-tmTNFα, and assessment of its effect on monolayer and tumor spheroids

3.3. Fabrication of microparticle stabilized recombinant transmembrane TNFα and evaluation of its functionality

Biotechnology Notes, Unver Revision, 2020.

Results and Discussion

Abstract: This work was pertaining to develop a suitable cargo for the stabilization and effective delivery of functional recombinant transmembrane TNFα (tmTNFα). The microcarrier was characterized for the delivery of the recombinant protein *in-vitro.* Functional integrity of the protein-loaded delivery vehicle was evaluated by cell viability assays. The results demonstrated remarkable physical properties of the microparticles, successful loading of the purified tmTNFα accompanied with retention of its functionality. A comparison of the cytotoxic profile of free recombinant protein and the calcium carbonate immobilized tmTNFα elucidated enhanced therapeutic efficacy of the later. This work bestows a positive lead towards formulating delivery platforms to achieve higher therapeutic efficacy of tmTNFα for biomedical applications.

The pGEX-4T-2 bacterial expression vector containing cloned tmTNFα gene was transformed into *E.coli* (BL21 DE3), a strain especially designed for the purification of recombinant proteins [113]. Following transformation, recombinant GST tagged tmTNFα was purified using glutathione agarose affinity chromatography according to the optimized purification protocol [49]. A legitimate band at 52 kDa was observed in 12% SDS PAGE, which established successful purification of the recombinant protein **(Figure 3.43)**. Subsequently, the protein was concentrated using a mini spin column concentrator (make: Corning), against a gradual gradient of Tris-HCl (pH 7.4) buffer to allow proper folding of the purified protein. To overcome the hurdles associated with the loss of bare recombinant proteins in solutions, an attempt was made to fabricate a delivery vehicle, considering all the necessary parameters. Since the transmembrane protein binds with TNFα receptors on the surface of the cells, it does not need internalization; rather, it functions as a ligand [15]. The net charge of the protein was calculated theoretically using the ExPASy ProtParam tool. The theoretical pI of the protein was estimated to be 5.3, necessarily indicating that the synthesized recombinant protein would have a net negative charge at physiological pH of 7.4,

which in turn would be beneficial to hinder the internalization of the protein by the cells. The surface charge of the delivery vehicle plays a crucial role in the binding of the protein with the carrier [114]. Therefore, a mildly positive charged particle was synthesized, which would allow better adsorption of the recombinant protein on its surface, concurrently, would not promote easy uptake by the negatively charged cell membrane [115]. To accomplish the intended purpose, calcium carbonate microparticles were engineered by a slight modification of the process reported by Wu et al. [96]. Although the size of a nanoparticle is one of the prime factors that should be taken into consideration while designing an appropriate protein cargo, to date, there is no such strict doctrine that one can follow to tailor the size, particularly for a specific purpose [116]. However, the general trend reveals that the bigger the size of a nanoparticle, the lesser is its uptake efficiency [117,118].

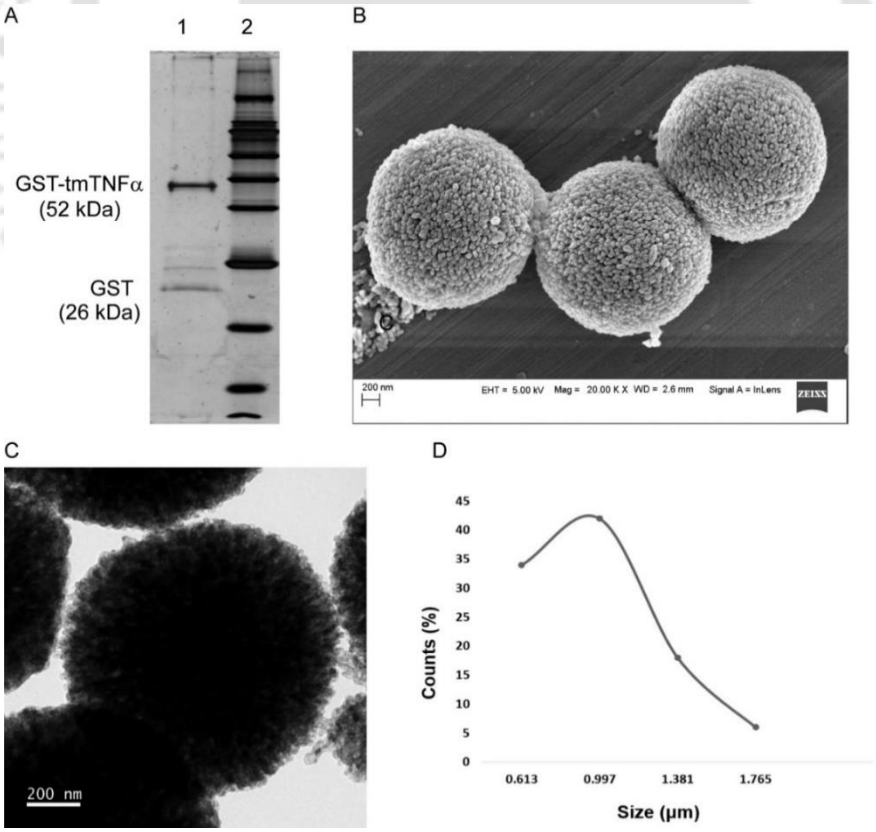

Figure 3.43: (A) Lane 1 demonstrates a band of purified GST-tmTNFα at 52 kDa as observed after silver staining a 12% SDS-PAGE, a band of cleaved GST was also visible at 26 kDa, Lane 2 is the molecular marker. (B) FESEM image of the as-

synthesized microspheres. (C) TEM analysis of the particles. (D) Graphical representation of particle size distribution as calculated by ImageJ software

So, a relatively large-sized delivery vehicle was tailored by modifying the concentration of soluble starch used in the synthesis procedure. The fabricated microparticles were characterized by FESEM and TEM, which demonstrated a relatively large size and the perfectly spherical morphology of the particles **(Figure 3.43 B, C)**. The average diameter of the microparticles was found to be 1.165 µm as calculated from FESEM images of 100 particles, using ImageJ software **(Figure 3.43 D)**.

The EDX analysis revealed **(Figure 3.44)** the presence of elemental calcium, carbon, and oxygen in the particle, which is advantageous for a carrier because these are three of the six elements present in the human body. The weight % data obtained from the elemental analysis revealed 42.4% of oxygen, 26.7% of carbon and 19.3% of calcium. Apart from the three principal components – calcium, carbon and oxygen, which is present in calcium carbonate , the data also illustrated the presence of 1.4% sodium and 1.5 % of chlorine. These is essentially the traces of the by-product which was obtained in the synthesis procedure along with calcium carbonate. Furthermore, since the glass slide surface for FESEM analysis was coated with aluminium foil for better conductivity, EDX data also indicates the presence of 8.6% aluminium.

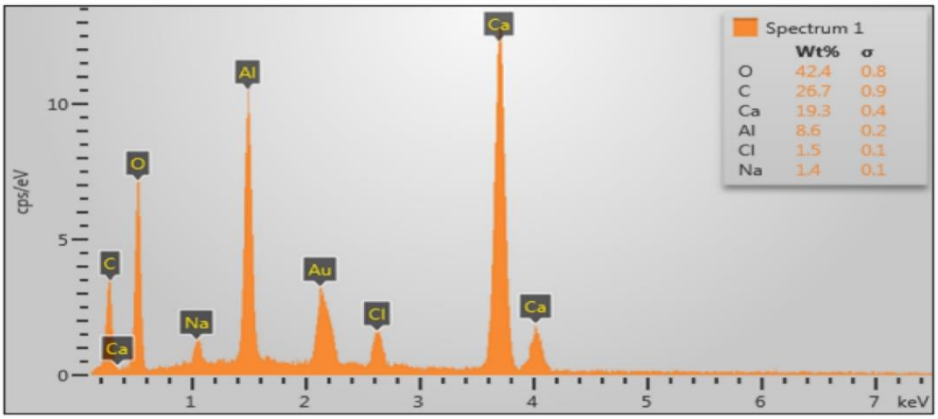

Figure 3.44: Elemental analysis showing the presence of Ca, C, and O in the synthesized microparticles

To understand the softness of the synthesized calcium carbonate microparticle thermo gravimetric analysis (TGA) was carried out. The TGA curve (**Figure 3.45)** illustrated two weight loss phases. One around 250-300 °C, which may be due to the combustion of soluble starch which was used for the preparation. The final dip observed after 700 °C, is the characteristic of decomposition of calcium carbonate.

Reaction of Decomposition- $CaCO_3$ ->$CaO + CO_2$

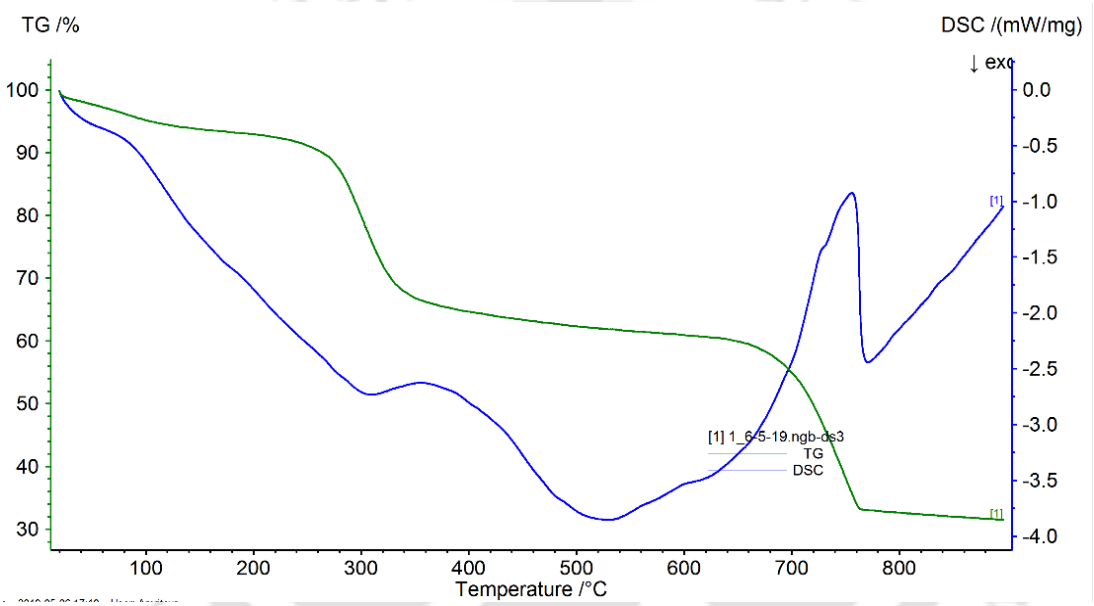

Figure 3.45: TGA analysis of calcium carbonate microparticle.

Furthermore, it is interesting to mention that $CaCO_3$ is naturally present in three states calcite, aragonite, and vaterite phase; in the decreasing order of their stability. Calcite and aragonite polymorphs are crystalline, while the vaterite phase is spherical. Vaterite, the metastable phase, gained the limelight among the other two polymorphs because of their high porosity, high specific surface area, and the ability to gradually convert into the calcite phase facilitating sustained drug release [119]. Characteristic peaks were generated when XRD analysis was performed to probe the phase of the as-synthesized microparticles. The peaks obtained were

examined using Match! (Phase Identification from Powder Diffraction) software, which elucidated that 89.3% of the synthesized microparticles were in the vaterite phase **(Figure 3.46).**

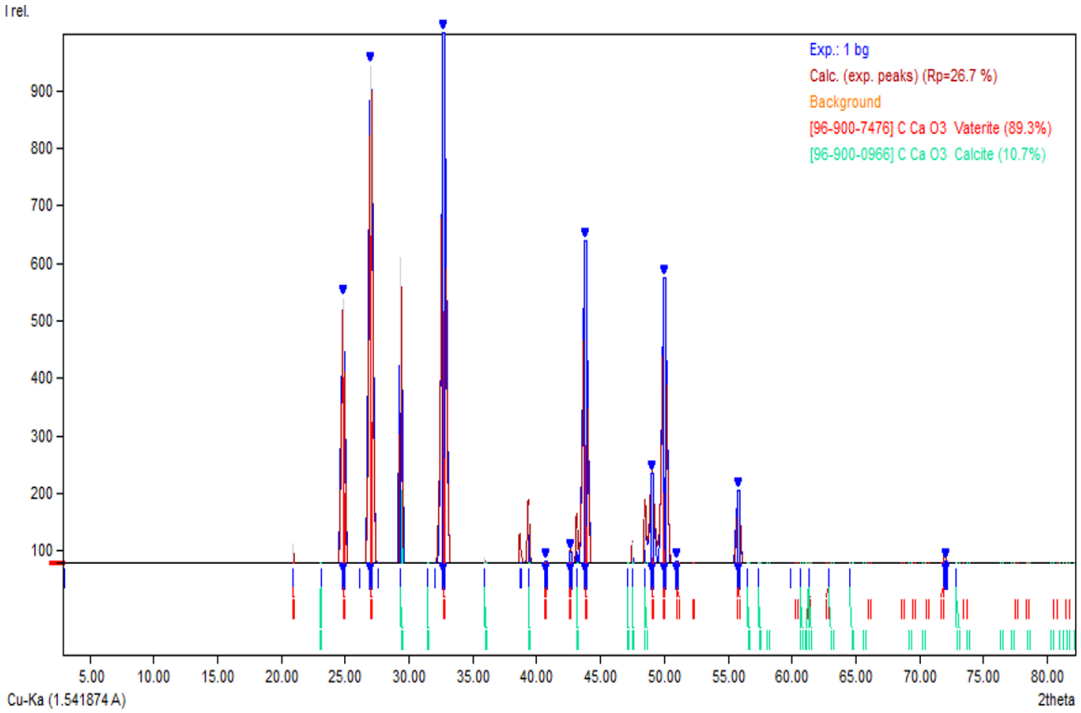

Figure 3.46: XRD pattern of the synthesized calcium carbonate microparticles illustrating the dominance of vaterite phase (89.3%). The peaks corresponding to vaterite have been marked with inverted arrowheads**.**

Notably, the porous architecture of the synthesized particles was well evident from the FESEM and TEM images. This imparted an additional benefit because it can promote better adsorption of the recombinant protein on the microparticles by providing greater surface area. BET analysis was performed to assess the specific pore surface area, and it was found to be 14.499 m^2/g. The total pore volume of the microparticles was 0.0956 cc/g, and Barrett Joyner and Halenda (BJH) desorption summary revealed that the pores had 1 to 153 nm diameter, with the average diameter of the pores being 30.018 nm **(Figure 3.47 A)**. This was indicative of dominant mesopores in the synthesized material [120].

Binding of the recombinant protein on the calcium carbonate microparticles was evaluated by probing the amount of protein left in the supernatant portion using

Bradford Assay. The maximum binding percentage was found to be 48% for the recombinant protein with 500 μg/ml of calcium carbonate microparticles **(Figure 3.47 B)**. The average hydrodynamic diameter of the bare microparticles was recorded to be 1044 nm **(Figure 3.47 C i)** by the Zetasiser, while the average hydrodynamic diameter of the tmTMFα immobilized particles was 1266 nm **(Figure 3.47 C ii)**. This increase in the hydrodynamic diameter, in comparison with the bare calcium carbonate microparticles, also denotes successful protein binding. It needs to be mentioned here that there is a difference between the hydrodynamic diameters of the particles, and the diameters of the particles, as observed by FESEM, probably because of the hydration layer formation. Moreover, the successful binding was also evaluated by recording the zeta potential, which demonstrated a slight shift in the surface charge of the tmTNFα immobilized microparticles in comparison to the bare calcium carbonate. The calcium carbonate microparticles had a net positive charge of 2 mV, which upon binding with the negatively charged protein, was recorded to be – 1.52 mV, indicative of protein binding **(Figure 3.47 D)**.

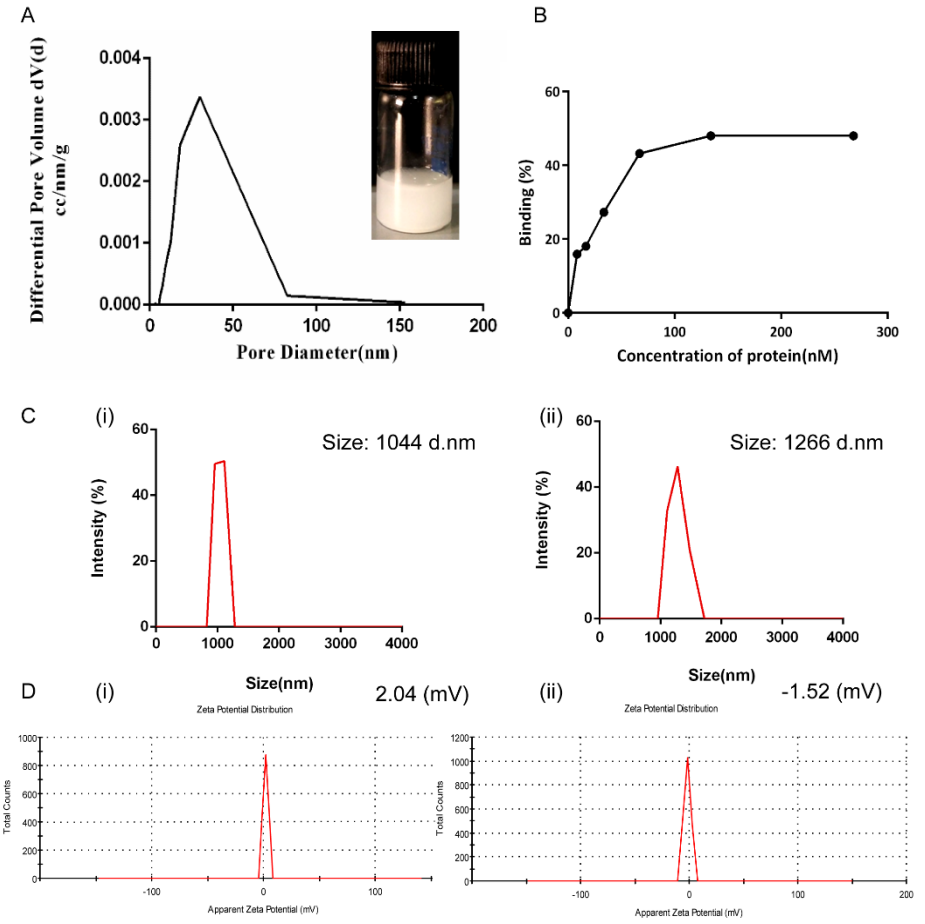

Figure 3.47: (A) Graph depicting pore diameter size distribution v/s the pore volume of calcium carbonate microparticles. (B) Binding percentage of recombinant tmTNFα on calcium carbonate microparticles. (C) Zeta potential distribution of the Calcium carbonate microspheres (i) before and (ii) after protein loading, (D) Hydrodynamic diameter of the microparticles before and after protein loading.

Upon successful confirmation of the binding, it was imperative to assess the function of the bio-macromolecule. Therefore, the functional integrity of the engineered recombinant protein-loaded microparticles was scrutinized by performing MTT cell viability assay. For this purpose, the HeLa cell line was selected because these cells are reported to have an abundant expression of TNFα specific receptors on their surface [49]. The cells were treated with increasing concentrations of calcium carbonate microparticles - ranging from 0.075-0.3 mg/ml concentration and with the same concentration of protein loaded microparticles

having recombinant protein concentration varying from 9-36 nM, for 48 h. Cell viability percentage was calculated, and the results **(Figure 3.48 A)** demonstrated a dose-dependent decrease in cell proliferation in the cells treated with tmTNFα-loaded calcium carbonate. At the same time, there was no substantial decrease in cell viability for the group, which was subjected to only calcium carbonate microparticles treatment. IC_{50} concentration of the tmTNFα-loaded calcium carbonate microparticles on HeLa cells **(Figure 3.48 B)** was evaluated to be of 15.56 nM.

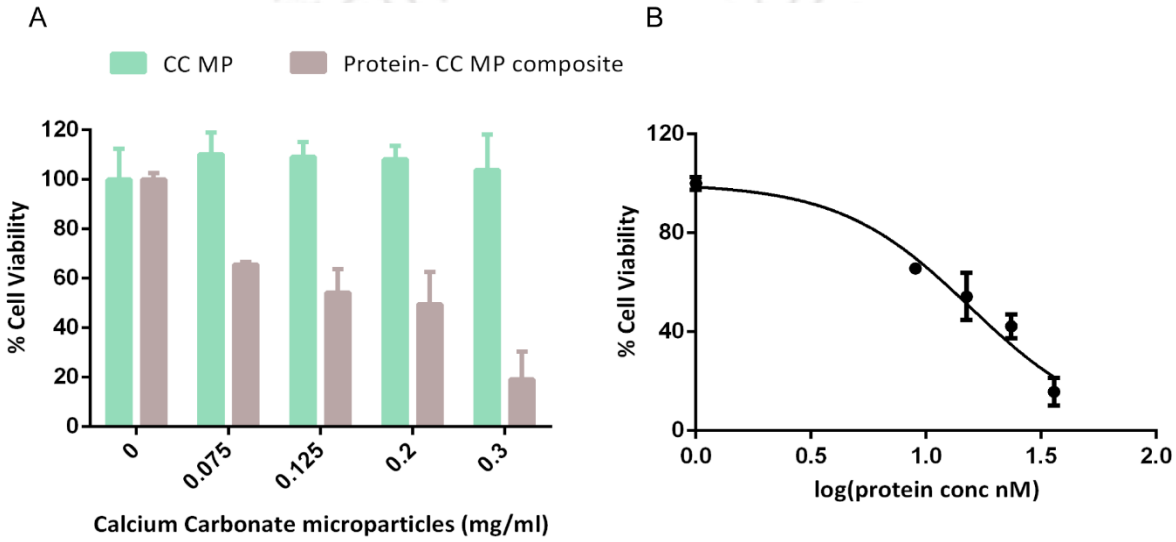

Figure 3.48 (A) Assessment of cell viability upon treatment with increasing concentrations of calcium carbonate microparticles and with recombinant tmTNFα loaded calcium carbonate microparticles. The concentration of the recombinant protein loaded on the microparticles were 9 nM, 15 nM, 24 nM, and 36 nM for 0.075, 0.125, 0.2 and 0.3 mg/ml microparticles respectively. (B) Evaluation of the IC_{50} concentration of recombinant tmTNFα loaded calcium carbonate microparticles on HeLa cells.

Interestingly, it is worth stating here that this concentration is far below the reported IC_{50} value (23 nM) of recombinant tmTNFα alone on HeLa cells. This enhancement of cytotoxic potential of recombinant tmTNFα upon successful stabilization on calcium carbonate microparticles, consequently, provided a categorical evidence supporting the prime objective of this study. The essence of the work has been illustrated in **Scheme 3.4** below**:**

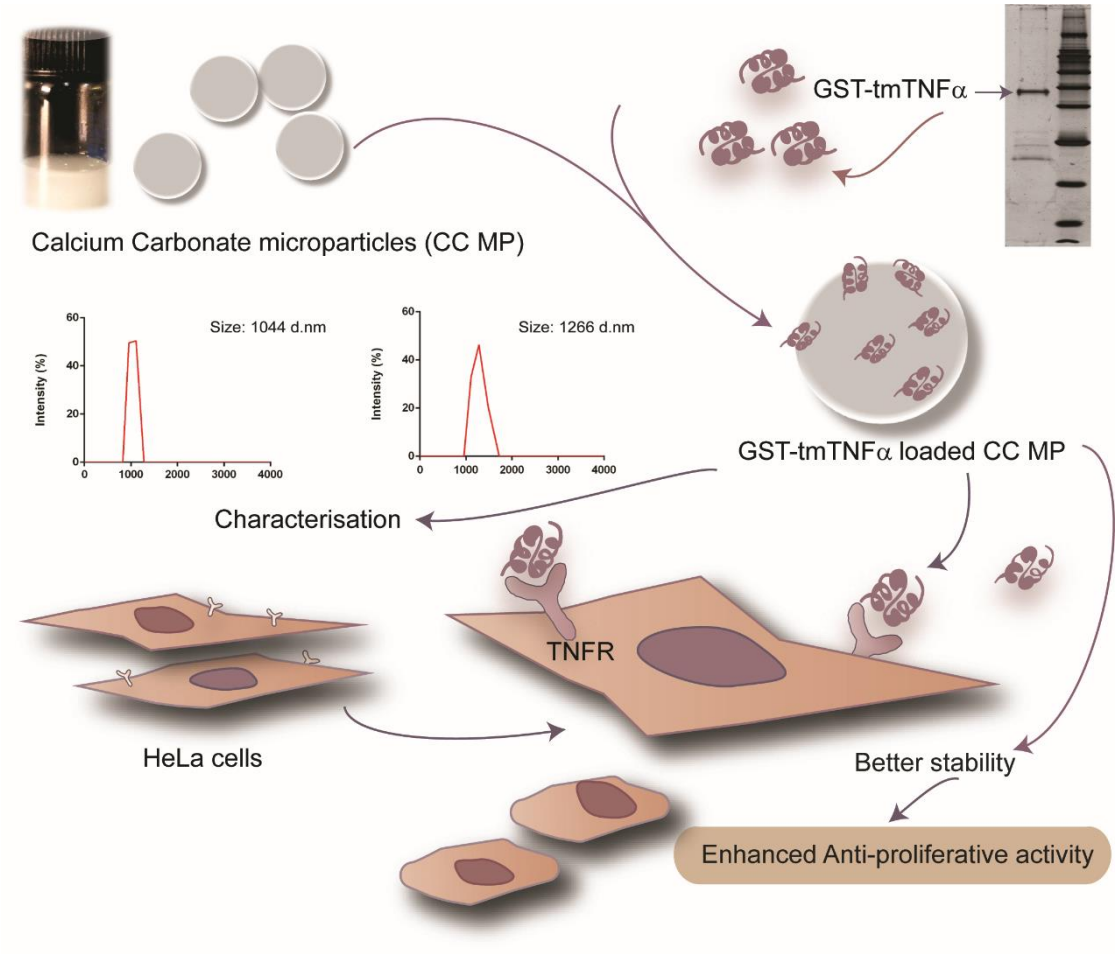

Scheme 3.4: Schematic portraying immobilization of GST-tmTNFα on calcium carbonate microparticle and evaluation of its functional efficacy

Section 4

Conclusion and Future Prospects

Conclusion and Future Prospects

Considering the contradicting nature of soluble TNFα, its precursor- tmTNFα, could be explored as an attractive option, as it lacks the cell proliferative property. The current study has focused on finding the therapeutic relevance of tmTNFα, by exploiting the ligand function of the moiety through forward signaling. The salient conclusions of the work have been categorized under three major subheadings and delineated below:

Generation of tmTNFα-expressed macrophage membrane-coated nanoparticles and evaluation of their anti-cell proliferative activity

- Therapeutically relevant transmembrane- TNFα expressed macrophage membrane has been coated on nontoxic chitosan nanoparticles to formulate a nanoassembly.
- Upon LPS induction, TNFα imparted therapeutic efficiency to the otherwise non-cytotoxic macrophage membrane.
- Excellent stability, hemocompatibility, and biocompatibility of the fabricated nanoassembly paved the way to explore its functional integrity.
- The membrane coated nanoparticles retained dose-dependent anti-cell proliferative properties when examined on three different cancer cells.
- Evaluation of the mode of cell death unveiled the triggering of apoptosis in the cells after treatment with the nanoassembly.
- The successful regressive effect of the nanoassembly on spheroids boosts the biological significance of the study in the perspective of a new regime in cancer therapy, as the spheroids closely mimic the *in vivo* tumor microenvironment. The translation of cell retardation activity confirms the immense potential of this novel therapeutic nanoassembly as a 'nanodrug'

Cloning, expression, purification of recombinant tmTNFα and investigation of its functional effects

- Successful expression, cloning, and purification of tmTNFα protein in a homogenous form and subsequent biophysical characterizations depicted the integrity of this novel recombinant protein.
- While cytotoxic assays unveiled functionality, microscopic experiments and flow cytometry-based studies established apoptotic mode of cell death, a more desirable process as opposed to necrosis.
- Treatment of tumor spheroids with the recombinant protein efficiently reduced the spheroid's size as well as the viability.

Fabrication of microparticle stabilized recombinant transmembrane TNF-α and assessment of their functionality

- Engineering a suitable cargo for the proper delivery and stabilization of recombinant therapeutic proteins is an emerging avenue in the realm of health care.
- Successful design of a carrier, modulating all the essential parameters for the stabilization and delivery of recombinant tmTNFα protein.
- Detailed characterization of the microparticles unveiled its size, shape, and porous morphology of the meticulously tailored delivery vehicle.
- Subsequently, the results of binding studies indicated effective immobilization of the recombinant protein.
- The results of MTT assay demonstrated that the cytotoxic potential of the recombinant protein was retained after binding.
- Moreover, the higher antiproliferative potential of the recombinant tmTNFα immobilized on the calcium carbonate microparticles compared to

free recombinant tmTNFα indicated better stabilization of the protein on adsorption with the microparticles.

- In a nutshell, equipped with promising results, the present work addresses the limitations in protein stabilization. It confers a decisive lead for the further evaluation of recombinant tmTNFα immobilized biocompatible carriers for clinical translation.

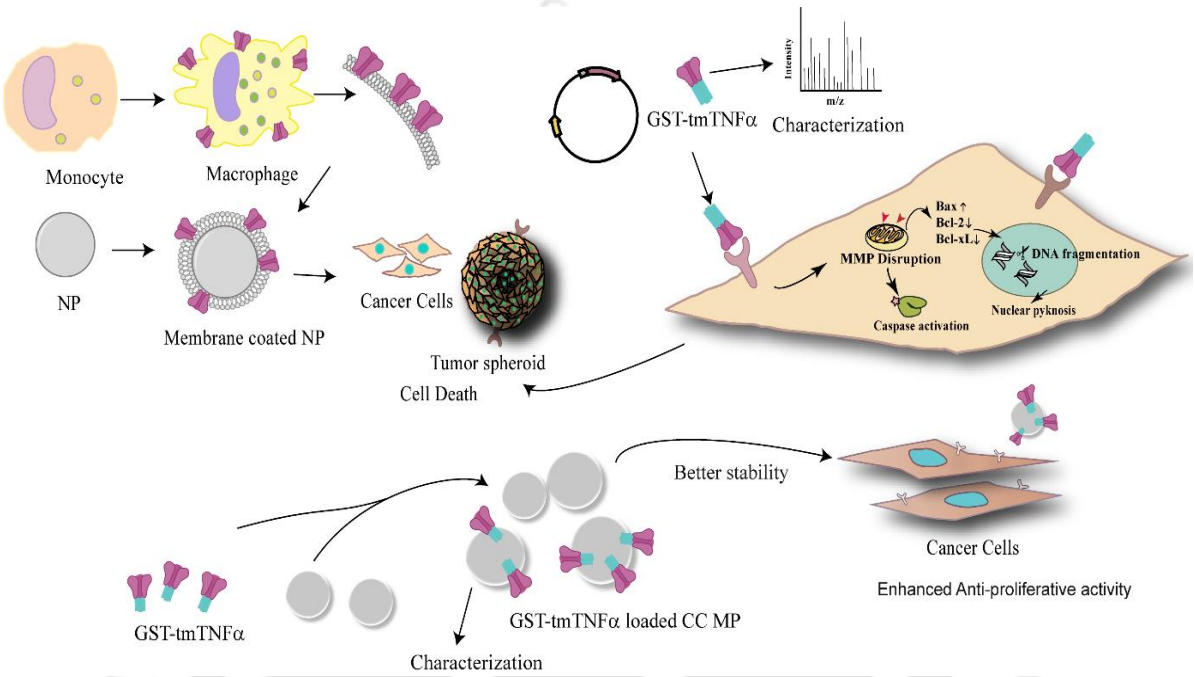

Scheme 4.1: Pictorial depiction of the current thesis work

Future prospects of the current study include:

- Insight into the signaling pathways rewired by recombinant tmTNFα may open a new vista in the realm of protein therapy
- The issues of safe delivery of the transmembrane moiety need further experimental validations
- Non-cleavable mutant recombinant proteins can also be synthesized to increase the therapeutic efficiency of tmTNFα

- This work provides a future scope of testing efficacy of tmTNF*α* *in vivo* for its translational potential

References

1. Rhind, N. & Russell, P. Signaling pathways that regulate cell division. *Cold Spring Harb. Perspect. Biol.* **4**, (2012).
2. Agnello, M., Bosco, L., Chiarelli, R., Martino, C. & Roccheri, M. C. The Role of Autophagy and Apoptosis During Embryo Development. in *Cell Death - Autophagy, Apoptosis and Necrosis* (InTech, 2015). doi:10.5772/61765.
3. Leader, B., Baca, Q. J. & Golan, D. E. Protein therapeutics: a summary and pharmacological classification. *Nat. Rev. Drug Discov.* **7**, 21–39 (2008).
4. Hirsch, I. B. Insulin analogues. *N. Engl. J. Med.* **352**, 174–183 (2005).
5. Walczak, H. Death receptor-ligand systems in cancer, cell death, and inflammation. *Cold Spring Harb. Perspect. Biol.* **5**, (2013).
6. Lunney, J. K. Cytokines orchestrating the immune response. *Rev. sci. tech. Off. int. Epiz* **17**, 84–94 (1998).
7. THAYER, A. Interleukin-2 wins FDA market clearance. *Chem. Eng. News* **70**, 5 (1992).
8. Asmana Ningrum, R. Human interferon alpha-2b: a therapeutic protein for cancer treatment. *Scientifica (Cairo).* **2014**, 970315 (2014).
9. Cai, W., Kerner, Z. J., Hong, H. & Sun, J. Targeted Cancer Therapy with Tumor Necrosis Factor-Alpha. *Biochem. Insights* **1**, BCI.S901 (2008).
10. Ruggiero, V., Latham, K. & Baglioni, C. Cytostatic and cytotoxic activity of tumor necrosis factor on human cancer cells. *J. Immunol.* **138**, 2711–7 (1987).
11. Sedger, L. M. & McDermott, M. F. TNF and TNF-receptors: From mediators of cell death and inflammation to therapeutic giants - past, present and future. *Cytokine Growth Factor Rev.* **25**, 453–472 (2014).
12. Sacchi, A. *et al.* Synergistic antitumor activity of cisplatin, paclitaxel, and gemcitabine with tumor vasculature-targeted tumor necrosis factor-α. *Clin. Cancer Res.* **12**, 175–182 (2006).
13. van Horssen, R., Ten Hagen, T. L. M. & Eggermont, A. M. M. TNF-alpha in cancer treatment: molecular insights, antitumor effects, and clinical utility. *Oncologist* **11**, 397–408 (2006).
14. Aggarwal, B. B. Signalling pathways of the TNF superfamily: a double-edged sword. *Nat. Rev. Immunol.* **3**, 745–756 (2003).
15. Jiang, Y. *et al.* STAT1 mediates transmembrane TNF-alpha-induced formation of death-

inducing signaling complex and apoptotic signaling via TNFR1. *Cell Death Differ.* **24**, 660–671 (2017).

16. Zhang, H. *et al.* Transmembrane TNF-α mediates "forward" and "reverse" signaling, inducing cell death or survival via the NF-κB pathway in Raji Burkitt lymphoma cells. *J. Leukoc. Biol.* **84**, 789–797 (2008).
17. Hoption Cann, S. A., Van Netten, J. P. & Van Netten, C. Dr William Coley and tumour regression: A place in history or in the future. *Postgraduate Medical Journal* vol. 79 672–680 (2003).
18. Bickels J, Kollender Y, Merinsky O & Meller I. Coley's Toxin: Historical Perspective. *Isr Med Assoc J* **4**, 471–472 (2002).
19. McCarthy, E. F. The toxins of William B. Coley and the treatment of bone and soft-tissue sarcomas. *Iowa Orthop. J.* **26**, 154–158 (2006).
20. Tang, D. *et al.* TNF-Alpha Promotes Invasion and Metastasis via NF-Kappa B Pathway in Oral Squamous Cell Carcinoma. *Med. Sci. Monit. Basic Res.* **23**, 141–149 (2017).
21. Parameswaran, N. & Patial, S. Tumor necrosis factor-a signaling in macrophages. *Critical Reviews in Eukaryotic Gene Expression* vol. 20 87–103 (2010).
22. O'malley, W. E., Achinstein, B. & Shear, M. J. Action Of Bacterial Polysaccharide On Tumors. III. Repeated Response Of. *Cancer Res.* **23**, 890–895 (1963).
23. O'malley, W. E., Achinstein, B. & Shear, M. J. Action of Bacterial Polysaccharide on Tumors. II. Damage of Sarcoma 37 by Serum of Mice Treated with Serratia Marcescens Polysaccharide, and Induced Tolerance. *Nutr. Rev.* **46**, 389–391 (2009).
24. Carswell, E. A. *et al.* An endotoxin induced serum factor that cuases necrosis of tumors. *Proc. Natl. Acad. Sci. U. S. A.* **72**, 3666–3670 (1975).
25. Pennica, D. *et al.* Human tumour necrosis factor: Precursor structure, expression and homology to lymphotoxin. *Nature* **312**, 724–729 (1984).
26. Aggarwals, B. B. *et al. The Journal Of Biological Chemistry Human Tumor Necrosis Factor Production, Purification, And Characterization**. vol. 260 (1985).
27. Wang, X. & Lin, Y. Tumor necrosis factor and cancer, buddies or foes? *Acta Pharmacologica Sinica* vol. 29 1275–1288 (2008).
28. Horiuchi, T., Mitoma, H., Harashima, S. I., Tsukamoto, H. & Shimoda, T. Transmembrane TNF-α: Structure, function and interaction with anti-TNF agents. *Rheumatology* vol. 49 1215–1228 (2010).
29. Sellati, T. J. & Sahay, B. Cells of Innate Immunity: Mechanisms of Activation. in *Pathobiology of Human Disease: A Dynamic Encyclopedia of Disease Mechanisms* 258–274

(Elsevier Inc., 2014). doi:10.1016/B978-0-12-386456-7.01804-9.

30. Josephs, S. F. *et al.* Unleashing endogenous TNF-alpha as a cancer immunotherapeutic. *Journal of Translational Medicine* vol. 16 242 (2018).

31. Zheng, F. *et al.* Leader sequence is required for activity of transmembrane tumor necrosis factor-α. *Mol. Immunol.* **46**, 3336–3344 (2009).

32. Kollias, G. & Petros, P. S. *TNF Pathophysiology: Molecular and Cellular Mechanisms*. *TNF Pathophysiology: Molecular and Cellular Mechanisms* vol. 11 (S. Karger AG, 2010).

33. Tracey, M.D, K. J. & Cerami, A. Tumor Necrosis Factor: A Pleiotropic Cytokine and Therapuetic Target. *Annu. Rev. Med.* **45**, 491–503 (1994).

34. Bertazza, L. & Mocellin, S. The Dual Role of Tumor Necrosis Factor (TNF) in Cancer Biology. *Curr. Med. Chem.* **17**, 3337–3352 (2012).

35. Cruceriu, D., Baldasici, O., Balacescu, O. & Berindan-Neagoe, I. The dual role of tumor necrosis factor-alpha (TNF-α) in breast cancer: molecular insights and therapeutic approaches. *Cellular Oncology* vol. 43 1–18 (2020).

36. Sedger, L. M. & McDermott, M. F. TNF and TNF-receptors: From mediators of cell death and inflammation to therapeutic giants – past, present and future. *Cytokine Growth Factor Rev.* **25**, 453–472 (2014).

37. Cai, W., Kerner, Z. J., Hong, H. & Sun, J. *Targeted Cancer Therapy with Tumor Necrosis Factor-Alpha*. *Biochemistry Insights* https://journals.sagepub.com/doi/pdf/10.4137/BCI.S901 (2008).

38. Schütze, S., Wiegmann, K., Machleidt, T. & Krönke, M. TNF-Induced Activation of NF-κB. *Immunobiology* **193**, 193–203 (1995).

39. Tang, D. *et al.* TNF-Alpha Promotes Invasion and Metastasis via NF-Kappa B Pathway in Oral Squamous Cell Carcinoma. *Med. Sci. Monit. Basic Res.* **23**, 141–149 (2017).

40. Ardestani, S. *et al.* Membrane versus Soluble Isoforms of TNF-α Exert Opposing Effects on Tumor Growth and Survival of Tumor-Associated Myeloid Cells. *Cancer Res.* **73**, 3938–3950 (2013).

41. Utsumi, T. *et al.* Transmembrane TNF (pro-TNF) is palmitoylated. *FEBS Lett.* **500**, 1–6 (2001).

42. Kriegler, M., Perez, C., DeFay, K., Albert, I. & Lu, S. D. A novel form of TNF/cachectin is a cell surface cytotoxic transmembrane protein: Ramifications for the complex physiology of TNF. *Cell* **53**, 45–53 (1988).

43. Zheng, F. *et al.* Mutational analysis of region-cytotoxicity relationship in human transmembrane tumor necrosis factor-alpha. *Chinese-German J. Clin. Oncol.* **1**, 38–41 (2002).

44. Jiang, Y. *et al.* STAT1 mediates transmembrane TNF-alpha-induced formation of death-inducing signaling complex and apoptotic signaling via TNFR1. *Cell Death Differ.* **24**, 660–671 (2017).

45. Zhang, H. *et al.* Transmembrane TNF-alpha mediates 'forward' and 'reverse' signaling, inducing cell death or survival via the NF-kappaB pathway in Raji Burkitt lymphoma cells. *J. Leukoc. Biol.* **84**, 789–97 (2008).

46. Yang, L. *et al.* Comparison of cell deaths induced by transmembrane and secretory TNF-α. *J. Huazhong Univ. Sci. Technol. - Med. Sci.* **27**, 117–119 (2007).

47. Yang, L. *et al.* Comparison of cell deaths induced by transmembrane and secretory TNF-α. *J. Huazhong Univ. Sci. Technol. - Med. Sci.* **27**, 117–119 (2007).

48. Li, X. *et al.* Correlation of cytotoxic effect of transmembrane and secretory TNF-α to cell cycle. *J. Huazhong Univ. Sci. Technolog. Med. Sci.* **32**, 806–809 (2012).

49. Bhattacharyya, S. & Ghosh, S. S. Deciphering insights of novel recombinant tmTNFα in cell growth inhibition. *Mol. Biol. Rep.* **47**, 3949–3961 (2020).

50. Li, Q. *et al.* Mechanism of action differences in the antitumor effects of transmembrane and secretory tumor necrosis factor-alpha in vitro and in vivo. *Cancer Immunol. Immunother.* **55**, 1470–1479 (2006).

51. Yu, M. *et al.* Influence of reverse signaling via membrane TNF-α on cytotoxicity of NK92 cells. *Eur. J. Cell Biol.* **88**, 181–191 (2009).

52. Zhang, Z. *et al.* Transmembrane TNF-alpha promotes chemoresistance in breast cancer cells. *Oncogene* **37**, 3456–3470 (2018).

53. Yu, M. *et al.* Targeting transmembrane TNF-α suppresses breast cancer growth. *Cancer Res.* **73**, 4061–4074 (2013).

54. Yan, D. *et al.* Expression of TNF-alpha leader sequence renders MCF-7 tumor cells resistant to the cytotoxicity of soluble TNF-alpha. *Breast Cancer Res. Treat.* **116**, 91–102 (2009).

55. Grell, M. *et al.* The transmembrane form of tumor necrosis factor is the prime activating ligand of the 80 kDa tumor necrosis factor receptor. *Cell* **83**, 793–802 (1995).

56. Lee, W. H., Seo, D., Lim, S. G. & Suk, K. Reverse Signaling of Tumor Necrosis Factor Superfamily Proteins in Factor Superfamily Proteins in Macrophages and microgia: Superfamily portrait in the neuroimmune interface. *Front. Immunol.* **10**, 262 (2019).

57. Sun, M. & Fink, P. J. A New Class of Reverse Signaling Costimulators Belongs to the TNF Family. *J. Immunol.* **179**, 4307–4312 (2007).

58. Qu, Y., Zhao, G. & Li, H. Forward and reverse signaling mediated by transmembrane

tumor necrosis factor-alpha and TNF receptor 2: Potential roles in an immunosuppressive tumor microenvironment. *Front. Immunol.* **8**, (2017).

59. Yan, D. *et al.* Expression of TNF-α leader sequence renders MCF-7 tumor cells resistant to the cytotoxicity of soluble TNF-α. *Breast Cancer Res. Treat.* **116**, 91–102 (2009).
60. Neumeyer, J. *et al.* TNF-receptor I defective in internalization allows for cell death through activation of neutral sphingomyelinase. *Exp. Cell Res.* **312**, 2142–2153 (2006).
61. Chen, H., Leng, Y. & Li, Z. β-Actin in the signaling of transmembrane TNF-α-Mediated cytotoxicity. in *Methods in Molecular Biology* vol. 1155 55–68 (Humana Press Inc., 2014).
62. Chen, H. *et al.* The involvement of β-actin in the signaling of transmembrane TNF-α-mediated cytotoxicity. *J. Leukoc. Biol.* **89**, 917–26 (2011).
63. Oeckinghaus, A. & Ghosh, S. The NF-kappaB family of transcription factors and its regulation. *Cold Spring Harbor perspectives in biology* vol. 1 (2009).
64. Tummers, B. & Green, D. R. Caspase-8: regulating life and death. *Immunol. Rev.* **277**, 76–89 (2017).
65. Chen, H. *et al.* The involvement of β-actin in the signaling of transmembrane TNF-α-mediated cytotoxicity. *J. Leukoc. Biol.* **89**, 917–926 (2011).
66. Bidkar, A. P., Sanpui, P. & Ghosh, S. S. Efficient induction of apoptosis in cancer cells by paclitaxel-loaded selenium nanoparticles. *Nanomedicine* **12**, 2641–2652 (2017).
67. Wu, W., Liu, P. & Li, J. Necroptosis: An emerging form of programmed cell death. *Critical Reviews in Oncology/Hematology* vol. 82 249–258 (2012).
68. Hanson, B. Necroptosis: A new way of dying? *Cancer Biology and Therapy* vol. 17 899–910 (2016).
69. Ardestani, S., Deskins, D. L. & Young, P. P. Membrane TNF-alpha-activated programmed necrosis is mediated by Ceramide-induced reactive oxygen species. *J. Mol. Signal.* **8**, (2013).
70. Green, D. R., Droin, N. & Pinkoski, M. Activation-induced cell death in T cells. *Immunological Reviews* vol. 193 70–81 (2003).
71. Zhang, M. *et al.* Transmembrane TNF-α promotes activation-induced cell death by forward and reverse signaling. *Oncotarget* **8**, 63799–63812 (2017).
72. Wu, J. & Lanier, L. L. Natural Killer Cells and Cancer. *Adv. Cancer Res.* **90**, 127–156 (2003).
73. Eissmann, P. Natural Killer Cells | British Society for Immunology. https://www.immunology.org/public-information/bitesized-immunology/cells/natural-killer-cells.
74. Moon, W. Y. & Powis, S. J. Does Natural Killer Cell Deficiency (NKD) Increase the Risk of Cancer? NKD May Increase the Risk of Some Virus Induced Cancer. *Frontiers in*

immunology vol. 10 1703 (2019).

75. Tang, Y. P. *et al.* Prognostic value of peripheral blood natural killer cells in colorectal cancer. *BMC Gastroenterol.* **20**, 31 (2020).
76. Hanna, N. Role of natural killer cells in control of cancer metastasis. *Cancer Metastasis Rev.* **1**, 45–64 (1982).
77. Jiang, Y., Chen, J., Deng, C., Suuronen, E. J. & Zhong, Z. Click hydrogels, microgels and nanogels: Emerging platforms for drug delivery and tissue engineering. *Biomaterials* vol. 35 4969–4985 (2014).
78. Rizvi, S. A. A. & Saleh, A. M. Applications of nanoparticle systems in drug delivery technology. *Saudi Pharmaceutical Journal* vol. 26 64–70 (2018).
79. Garg, U., Chauhan, S., Nagaich, U. & Jain, N. Current advances in chitosan nanoparticles based drug delivery and targeting. *Advanced Pharmaceutical Bulletin* vol. 9 195–204 (2019).
80. Li, Q., Dunn, E. T., Grandmaison, E. W. & Goosen, M. F. A. Applications and Properties of Chitosan. *J. Bioact. Compat. Polym.* **7**, 370–397 (1992).
81. Elgadir, M. A. *et al.* Impact of chitosan composites and chitosan nanoparticle composites on various drug delivery systems: A review. *Journal of Food and Drug Analysis* vol. 23 619–629 (2015).
82. Alexis, F., Pridgen, E., Molnar, L. K. & Farokhzad, O. C. Factors affecting the clearance and biodistribution of polymeric nanoparticles. in *Molecular Pharmaceutics* vol. 5 505–515 (2008).
83. Rao, L. *et al.* Red Blood Cell Membrane as a Biomimetic Nanocoating for Prolonged Circulation Time and Reduced Accelerated Blood Clearance. *Small* **11**, 6225–6236 (2015).
84. Ishida, T. *et al.* Injection of PEGylated liposomes in rats elicits PEG-specific IgM, which is responsible for rapid elimination of a second dose of PEGylated liposomes. *J. Control. Release* **112**, 15–25 (2006).
85. Tan, S., Wu, T., Zhang, D. & Zhang, Z. Cell or cell membrane-based drug delivery systems. *Theranostics* vol. 5 863–881 (2015).
86. Rao, L. *et al.* A Biomimetic Nanodecoy Traps Zika Virus to Prevent Viral Infection and Fetal Microcephaly Development. *Nano Lett.* **19**, 2215–2222 (2019).
87. Rao, L. *et al.* Cancer Cell Membrane-Coated Upconversion Nanoprobes for Highly Specific Tumor Imaging. *Adv. Mater.* **28**, 3460–3466 (2016).
88. Wu, M. *et al.* Cell membrane camouflaged nanoparticles: a new biomimetic platform for cancer photothermal therapy. (2019) doi:10.2147/IJN.S200284.
89. Zhang, Y. *et al.* Macrophage-Membrane-Coated Nanoparticles for Tumor-Targeted

Chemotherapy. *Nano Lett.* **18**, 1908–1915 (2018).

90. Madsen, S. J. *et al.* Nanoparticle-loaded macrophage-mediated photothermal therapy: potential for glioma treatment HHS Public Access. *Lasers Med Sci* **30**, 1357–1365 (2015).

91. Ueno, Y., Futagawa, H., Takagi, Y., Ueno, A. & Mizushima, Y. Drug-incorporating calcium carbonate nanoparticles for a new delivery system. *J. Control. Release* **103**, 93–98 (2005).

92. Mailafiya, M. M. *et al.* Cockle shell-derived calcium carbonate (aragonite) nanoparticles: A dynamite to nanomedicine. *Applied Sciences (Switzerland)* vol. 9 2897 (2019).

93. Maleki Dizaj, S., Barzegar-Jalali, M., Zarrintan, M. H., Adibkia, K. & Lotfipour, F. Calcium carbonate nanoparticles as cancer drug delivery system. *Expert Opinion on Drug Delivery* vol. 12 1649–1660 (2015).

94. Arora, N., Shome, R. & Ghosh, S. S. Deciphering therapeutic potential of PEGylated recombinant PTEN-silver nanoclusters ensemble on 3D spheroids. *Mol. Biol. Rep.* **46**, 5103–5112 (2019).

95. Bhattacharyya, S. & Ghosh, S. S. Transmembrane TNFα-Expressed Macrophage Membrane-Coated Chitosan Nanoparticles as Cancer Therapeutics. *ACS Omega* **5**, 1572–1580 (2020).

96. Xiang, Y. *et al.* Efficient Synthesis of Starch-Regulated Porous Calcium Carbonate Microspheres as a Carrier for Slow-Release Herbicide. *ACS Sustain. Chem. Eng.* **6**, 3649–3658 (2018).

97. Tobias, P. S. & Ulevitch, R. J. Lipopolysaccharide binding protein and CD14 in LPS dependent macrophage activation. *Immunobiology* **187**, 227–232 (1993).

98. Bidkar, A. P., Sanpui, P. & Ghosh, S. S. Red Blood Cell-Membrane-Coated Poly(Lactic- co -glycolic Acid) Nanoparticles for Enhanced Chemo- and Hypoxia-Activated Therapy . *ACS Appl. Bio Mater.* **2**, 4077–4086 (2019).

99. Bidkar, A. P., Sanpui, P. & Ghosh, S. S. Efficient induction of apoptosis in cancer cells by paclitaxel-loaded selenium nanoparticles. *Nanomedicine* **12**, 2641–2651 (2017).

100. Basmaciyan, L., Azas, N. & Casanova, M. Calcein+/PI- as an early apoptotic feature in Leishmania. *PLoS One* **12**, (2017).

101. McIlwain, D. R., Berger, T. & Mak, T. W. Caspase functions in cell death and disease. *Cold Spring Harb. Perspect. Biol.* **5**, 1–28 (2013).

102. Harper, S. & Speicher, D. W. Purification of Proteins Fused to Glutathione S-Transferase. in 259–280 (Humana Press, 2011). doi:10.1007/978-1-60761-913-0_14.

103. Gopal, G. J. & Kumar, A. Strategies for the Production of Recombinant Protein in Escherichia coli. *Protein J.* **32**, 419–425 (2013).

104. Arora, N. & Ghosh, S. S. Functional characterizations of interactive recombinant PTEN–silica nanoparticles for potential biomedical applications. *RSC Adv.* **6**, 114944–114954 (2016).

105. Ghoshal, A. & Ghosh, S. S. Expression, Purification, and Therapeutic Implications of Recombinant sFRP1. *Appl. Biochem. Biotechnol.* **175**, 2087–2103 (2014).

106. Riazance-Lawrence, J. H., Toumadje, A. & Johnson, W. C. The circular dichroism of tumor necrosis factor-?: Measurement into the vacuum UV and analysis for secondary structure. *Chirality* **3**, 254–256 (1991).

107. Grell, M., Wajant, H., Zimmermann, G. & Scheurich, P. The type 1 receptor (CD120a) is the high-affinity receptor for soluble tumor necrosis factor. *Proc. Natl. Acad. Sci. U. S. A.* **95**, 570–575 (1998).

108. Franco, D. L., Nojek, I. M., Molinero, L., Coso, O. A. & Costas, M. A. Osmotic stress sensitizes naturally resistant cells to TNF-a-induced apoptosis. *Cell Death Differ.* **9**, 1090–1098 (2002).

109. Gong, D. *et al.* Cyclin A2 Regulates Nuclear-Envelope Breakdown and the Nuclear Accumulation of Cyclin B1. *Curr. Biol.* **17**, 85–91 (2007).

110. Saraste, A. & Pulkki, K. Morphologic and biochemical hallmarks of apoptosis. *Cardiovasc. Res.* **45**, 528–537 (2000).

111. Brunelle, J. K. & Letai, A. Control of mitochondrial apoptosis by the Bcl-2 family. *J. Cell Sci.* **122**, 437–441 (2009).

112. Friedrich, J., Seidel, C., Ebner, R. & Kunz-Schughart, L. A. Spheroid-based drug screen: considerations and practical approach. *Nat. Protoc.* **4**, 309–324 (2009).

113. Rosano, G. L. & Ceccarelli, E. A. Recombinant protein expression in Escherichia coli: Advances and challenges. *Frontiers in Microbiology* vol. 5 (2014).

114. Welsch, N., Lu, Y., Dzubiella, J. & Ballauff, M. Adsorption of proteins to functional polymeric nanoparticles. *Polymer* vol. 54 2835–2849 (2013).

115. Ghoshal, A., Goswami, U., Raza, A., Chattopadhyay, A. & Ghosh, S. S. Recombinant sFRP4 bound chitosan-alginate composite nanoparticles embedded with silver nanoclusters for Wnt/β-catenin targeting in cancer theranostics. *RSC Adv.* **6**, 85763–85772 (2016).

116. Albanese, A., Tang, P. S. & Chan, W. C. W. The effect of nanoparticle size, shape, and surface chemistry on biological systems. *Annual Review of Biomedical Engineering* vol. 14 1–16 (2012).

117. Ghoshal, A., Goswami, U., Sahoo, A. K., Chattopadhyay, A. & Ghosh, S. S. Targeting Wnt

Canonical Signaling by Recombinant sFRP1 Bound Luminescent Au-Nanocluster Embedded Nanoparticles in Cancer Theranostics. *ACS Biomater. Sci. Eng.* **1**, 1256–1266 (2015).

118. Prabha, S., Arya, G. & Chandra, R. Effect of size on biological properties of nanoparticles employed in gene delivery. *Nanomedicine, Biotechnol.* **44**, 83–91 (2016).

119. Salomão, R., Costa, L. M. M. & Olyveira, G. M. de. Precipitated Calcium Carbonate Nano-Microparticles: Applications in Drug Delivery. *Adv. Tissue Eng. Regen. Med. Open Access* **3**, (2017).

120. Anovitz, L. M. & Cole, D. R. Characterization and analysis of porosity and pore structures. *Rev. Mineral. Geochemistry* **80**, 61–164 (2015).

Publications and Conferences

Journal Publications:

From thesis work-

1. Bhattacharyya, S. & Ghosh, S. S. "Deciphering insights of novel recombinant tmTNFα in cell growth inhibition." ***Molecular Biology Reports,* 47**, 3949–3961, 2020.

2. Bhattacharyya, S. & Ghosh, S. S. "Transmembrane TNFα-Expressed Macrophage Membrane-Coated Chitosan Nanoparticles as Cancer Therapeutics." ***ACS Omega*** 5, 3, 1572–1580, 2020.

3. Bhattacharyya, S. & Ghosh, S. S. "Unfolding Transmembrane TNFα Dynamics in Cancer Therapeutics" [**Revision Submitted in *Cytokine***].

4. Bhattacharyya, S. Saha, M. Ghosh, S. S. "Fabrication of transmembrane TNFα loaded calcium carbonate microparticles with enhanced therapeutic efficacy against HeLa cells" [**Manuscript under Revision**].

From collaborative work-

5. Das, M. Goswami,U. **Bhattacharyya, S.** Kandimalla, R. Chattopadhyay, A& Ghosh,SS "Integration of Nonsteroidal Anti-Inflammatory Drug with Luminescent Copper for in vivo Cancer Therapy in Mouse Model. "***ACS Applied Bio Materials,*** 3, 1, 227-238, 2020.

6. Das, A. **Bhattacharyya, S.** Uppaluri, R. Das, C. "Optimality of poly-vinyl alcohol/starch/glycerol/citric acid in wound dressing applicable composite films" ***International Journal of Biological Macromolecules,*** 26;155:260-272, 2020.

7. Ali, R, **Bhattacharyya, S**. Ali, S. Yashmin, S. Gattu, R. Mondal, S. Ghosh, S.S. and Khan, A.T. "Fused benzoquinoline: A potential fluorescent probe for selective

and sensitive detection of fluoride ion in different medium" (**Manuscript Under review, 2020**)

8. Haridhasapavalan, K. Sundaravadivelu, P. **Bhattacharyya**, **S.** Ranjan, S. Raina, K. Thummer, R. "Generation of cell-permeant recombinant human transcription factor GATA4 from *E. coli*" **(Manuscript communicated, 2020)**

9. Dey, C. Thool, M. **Bhattacharyya, S.** Sudhagar, S. Thummer, R. "Codon optimization, cloning, expression, purification, and secondary structure determination of human transcription factor OCT4", **(Manuscript communicated, 2020)**

10. Haridhasapavalan, K. Ranjan, S. **Bhattacharyya**, **S.** Thummer, R. "Codon optimization, cloning, expression, purification, and secondary structure determination of human MESP1 transcription factor", **(Manuscript communicated, 2020)**

Conference presentations:

1. **Poster presentation by Bhattacharyya, S**. **"**Unravelling role of transmembrane TNFα for cancer therapy", **World Congress On Cancer,** Mahatma Gandhi Medical College and Hospital Jaipur, February 3-5, 2020, jointly organized by the Mahatma Gandhi University of Medical Sciences and Technology (MGUMST), Jaipur, Cancer Institute, Chennai, Ichan School of Medicine at Mount Sinai, New York and National Institute of Immunology, New Delhi, India [***Received Best Poster Award***].
2. **Poster presentation by Bhattacharyya, S**. **"**Recombinant tmTNF α in Cancer Therapeutics", **Fourth International Conference on Nutraceuticals and Chronic Diseases (INCD-2019),** Jointly organized by IIT Guwahati, Society for Nutraceuticals and Chronic Diseases**,** Society for Translational Cancer Research**,** DAICENTER (DBT-AIST International Center for Translational and Environmental Research), Japan**,** National Institute of

Pharmaceutical and Educational Research (NIPER), India [***Received Best Poster Award***].

3. **Poster presentation** by **Bhattacharyya, S**. **"**Transmembrane TNFα Expressed Macrophage Membrane Coated Chitosan Nanoparticles as Cancer Therapeutics", **6th International Conference on Advanced Nanomaterials and Nanotechnology (ICANN2019)**, organized by Centre for Nanotechnology, IIT Guwahati, India, Dec 18-21, 2019.

Appendix

Buffers and their composition:

4 X protein loading dye (for 10 ml)	2 ml 1M Tris-HCl (pH 6.8), 0.8 g SDS, 4.0 ml 100 % glycerol, 0.4 ml 14.7 M β- mercaptoethanol, 8 mg bromophenol blue in water
6 X DNA loading dye	0.25 (%) (w/v) bromophenol blue, 0.25 % (w/v) xylene cyanol FF, 30 % (v/v) glycerol in water
30% Acrylamide solution	29.2 % (w/w) Acrylamide, 0.8 % (w/w) N, N' - methylenebisacrylamide.
Alkaline lysis solution for plasmid isolation I	50 mM glucose, 25 mM Tris-Cl (pH 8.0), EDTA (10 mM)
Alkaline lysis solution for plasmid isolation II	0.2 N NaOH, (freshly diluted from 10 N stock), 1 % (w/v) SDS
Alkaline lysis solution for plasmid isolation III	5 M potassium acetate (60 ml), glacial acetic acid (11.5 ml), water (28.5 ml)
Blocking buffer for western blot	3 % (w/v) BSA in PBST/ TBST
Cleansing buffer I for column regeneration (pH – 8.5)	0.1 M boric acid, 0.5 M NaCl, adjust the pH 8.5 with sodium hydroxide
Cleansing buffer II for column regeneration (pH – 4.5)	0.1 M sodium acetate, 0.5 M NaCl, adjust the pH 4.5 with acetic acid
Gel running buffer(10x)	250 mM Tris base, 1.92 M glycine, and 1 % SDS
Lysis Buffer for GST-TNF α purification	50 mM Tris-HCl (pH-8), 150 mM NaCl, 0.1% β mercaptoethanol, 1.4 mM PMSF

Protein elution buffer	15 mM L-reduced glutathione in 50 mM Tris–HCl (pH 8).
Phosphate buffer saline	137 mM NaCl, 2.68 mM KCl, 7.98 mM Na_2HPO_4, 1.4 mM KH_2PO_4, pH 7.4
Tris buffered saline	Tris-HCl (50Mm), NaCl (150 mM), pH 7.5
Tris buffered saline Tween -20 (TBST)	Tris-HCl (50Mm), NaCl (150 mM), Tween 20 (0.1% v/v) pH 7.5
Tris acetate EDTA(TAE) 50 X, (100 ml)	24.2 g Tris base, 5.71 ml of glacial acetic acid, 10 ml of 0.5 EDTA (pH 8)
Towbin Buffer (5X)	25 mM Tris base, 192 mM glycine, and 20 % methanol
TSS Buffer for transformation	10% (w/v) PEG 8000, 0.6% (w/v) $MgCl_2.6H_2O$, 5% (v/v) DMSO in LB